THE INFLUENCE OF TWO-DIMENSIONAL BED ROUGHNESS ON THE FLOW STRUCTURE OF A TURBULENT BOUNDARY LAYER

BY

MUHAMMAD IJAZ KHAN

A Thesis submitted for the Degree of Doctor of Philosophy in the University of London.

DEPARTMENT OF CIVIL AND ENVIRONMENTAL ENGINEERING
UNIVERSITY COLLEGE LONDON, 2004

ProQuest LLC
789 East Eisenhower Parkway
P.O. Box 1346
Ann Arbor, MI 48106-1346

To my dear wife, SADIA, and our lovely daughter, HINA

ABSTRACT

Experiments have been performed to investigate the relationship between the geometry of an idealised bed roughness and the structure of the turbulent boundary layer above. This work has particular applications in relation to architecture and environmental health, designing comfort for pedestrians and managing environmental pollution. Experiments were carried out in a laboratory water flume to study the turbulence structure generated under both rough and smooth bed conditions. The relationship between small scale turbulent eddies formed between the elements of a two-dimensional bed roughness and the intermittent turbulent structure of the boundary layer was established in the form of roughness length scale and friction velocity using LDV measurements from the mean velocity profile. Turbulence production was also determined from measurements of the Reynolds stress and velocity gradient. This was compared with the diffusion characteristics of the flow. Spacing between the roughness slats was varied for different tests to produce isolated (k-type) bed roughness, skimming (d-type) flow, and wake interference flow for transitional roughness. Transition between these regimes was further investigated using flow visualisation, and a clear correlation established between the vortices at the bed and the turbulence characteristics of the boundary layer.

The effect of sudden changes in bed geometry on the turbulence structure was investigated for flows aligned perpendicular to the roughness elements forming simulated urban environment. These results were compared for a similar model street canyon with and without a large scale upstream approach roughness. The turbulence generated as a result of the change in local bed geometry has a significant influence on the dispersion of dye tracer used to simulate pollutant. It was found that uniformity in height of buildings along parallel streets in an urban environment promotes shear at roof-level, thereby trapping fluid and pollution within the canyon. On the other hand, non-uniformity in building height and the presence of substantial upstream buildings promotes turbulence which helps in ventilation of street canyons.

ACKNOWLEDGEMENTS

I acknowledge with pleasure and sincere thanks the kind and sound guidance provided by Dr. Richard Simons during my research work. Richard has always shown a sincere interest in my research work which spanned over a period of three years. I found him a source of inspiration and a generous benefactor in the advancement of my professional career. I am grateful to him for his special interest in the analysis of my experimental data, discussions and help in my thesis and publications.

I am grateful to Prof. Grass for his continuous encouragement. I always found him very supportive and helpful. He addressed the needs for my research study at the right time. I must also acknowledge help of Prof. Grass wife, Adele; she has the skills to handle difficult situations in a right direction.

I want to acknowledge the help from Dr. Gert Van der Heijden (Non-linear dynamics group, UCL) for discussion on the numerical methods. Thanks must go to Dr. Ian Eames (Mechanical Engineering Department, UCL) for his help on the numerical side and his keen interest in my experimental work in the laboratory. Dr. Martin Hyde (TSI) and Dr. David Selviah (EE, UCL) were very kind and their services were available to me for the LDV employed for the current research is gratefully acknowledged.

I would like to thank Mr. Keith Harvey for his technical assistance. Thanks also go to other departmental technician staff of which special thanks are extended to Ian, Muhammad Saleem, Les, John, Simon, Harry, Paul and Bill for tapping large amount of slats for my experiments.

Thanks also go to UCL colleagues, Dr Achilleas Kalopedis, Dr. Yuan Shiang, Dr. Ruairi MacIver, and Mr. Amar Bahra who provided support and encouragement throughout this work.

To my wife, Sadia; I am grateful for her patience and encouragement at all times for the successful completion of this work. Sadia is a determined wife and has got the selfless devotion and understanding which has been my strength and confidence under demanding circumstances.

Finally, financial support from the University College London, through Graduate School Research award is gratefully acknowledged.

CONTENTS

LIST OF TABLES

LIST OF FIGURES

NOMENCLATURE

Co-ordinate System

x	Stream wise distance (along channel)
y	Transverse distance (across channel)
z	Vertical distance from the effective origin of mean velocity profile
U (=u+u')	Instantaneous stream wise velocity
V (=v+v')	Instantaneous transverse velocity
W(=w+w')	Instantaneous vertical velocity
u	Local mean stream wise velocity
v	Local mean transverse velocity
w	Local mean vertical velocity
u'	Fluctuating stream wise velocity component
v'	Fluctuating transverse velocity component
w'	Fluctuating vertical velocity component

Notation

b	Thickness of the roughness element
c	Cavity plume width
c1	Injector at the top of the centre of the element
Cd	Turbulent diffusion coefficient
d1	Injector inside the cavity release dye in direction of flow
D	Flow depth at test section
H	Hyperbolic hole
Hd	Height of downstream element of large scale roughness
Hu	Height of upstream element of the large scale roughness
λ	Mixing length scale
L1	Shortest distance dye touch the water surface

$L2$	Average distance dye touch the water surface
s	Gap distance between the roughness elements
$u1$	Injector inside the cavity release dye against flow direction
u_τ	Bed shear velocity
urms	Root mean square value for U
$\overline{u}$	Depth average mean velocity
U_∞	Free stream velocity
V_T	Turbulent viscosity
wo	Initial plume width
$w1$	Plume width at shortest distance dye touching water surface
$w2$	Plume width at average distance dye touching water surface
wrms	Root mean square value for W
z'	Vertical distance from the roof level of roughness element
z''	Vertical distance from the wall to the roof level of the roughness element
z'''	Vertical distance from the tall roughness element
z_d	Zero plane displacement height from the wall to the effective origin of mean velocity profile
z_o	Roughness length scale
z^+	Non-dimensional wall distance $\frac{zu_\tau}{\upsilon}$
υ	Kinematic viscosity of water
μ	Dynamic viscosity of water
ρ	Density of water
$-\rho\overline{u'w'}$	Reynolds stress
τ	Shear stress
τ_0	Bed shear stress

ε	Effective origin for z below roughness element crest
κ	Von Karman's constant
k	Roughness element height
λ	Face to face spacing between roughness elements
a	Streamwise position between the roughness elements
λ_d	Roughness parameter

Further symbols are specifically defined within the text.

Unit Abbreviations

fps	Frames per second
Hz	Hertz
m	Meters
mm	Millimetres
ms	Milliseconds
sec	Seconds
μs	Microseconds

CHAPTER 1

INTRODUCTION

1.1 General introduction

The interaction of wind with an urban environment is one of the major scientific issues to be addressed by society by professionals, community participation and help of the government. Town planners, architects and engineers are going to be increasingly important drivers in providing a healthy environment for residents and workers. For this reason meteorological research is being carried out to gain a better understanding of the interaction between ground roughness (particularly in cities) and flow in the turbulent atmospheric boundary layer. From this research study it is hoped to parameterise the influence of the systematic variation of two-dimensional surface roughness on the surface drag, length scale, and dispersion behaviour of the flow.

The boundary layer structure can be divided into various regions where different length scales and different driving mechanisms are important as shown in figure 1.1.

The surface layer defines the region in which surface effects are dominant. Within this layer, the roughness sublayer extends from the surface up to 2-5 canopy heights (or height of the roughness elements), and here the surface roughness influences the turbulence and flow parameters. The roughness sublayer is a layer of spatial inhomogeneity where the different length scales of the surface geometry are important. Significant spatial variations in the properties of the flow are predicted from surface layer theory within the roughness sublayer. Turbulence here is generated by both wake production in the low-pressure region behind roughness elements and by shear production (Raupach et al. 1986). Removal of turbulence through viscous dissipation is especially important close to the ground. The important length scales in

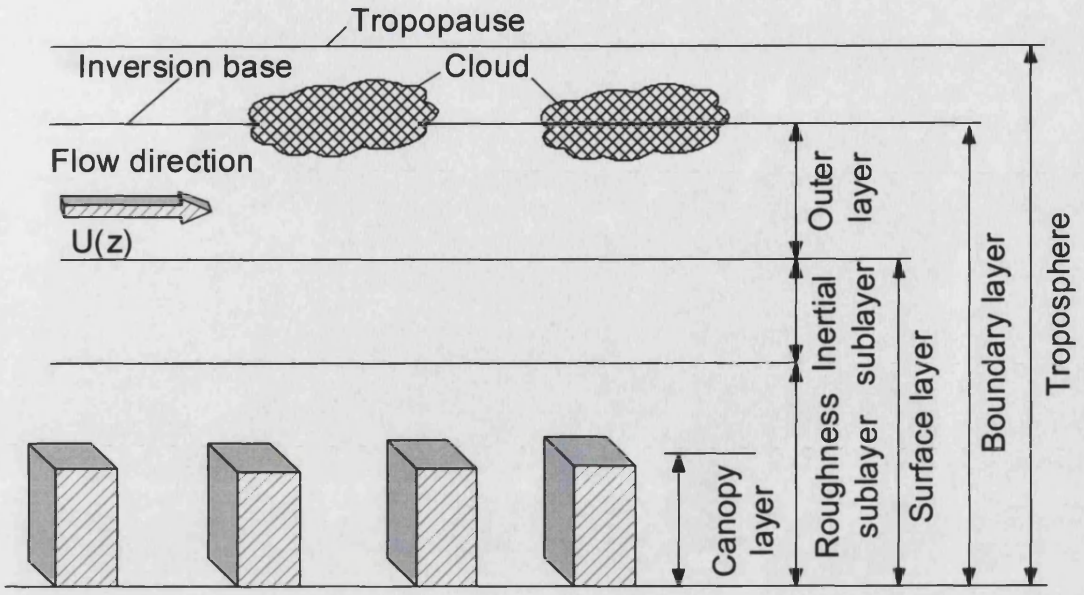

Figure 1.1 A schematic of the atmospheric boundary layer structure

the roughness sublayer include the roughness length scale (representing the drag induced by the roughness elements) and roughness parameters density and shape. Above the roughness sublayer, the inertial sublayer can be thought of as the region of overlap of the roughness sublayer and the outer layer. In this region shear production and viscous dissipation of turbulent kinetic energy are negligible (Finnigan and Brunet, 1995). The dominant turbulent process here is the conversion of large scale eddies to small scale eddies via the energy cascade process. Beyond the surface layer is the outer layer where turbulent effects predominate and turbulent stress is principally due to turbulent Reynolds stress. The governing length scale in the inertial sublayer is the roughness length scale which is commonly found from the logarithmic mean velocity profile.

This thesis is concerned with the mean velocity profile of flow within and above the canopy layer for two-dimensional roughness elements (slats), which is found to depend on certain roughness parameters. Of these, the friction velocity represents the effect of the shear stress at the ground, the roughness length scale represents the drag induced by the roughness, and the zero-plane displacement represents the

displacement of the flow above the flat plate surface. These parameters help in understanding and quantifying the momentum exchange and complex interaction between the canopy and the boundary layer. Specific applications include the parameterisation of surface drag for use in atmospheric models, calculation of wind load on buildings and trees, and pollutant dispersal modelling. In dispersion modelling the roughness length scales is an important input parameter.

A water flume is used for this research project because of several advantages over the wind tunnel i.e. the lower kinematic viscosity permits lower mean flow velocities, thus slowing down the turbulent dispersion process. This facilitates high quality flow visualization with a dye tracer and polystyrene beads. Mineral particles present in typical quality laboratory water also provide natural seeding for laser Doppler velocimetry measurements.

1.2 Turbulence structure

Turbulent flows have been the subject of many experimental and theoretical investigations. They arise in numerous engineering applications involving the interaction between man and his surroundings, for example in the form of smoke stacks, cooling towers, flow around buildings, and the dispersion of pollutants in the atmosphere and rivers. In addition, the transportation of fluids such as in chemical reactors, heat exchangers, gas turbines and aircraft intakes involves turbulent flow. The study of turbulence can be achieved experimentally using techniques such as hot wire and hot film anemometry; where a non-intrusive method is essential, laser Doppler velocimetry and particle image velocimetry can be used for flow visualisation.

Theodorsen (1952) was the first to postulate the turbulent boundary layer is made of coherent eddy structures or vortex loops (figure 1.2) also variously referred to as 'horseshoe' or 'hairpin' vortices.

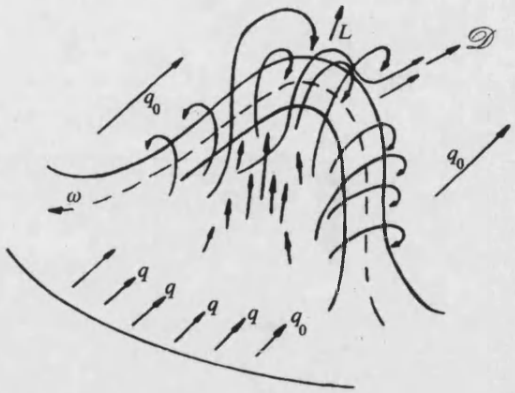

Figure 1.2 Horseshoe Vortex Model first proposed by Theodorsen (1952)

He proposed a vortex model as the central element of the turbulence generation process in shear flows. The horseshoe-shaped vortical structure is inclined in the direction of shear and loops either upwards, in response to positive perturbation velocities such as occur during ejection events, or downwards for negative velocities produced by sweep events. In ejections, low speed fluid is observed to be ejected away from the wall region into the outer flow. On the other hand when high velocity fluid moves toward the bed, it is generally described as an "inrush" or "sweep" event. Near the wall, coherent structures in a turbulent boundary layer lead to intense variations of the shear stress. Ejection events are an important feature in the evolution of the near wall flow structures. Flow visualisation experiments by Kline et al. (1967) observed a gradual uprising of the low speed streaks towards the external region of the boundary layer. A streak forms in the region between two vortices, because the streamwise velocity there is lower than the mean velocity of the surrounding fluid. This can be observed by injecting dye or smoke at a fixed point for an interval of time. Another important advance they made was to observe that the inner part of the wall layer in the range $5 < z^+ < 70$ is not at all passive, as one might think. In fact, it is perhaps dynamically the most active, in spite of the fact that it occupies about 1% of the

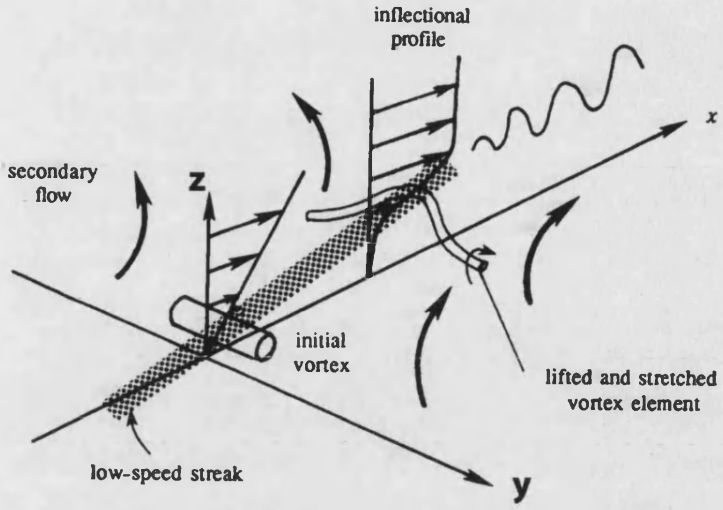

Figure 1.3 Mechanics of streak break up. [S.J.Kline (1967)]

total thickness of the boundary layer. This was shown from their hydrogen bubble visualisation of the viscous sublayer at a distance $z^+ = 2.7$ from the wall. It was shown that the streaky structure of the near bed flow is generated by regions of fluid moving downstream faster or slower than the average. The hydrogen bubble visualisation revealed that the streaks of low speed fluid are quasi-periodic in the spanwise direction. From time to time these slowly moving streaks lifted up into the buffer region, where they underwent a characteristic oscillation. The oscillations ended violently and abruptly as the lifting fluid broke up into small scale eddies. The whole cycle is called bursting, or eruption, and is essentially an ejection of slower fluid into the flow above. The flow into which ejections occur decelerates, causing a point of inflection in the profile $u(z)$ shown in figure 1.3. The secondary flow associated with the eruption motion causes the stretching of the spanwise vortex lines, as shown in the figure 1.3. These vortex lines amplify due to the inherent instability of an inflectional profile, and readily break up, producing a source of small scale turbulence. The strengths of the eruptions vary, and the strong ones can go right through to the edge of the boundary layer. Kline et al. (1967) linked this streaky structure to the bursting process, which they described as a randomly

occurring event comprising the gradual lift-up of the low speed streak from the wall region, sudden oscillation and break-up.

The ejection and inrush events form part of a randomly occurring yet linked cyclical process of turbulence generation in the boundary layer which has been shown to be responsible for most of the turbulence energy production and major contribution to the Reynolds stress momentum transport in the wall layers [Grass (1971)]. Grass also showed that the bursting event with its linked ejection of low momentum fluid from the wall region out into the main body of the flow, and the subsequent inrush event with its return high momentum fluid, were common features of both smooth and rough wall flows. During bursting and ejection events, the visualised erupting flow structure appears on slow motion films produced by Grass (1967) literally to 'rear up' from the bed. This behaviour is particularly pronounced in the case of the violent bursting and resulting highly disturbed flow field over a rough boundary.

Schoppa and Hussain (1997, 2000) suggested a cycle was controlling the wall turbulence in which low speed streaks are considered responsible for the initial generation of vortices, which in turn generate the ejection and sweep events. The generated ejection and sweep events contribute to maintain the low speed streaks. Schoppa and Hussain investigated the behaviour of a single low speed streak. It was found to be sinuous and, in time, oscillated with a meandering motion in the span wise direction. One single low speed streak has a longer life than the quasi-streamwise vortices and survives a number of vortex generations. In practice, if a lifted low speed streak which is found to be more stable to spanwise perturbation, it would reduce its meandering and reduced the tripping frequency of the quasi-streamwise vortices. This in turn would reduce the frequency and the intensity of the turbulence production events (ejection and sweeps). In other words,

lateral instability of lifted low speed streaks dominates turbulence production, drag and heat transfer.

Eames and Gilbertson (2004) reported that these coherent vortical structures generate regions of significant strain and are the primary agents for dispersing and mixing particles. Roy et al. (2004) reported that the size of the coherent structures on a smooth bed is twice the flow depth and their lateral and vertical extent is more or less equal to the flow depth. In flows over a smooth bed, large scale flow structures are generated in the near bed region and they are formed by the expansion and amalgamation of individual bursting motions. While one group of researchers believes that large scale flow structures act as a trigger, another focuses on the bursting cycle. Roy's (2004) experiments on a gravel river, bed showed that there is a convergence between flume studies over smooth as well as rough beds and their results in a gravel bed river. They found that large scale flow structures were enhanced by a feed back mechanism due to shedding motions from the lee side of the protruding obstacles and bursting motions from the near bed flow region.

Stuart (1984) carried out detailed flow visualisation experiments over a *k-type* bed roughness, and identified three dimensional vortex loops from direct simultaneous measurements of the spatial distribution of the three dimensional vorticity vector in the boundary layer of an open channel flow. These vortex structures and their self induced patterns of migration are a key element in the turbulence bursting process and the linked transport of mass, momentum and pollutants across the boundary layer.

Robinson (1991) proposed that coherent structures are the "skeleton" of the wall turbulence, responsible for the most part of turbulence production, dissipation, and transport phenomena. Holmes et al. (1996) and Jimenez and Pinelli (1997) argued that the dynamics of a coherent structures is the bursting process, which is linked to the

self-sustaining cycle and defines the alternation of sweeps and ejections near the wall. When the coherent structure becomes unstable, a burst occurs with an ejection of slow moving fluid toward the core of the flow; this is followed by an ensuing sweep of faster moving fluid towards the wall.

Wallace et al. (1972) classified the streamwise u' and vertical w' turbulence intensities by means of "quadrant analysis" shown graphically in figure 1.4. During an ejection, jets of low streamwise momentum are observed to be ejected away from the wall region into the outer flow. This ejected fluid combines low streamwise velocity with a positive velocity away from the wall, which can be expressed as $u' < 0$ and $w' > 0$ respectively. The product $\rho\overline{u'w'}$ is therefore negative, and since negative Reynolds stresses contribute, i.e. to positive turbulence production, thus their increase corresponds in general to an increase in drag. In physical terms, the ejection process provides a means of transferring wall shear stress into the outer flow. Diametrically opposite the ejection quadrant is a further quadrant where the Reynolds stress contribution is negative, due to $u' > 0$ and $w' < 0$. This represents jets of high streamwise momentum directed towards the wall and is generally described as an "inrush" or "sweep" event. In the remaining two quadrants, the contribution to Reynolds stress is positive i.e. negative turbulence production, and their increase corresponds in general to a decrease in drag. These are termed "interaction" regions.

A similar analysis was carried out by Lu and Willmarth (1973) in which the Reynolds stress at a point of the (u,w) plane is presented as the sum of the contributions measured in the four quadrants of the (u,w) plane. During an ejection, $u' < 0$ and $w' > 0$, the corresponding point is located in the second quadrant (Q_2).

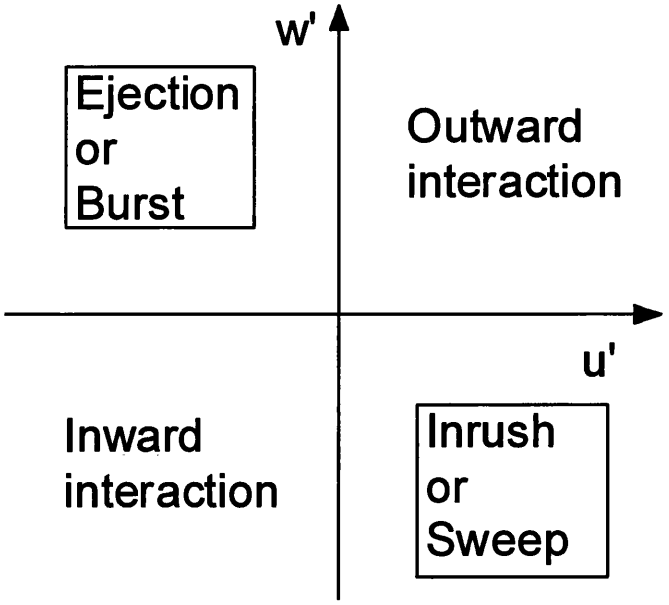

Figure 1.4 Quadrant representation of velocity fluctuations

During a sweep, when $u'>0$ and $w'<0$, the point can be plotted in a similar way in the fourth quadrant (Q_4). The contribution to the Reynolds stress determined in the Q_i quadrant outside the central region limited by four hyperbola is as follows:

$$(\overline{u'w'})_{Q_i} = \lim_{T\to\infty} \frac{1}{T} \int_0^T (u'w')_{Q_i} \, I \, dt \qquad (1.1)$$

where I is the detection indicator function related to the occurance of ejection and sweep events. For an ejection event, I was defined so that

$I = 1$, If $u'w' < -H(urms \times wrms)$ and $u' < 0$

$I = 0$, Otherwise

For a sweep, the detection indicator function I was defined so that

$I = 1$, If $u'w' < -H(urms \times wrms)$ and $u' > 0$

$I = 0$, Otherwise

The size of the hyperbolic hole determines the strength of the ejections and sweeps that are recorded; only points located outside a hyperbolic hole of size H are included in the analysis.

1.3 Atmospheric boundary layer

Turning now to specific aspects of urban boundary layer, the dispersion of pollution from a line source depends on the meteorological process and the associated turbulence. Pollution from the source comes in contact with the atmospheric boundary layer (the shear layer which couples the interaction of the atmosphere with the earth's surface) and starts interacting with the wind, at a range of spatial scales. Diffusion of the plume (caused by the line source of pollution) is driven by atmospheric turbulence. The turbulence in the boundary layer is generated mechanically, because of the velocity gradients, or thermally, due to the temperature gradients. This turbulence is dissipated or enhanced depending on the meteorological conditions.

The boundary layer or the mixing layer is the lower stratum of the atmosphere and extends to about one km above the earth's surface. This is a zone of transition from the disturbed flow near the surface to the smooth frictionless flow of the free atmosphere. Wind structures in this layer are generated by pressure gradients, Coriolis force and residual frictional effects of the Earth's surface.

The intense turbulent mixing in the boundary layer is initiated in two ways. The first relates to the variation in wind speed with height inducing vertical shear. The second source for turbulence production can be thermal, due to temperature differences between the ground and the air above. The enhancement and suppression of the turbulence depends on the variable balance of thermal energy into and out of the boundary layer and corresponding temperature (and density) profiles. In addition to the intense turbulent mixing, the boundary layer acts as a buffer zone in which heat, moisture and pollution from sources at the surface are stored for a time, before being released upwards into the troposphere (see figure 1.1). However temperature gradient is not the main subject of this thesis and will not be considered further.

Table 1.1 Horizontal scale of pollution dispersion from source in atmospheric boundary layer

Definition	Micro-scale	Local-scale	Meso-scale	Macro-scale
Oke (1987)	10^{-2}m to 10^{3}m	10^{2}m to 5×10^{4} m	10^{4}m to 2×10^{5} m	10^{5}m to 10^{8}m
Panofsky and Dutton (1984)	Small scale waves	×	10-500kms	Synoptic observing networks

Panofsky and Dutton (1984) and Oke (1987) divided the motions of the atmosphere on the basis of the horizontal dimensions of the turbulent flow in the boundary layer. Panofsky and Dutton (1984) described three broad groups: macro scale, meso scale, and micro scale. In addition to these, Oke (1987) suggested a local scale. Table 1.1 summarises the definition of Panofsky and Dutton (1984) and Oke (1987).

Pollutants released near the ground surface and taken up by the atmosphere are advected and diffused over the entire range of atmospheric scales defined above. The length scales of horizontal and vertical transport for any pollutant range from a scale of a few meters near the source, up to a global scale. The time scales involved for pollutants to spread and mix over these length scales range from minutes to years (Table 1.2).

1.4 Flow over roughened surfaces

The surface roughness and flow in the boundary layer are in a process of interaction with each other. Roughness alters the momentum, heat and mass transfer within the boundary layer. The boundary layer in turn induces vorticity between the roughness elements, which affects the mixing with the boundary layer.

Research into the role played by flow over roughened surfaces in fluid mechanics has developed in two principal directions. The first one is concerned with the transition from a laminar to turbulent boundary layer and the influence of roughness in inducing

Table 1.2 Horizontal and vertical scale of pollution dispersion from source in atmospheric boundary layer (Boeker et al., 1995)

Horizontal scale			Vertical scale		
Horizontal distance	Dispersion scale	Time scale	Vertical distance	Atmospheric layer involved	Time scale
1 to 10m	Micro scale	Seconds	Ground surface to 100m-3km	Surface layer	Minutes to hours
10m to 1 km	Micro scale	Minutes	100m-3km to 10km-15km	Mixing layer to Troposphere	Days to weeks
3 to 30 km	Local scale	Hours	10km-15km to 50km	Troposphere to Stratosphere	Years
100 to 1000 km	Meso scale	Days			
Hemisphere	Macro scale	Months			
Globe	Global scale	Years			

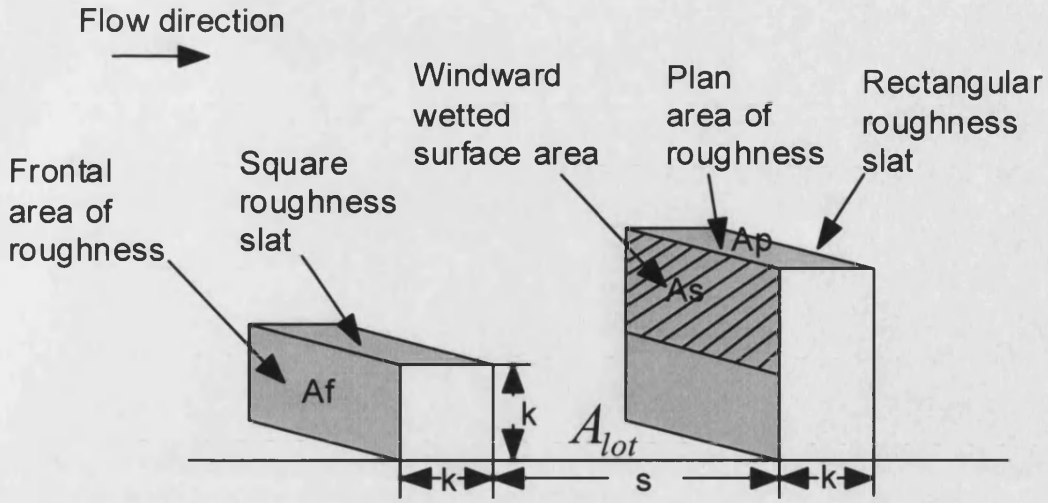

Figure 1.5 Roughness density parameterisation

transition. The second is concerned with the drag force exerted by the roughened surfaces in a fully developed turbulent boundary layer, as in rough pipes or in the atmospheric boundary layer.

Several workers have investigated the flow over "two-dimensional" roughness elements, while others have focussed on "three-dimensional" arrays of roughness elements with finite horizontal dimension. Two dimensional roughness refers to bars, ribs, or circular rods placed on a flat horizontal plate perpendicular to the flow direction as shown in figure 1.5. Two-dimensional roughness geometry can be described in terms of various parameters. These include the equivalent sand roughness height, k_s, pitch to height ratio $S_m = \lambda / k$, pitch to width ratio $S_f = \lambda / s$, the density roughness parameter $\lambda_d = \frac{S_m}{S_f}$, and an equivalent sand roughness density parameter defined by $\wedge = (\frac{S_m}{S_f})(\frac{A_f}{A_s})^{-1.6}$, where A_s is the windward wetted surface area, and A_f is the frontal area of the roughness element. The equivalent sand roughness height, k_s, is defined as the size of the sand grain which would give the same resistance as the particular roughness being investigated. Schlichting (1979) obtained values by

equating the wall intercept yielding: $\frac{ks}{k} = \exp[\kappa(3.0 + D)]$, where D is a function of geometry. With this definition Nikuradse's sand data can be applied to other types of roughness.

In contrast, "three-dimensional" roughness consists of arrangements of cubes, spheres, hemispherical elements, cones, angles, pyramids, screens, or sand grains along a surface. For three-dimensional roughness elements, a major difficulty is to define the texture of the roughness and to find a convenient means to explain its influence on the flow in the roughness sublayer. Theurer (1993) noted that roughness length scale z_o and zero plane displacement height z_d could be approximately related to two secondary parameters of the three-dimensional roughness. These are the ratio of the frontal area of the roughness elements to the total plan area occupied by the roughness elements.

$$\lambda_f = \frac{A_f}{A_d} \tag{1.2}$$

and the ratio of the plan area of the obstacles to the total area occupied by the roughness elements,

$$\lambda_p = \frac{A_p}{A_d} \tag{1.3}$$

For non-uniform obstacles, A_f is the total frontal area of the obstacles, A_p is the total plan area of the obstacles and A_d is the total area covered by the obstacles. For cubical elements, the two area densities are equal. Theurer found that z_o is mainly related to λ_f, while the displacement height was mainly a function of λ_p.

Fang and Sill (1991) reported that aerodynamic roughness length scales z_o for many natural conditions including forests, cities, crops, grass etc, can be approximated by the simple expression:

$$\frac{z_o}{k} = c \tag{1.4}$$

where k is the mean roughness height, and c a constant, approximately 0.1.

Lettau (1969) considered the density of the 3-D roughness elements and their frontal area in the special cases when roughness elements are uniform in size and evenly spaced for estimation of z_o. He concluded that:

$$\frac{z_o}{k} = 0.5\frac{A_f}{A_d} = 0.5\lambda_f \tag{1.5}$$

where k is the roughness height. A limitation of Lettau's equation is that it only applies to cases where roughness elements do not interfere too strongly with each other. The expression fails when the roughness area density $\lambda_p\,(or\ \lambda_f)$ increases beyond 20-30% due to aerodynamic interaction between the obstacles (wake interference flow) and the development of displacement height (z_d) in the velocity profile. Peterson (1997) found good agreement between the Lettau expression and roughness measurements for model refineries. This suggests that Lettau's expression is more representative of rounded obstacles, which have a lower drag by a factor of 2 than rectangular prisms.

Counihan (1971) measured z_o from velocity profiles over regular arrays of cubic roughness in a wind tunnel. He considered cubical roughness in the $\frac{A_p}{A_d}$ range from 0.08 to 0.45 and arrived at an expression which included the effect of a limited fetch of roughness upstream. He gave this expression as

$$\frac{z_o}{k} = 8.2\frac{k}{X_F} + 1.08\frac{A_p}{A_d} - 0.08 \tag{1.6}$$

where X_F is the fetch distance and A_p is the plan area of the obstacles. He suggested that z_o has a strong fetch dependence as shown in the above equation. But in reality the mean drag coefficient for rectangular blocks reduces with an increase in turbulence intensity, and turbulence length scales change with fetch. When the fetch is large, $\frac{k}{X_F} \to 0$ and the expression reduces to

$$\frac{z_o}{k} = 1.08\lambda_p - 0.08 \tag{1.7}$$

The use of roughness density by Counihan is not consistent with Lettau's expression. Macdonald (1998) reported a relationship between the roughness density and shape parameter: $A_f = 0.60A_p$, so that the above equation can be written as

$$\frac{z_o}{k} = 1.8\lambda_f - 0.08 \tag{1.8}$$

The above expression was reported valid over the range: $0.10 < \lambda_p < 0.25$ (*i.e.*$0.06 < \lambda_f < 0.15$).

The work done by Lettau (1969) and Counihan (1971) have not considered the effect of the displacement height and the non-linear variation of the roughness length scale z_o in relation to the increase in turbulent interaction between the roughness. Theurer (1993) found two expressions to approximate the displacement height z_d and roughness length scale z_o from full scale measurements in cities and wind tunnel experiments with systematic arrays of roughness.

These relationships of displacement height to bed roughness density parameter is valid for $\lambda_p < 0.6$,

$$\frac{z_d}{k} = 1.67\lambda_p \tag{1.9}$$

and

$$\frac{z_o}{k - z_d} = 1.6\lambda_f \tag{1.10}$$

Simplifying Equ. 1.9 and 1.10;

$$\frac{z_o}{k} = 1.6\lambda_f(1 - 1.67\lambda_p) \tag{1.11}$$

The change in flow regime from a single vortex dominating in a canyon to multiple vortices in the canyon there has a significant effect on zero plane displacement height. Theurer therefore limited his results to $\lambda_f < 0.25$ to avoid skimming flow effects within more densely packed roughness arrays.

Macdonald (1998) derived an improved version of the Lettau expression based on the assumption that there is negligible wake interference between the surface elements and that the mean velocity profile approaching each roughness is logarithmic. This alternative expression for $\frac{z_o}{k}$ look in the form:

$$\frac{z_o}{k} = \exp[-(0.5\frac{C_D}{k^2}\frac{A_f}{A_d})^{-0.5}] \tag{1.12}$$

substituting $C_D = 1.2$ and $\kappa = 0.4$ into Eq. 1.12 for the flow over a cube:

$$\frac{z_o}{k} = \exp(-.52\lambda_f^{-.5}) \tag{1.13}$$

Furthur improvement in estimating the roughness length scale (z_o) was made by the inclusion of the effect of zero plane displacement height as:

$$\frac{z_o}{k} = (1 - \frac{z_d}{k})\exp[\ -(0.5\frac{C_D}{\kappa^2}(1 - z_d/k)\frac{A_f}{A_d})^{-0.5}\ ] \tag{1.14}$$

This expression accounts for the reduction of z_o with increasing obstacle density. Macdonald considered the variation in displacement height by a simple monotonic expression. However z_d is not known *apriori* and represents another unknown in the problem.

From the above, it was found that various of the models are unable to estimate the roughness length scale and the displacement height when there is a transition between the flow pattern and change in the number of vortices in a canyon.

Cook (1985) developed different tables of terrain roughness. In these tables, ranges of z_o values and mean roughness height are given for each terrain category.

Many researchers (Perry et al. 1969 for instance) have quoted the work by Moore (1951), who studied roughness consisting of square bars mounted transversely to the flow. He carried out wind tunnel tests using arrays, .125in (3.17mm) by 63in (1600mm), and spaced about 4 times the bar width. His investigation focussed on the variation of total shear stress with distance downstream, so that the effect of varying boundary layer thickness could be observed. He found in his study that the surface friction factor depends only upon the physical roughness size. Morris (1959) reported evidence from his tests that quasi-smooth (or skimming flow) is only possible when the roughness height approaches the cavity width. Perry and Joubert (1963) used a similar configuration to that investigated by Moore (1951) and developed a refined version of the rough wall velocity origin location method originally introduced by Clauser (1956). This gave the displacement height referred to above and defined the effective origin of the logarithmic mean velocity profile. This definition of the velocity profile remains physically arbitrary but at least has the advantage of reproducibility and consistency.

The importance of gap (s) to height (k) ratio of the roughness array for the separation and reattachment of the stream lines in the canyon has been noted by many researchers. Surface roughness can be classified between 'k' type ($s \geq 3k$) and 'd' type ($s \leq k$) according to Perry et al. (1969), who made a comparison between the 'k' and 'd' type roughness by adjusting the spacing to produce the required roughness behaviour. In the case of 'k' type roughness, k is the controlling parameter. Eddies with a length scale proportional to k are shed into the flow above the crests of the elements. Furthur away from the crests, the roughness sublayer structure blends smoothly into the flow which is described by the velocity defect law. Flow visualisation studies by Perry et al. (1969) showed that the flow within these cavities between the elements is largely self contained, being separated from the outer flow by a shear layer across the top of the cavity. The outer flow rides over the crests of the elements undisturbed, with little eddy shedding from the rough wall into the main flow. Returning to 'k' type roughness, friction factor was found to depend on Reynolds number based on the shear velocity and on a length associated with the size of the roughness. There is a strong interaction between the flow over the crests of the roughness elements and the flow between the elements resulting in strong eddy shedding into the main flow. In the second, i.e. the 'd'type roughness, the friction factor does not depend on roughness scale i.e. does not produce a Reynolds number independent friction factor. Such a flow behaviour was termed "skimming flow".

The variation in 2-d roughness geometry was found by Oke (1987) to generate three kinds of flow pattern. These were referred to as isolated roughness flow, wake interference flow and skimming flow. The roughness geometry was characterised by its aspect ratio, which is the height 'k'of the canyon (gap between adjoining elements) divided by the width (s). For wide canyons ($s/k > 3.33$), the roughness

Table 1.3 Boundary between flow regimes (see figure 3.5)

Skimming flow	Wake interference flow	Isolated roughness flow
$0.5<s/k<1$ (Cheng-M.) $s/k=0.9$ (Perry et. al. k/s=1.11) $s/k<1.53$ (Oke)	$2<s/k<4$ (Cheng-M.) $s/k=2.713$ (Perry et al. $\lambda/k=3.6$) $1.53<s/k<3.33$ (Oke)	$s/k=6$ (Cheng-M.) $s/k=4$ (Stuart) $s/k>3.33$ (Oke)

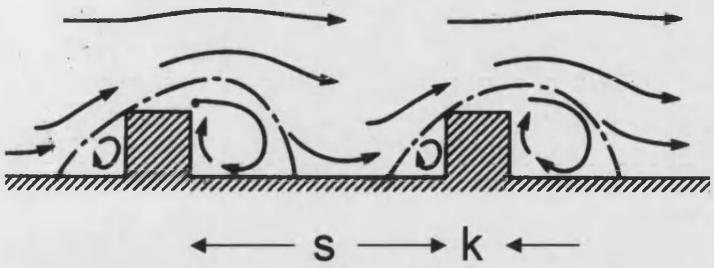

a) Isolated roughness flow s/k>3.33

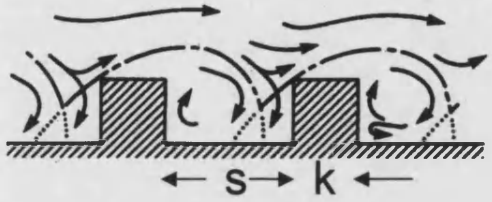

b) Wake interference flow 3.33>s/k>1.53

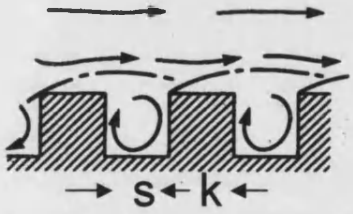

c) Skimming flow s/k<1.53

Figure 1.6 Flow pattern classifications a) Isolated roughness flow, b) Wake interference flow, and c) Skimming flow [Oke (1987)]

elements are well spaced and act essentially as isolated roughness elements (figure 1.6 a). As roughness become more closely spaced ($3.33 > s/k > 1.53$), the disturbed flow has insufficient distance to readjust (figure 1.6b). In the case of skimming flow ($s/k < 1.53$), the bulk of the flow skims over the canyon (figure 1.6c). The flow regimes in urban street canyons were also reported by Cheng and Meroney (2001). Their proposed boundaries are summarised in Table 1.3.

Pearson et al. (1997) reported tests with a single square cavity cut into a smooth surface. Flow visualisation confirmed that there exists an important communication via outflows and inflows between the groove and the overlying shear layer. Roberts et al. (1997) reported that ground level concentrations of a dense gas decrease with increased surface roughness length scale implying better ventilation.

Hunt and Eames (2001) reported the flow behaviour through a group of bluff bodies spaced sufficiently away to form wake interference flow. They reported that the wake was reduced by vorticity cancellation or by wake-wake interference. The former was reported to be associated with a staggered pattern of obstacles whereas the latter was reported to be associated with the 2-d roughness arrangement.

1.5 Dispersion over irregular surface

Elder (1958) reported the diffusion of marked fluid in turbulent open channel flow. The coefficients of longitudinal and lateral diffusion were scaled with friction velocity and depth of flow. Elder noticed that the longitudinal dispersion was 5 times the lateral dispersion. The concentration curves reported were more disturbed in front and a pronounced tail was seen behind. Townsend (1976) reported the necessary connection between the diffusion and the supply of energy to the turbulent motion is a fundamental characteristic of turbulent flow.

Gerdes and Olivari (1999) reported tests in a wind tunnel to study the effect of changes to the urban roughness, gap distance between two roughness elements, and height of downstream roughness on the flow pattern and concentration distribution in a test canyon intended to simulate a city street. Other tests were carried out with simulated roughness upstream of test section. The velocity inside the test street canyon increased with increasing ratio of street canyon width to height. A small gap between the elements did not allow any circulation to become established. Upstream

roughness did not change the concentration field. It was observed that flow approaching the canyon was parallel to the surface and flow circulation increased because a shear zone was formed at the top of the canyon and consequently the re-circulating eddies became much more stable in their position than in the case with no roughness. Better ventilation in the test section was observed in the case with no roughness than when urban roughness was located upstream. The flow pattern was seen to change when there was a change in building configuration. For flow with the windward element of the street canyon higher than the leeward element, pollutant was able to migrate into the upstream canyons. The combined effect of the upstream area and the ratio of the element heights of the street canyon determined the velocity field inside the canyon. The downstream tall element of the street canyon defined the flow pattern. For a ratio of downstream roughness height to upstream height of 5/3, the difference in terms of flow pattern between no-upstream roughness and the urban fabric case became smaller.

Meroney et al. (1996) carried out wind tunnel tests to study pollutant concentration. The experiments were mainly focused on the effects of wind speed and street canyon widths for pollutant dispersion released from a line source. The measurements showed that the dimensionless pollutant concentrations were almost independent of wind speeds for street canyon aspect ratio (gap distance/building height)=1 except at the two lowest wind speeds used. They also showed that the dimensionless pollutant concentrations decreased everywhere on the wall surfaces of the buildings with increasing street canyon width.

Xia and Leung (2001a) carried out a numerical study to investigate the effect of building configuration on pollutant dispersion near the ground. The first contained numerical comparison with the experimental results of Gerdes and Olivari (1999); the

second contained simulations with urban roughness placed upstream of the test section; the third contained simulations with roughness located at both upstream and downstream positions. A significant proportion of the pollutant within the test section was able to move upstream because of the blockage by higher buildings downstream. The thin wall (3% of gap width) in the simulations offered low resistance to upstream transport of pollutants. In further tests, Xia and Leung (2001a) reported that reverse flow at the top of buildings is reduced when the building width is increased to 30% of the gap width. The separation zone at the top of the roughness elements prevented flow entrainment into the upstream street canyon. It was also found that high buildings upstream or downstream increased the ventilation rate and reduced local pollutant concentration levels under certain configurations. However, two or more vortices stacked vertically in a street canyon were found to prevent pollutant from escaping the canyon when the height of the upstream and downstream buildings of street canyons was increased.

In a second paper, Xia and Leung (2001b) adopted a Lagrangian correction scheme to study the distribution of pollutant concentration in street canyons under different configurations. Lagrangian models calculate the trajectory of the "centre" of an individual puff (cloud of pollutant) while diffusion independently spreads the pollutant away from the puff centre. All the numerical simulations were conducted in a two dimensional digital tunnel 2m in length and .34m high. Again Xia and Leung (2001b) found that increasing building width prevented pollutant particles in the downstream canyon from moving upstream. In the case of multiple identical buildings with the same height, a stable vortex was formed in the street canyon resulting in higher pollutant concentration at the leeward side of the upstream building and lower pollutant concentration at the windward side of the downstream building.

Belcher et al. (2003) developed a general approach to how a deep boundary layer adjusts as flow moves over and through a canopy of roughness elements. Three stages of adjustment were reported. First the effects of the drag and finite volume of the canopy elements decelerates the air parcels; the associated pressure gradient decelerates the flow within an impact region upwind of the canopy. Secondly in an adjustment region downwind of the leading edge of the canopy, the flow within the canopy decelerates substantially until it comes into a local balance between downward transport of momentum by turbulent stresses and removal of momentum by the drag of the canopy elements.

Briggs et al (2001) discussed the theoretical aspects of the vertical entrainment velocity, w_e, and showed that, for a plume released near ground level, w_e is approximately proportional to another scaling velocity , the friction velocity u_τ. The proportionality factor, referred to as the entrainment coefficient, α, was found from the relation $w_e = \alpha u_\tau$ and is an important parameter in transport and dispersion models for releases of hazardous gases. This approach is useful particularly when considering passive and dense gas releases.

Britter et al.(2003) reported the growth of plumes. The vertical spread of the plume was characterised by the vertical entrainment velocity, w_e, which describes the effective "velocity" with which ambient air becomes part of the plume. This approach is often used in operational models for the dispersion of hazardous, particularly dense gases. He found that short range vertical dispersion of a passive contaminant in a neutrally stratified turbulent boundary can be characterised by the entrainment coefficient, $\alpha = \frac{w_e}{u_\tau} = .65 \pm 0.05$.

1.6 Objectives

The foregoing literature review presents a summary of current knowledge regarding turbulent boundary layers over smooth and rough surfaces. In order to clearly understand the connection between turbulence production and its effect on diffusion, an investigation will be described, involving tests over a regular array of two dimensional roughness elements spaced at different pitches. For this purpose tests have been performed in a water flume over sharp edge, 5mm square brass slats. The objective for the first series of tests was to investigate the relationship between small scale turbulent eddies formed between the elements of a two-dimensional bed roughness and the intermittent turbulent structure of the boundary layer. In the second series of tests the investigation focussed on the turbulence characteristics at and above roof-level and aimed to predict the behaviour of street pollution from dye dispersion by adopting different roughness conditions upstream and at a test street canyon. The main test programme focused on the influence of different bed geometry on the interaction of turbulent eddies generated at the wall, the turbulence structure of the boundary layer, and the dispersion of dye contaminants into the boundary layer. Spacing of the slats was varied for different tests to produce isolated, k-type bed roughness, skimming (d-type) flow, and wake interference flow for transitional roughness. Flow visualisation techniques were used to confirm the gross flow features and dispersion behaviour for the different roughness element spacing. The dispersion behaviour of the dye tracer inside the cavity was investigated using three injectors which allowed dye to be introduced into the flow at specific locations.

Other tests investigated the flow interaction at roof level, inside the cavity formed between the roughness elements, and above the roof level, for different bed geometry conditions including the variation in gap distance and height of the roughness

elements. A comparison has been made between a simulated urban environment with the model street canyon and its influence on the bed friction velocity. This study is important in relation to architecture and the management of environmental pollution.

CHAPTER 2

THEORY OF TURBULENCE

This chapter is devoted to a description of turbulent shear flows which include boundary layers, atmospheric boundary layers, flow past a flat plate and internal flows. When flow passes over a rough surface, vortices start extracting energy from the mean shear flow by a vortex stretching mechanism. It is important to understand this process and its relationship with turbulence production, diffusion and dispersion in order to identify the relevant and parametric range for the experiments.

2.1 Fully developed turbulence

Turbulence phenomena have been studied over decades. The developments can be divided into several stages. Between 1925 and 1930, Prandtl and Karman focussed on the qualitative analysis of turbulence which is now viewed as the classical theory. Between 1935 and 1937, Taylor published his statistical theory of isotropic turbulence resulting from air flow measurements made using hotwire anemometry. Kolmogorov (1941) went further and proposed a statistical theory of locally isotropic turbulence which led to the now well known -5/3 power law for the spectrum of shear-flow turbulence. Since 1945, additional equations for closure of the Reynolds equation have been proposed on the premise that quantities such as turbulent kinetic energy are transported by turbulent motion. Hence additional differential equations can be obtained from the equations of motion. They also contain some empirical constants. These equations, together with Reynolds equations, are then solved numerically. These are known as turbulence models.

Turbulence can be classified according to its structure and its spatial variation. It is said to be stationary or idealized when the flow shows a regular repeatable pattern, i.e. it has a distinct constant periodicity in time and space (Hinze,1959). The assumption of

fluctuations (in velocity, temperature, and pressure) being superimposed on stationary flow is central to the development of analytical techniques and models. Important exceptions are LES (Large Eddy Simulation) where the averaging time interval is finite, smoothing out the rapid fluctuations. On the other hand, in DNS (Direct Numerical Simulation), no averaging is performed. LES was introduced in 1970 with the multi equation models of turbulence. In this technique, modelling is narrowed down to the unresolved Sub-Grid Scale (SGS) eddies whose behaviour is close to isotropic. DNS refers to the solution of full Navier-Stokes and continuity equations without a model. This approach is capable of resolving a given flow field down to the smallest Kolmogorov turbulence length and time scales.

Turbulence is said to be isotropic if the individual velocity fluctuations are equal in all the three (x,z,y) directions. In other words, at a point $\overline{u'^2} = \overline{w'^2} = \overline{v'^2}$. True isotropy is hypothetical in practice because of the distorting influence of solid boundaries. Turbulence behind a grid of orthogonal bars in a wind or water tunnel has been shown to be closely isotropic i.e. turbulent shear stresses are zero because there is no mean velocity gradient. In other situations, when mean velocity shows a gradient, turbulence will be nonisotropic or anisotropic. For example, boundary layer flow or flow in a pipe near the boundary is anisotropic since $\overline{u'^2} \neq \overline{w'^2} \neq \overline{v'^2}$ at a point. A flow field where turbulence levels do not change from one point to another is called homogeneous. Thus, if one consider two points a and b in the flow field, and if $(\overline{u'^2})_a = (\overline{u'^2})_b$, $(\overline{w'^2})_a = (\overline{w'^2})_b$, $(\overline{v'^2})_a = (\overline{v'^2})_b$, the turbulence will be homogeneous. Flow downstream of a grid in a wind tunnel is isotropic homogeneous, if the mean flow has a constant velocity in the streamwise direction and a negligible lateral velocity gradient throughout the flow field. As a consequence turbulence dies out rather slowly, so that

homogeneity can be assumed. In all other situations where the mean velocity shows a varying gradient (turbulent boundary layer), the turbulence is anisotropic and non homogeneous.

In a turbulent flow, the large scale motions are affected by shear in the time averaged velocity. Vortex stretching breaks down the eddies into progressively by smaller scale motions and directional bias caused by the mean flow is gradually lost. The smallest eddies that are eventually dissipated to heat will be essentially isotropic in character. Thus a well developed turbulent field will be locally isotropic at the scale of the smallest eddies. Viscosity does not play a direct role in the dynamics of these scales. This will be true if the Reynolds number is high enough so that an "inertial-range" can develop. One can therefore argue that large scale turbulence interactions responsible for momentum transport are unaffected by the fluid viscosity. The fine scale motions responsible for viscous dissipation are to a large extent independent of the nature of mean flow as well as the large scale eddies. Garde (1994) reported about the fully developed turbulence is a turbulence which is free to develop without imposed constraints. The possible constraints are boundaries, external forces, or viscosity. The structure of flows of a scale comparable with the dimensions of the domain where the fluid evolves cannot deserve to be categorized as "developed" because the planetary scales are imposed by the constraints i.e as the rotation, thermal stratification and finite size of the planet. So no real turbulent flow, even at high Reynolds number, can be fully developed in the large energetic scales. The small three-dimensional turbulent scales of the earth's atmosphere and oceans are fully developed.

2.2 Navier-Stokes Equations

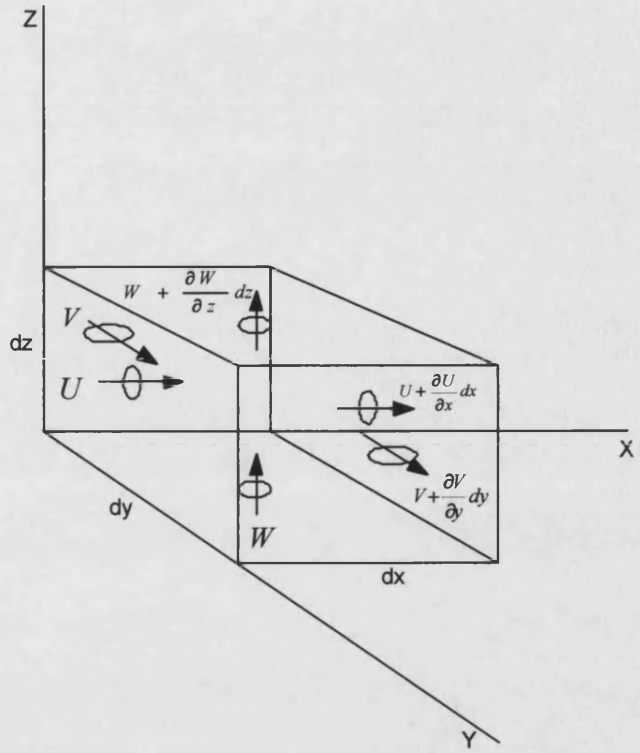

Figure 2.1 Fixed infinitesimal "Control Volume"

In the case of ideal fluid flow, laminar flow is analysed by using the equations of motion which are mathematical statements of Newton's Second law of motion. According to Newton's Second Law, the summation of the components of all external forces acting on a fluid in a given direction is equal to the mass of fluid multiplied by the total acceleration in that direction. Considering a unit volume of incompressible fluid, the equations of motion in a Cartesian coordinate system take the following form, when pressure, gravity and viscous forces control the motion.

$$\rho\left[\frac{\partial U}{\partial t}+U\frac{\partial U}{\partial x}+W\frac{\partial U}{\partial z}+V\frac{\partial U}{\partial y}\right]=X-\frac{\partial P}{\partial x}+\mu\left[\frac{\partial^2 U}{\partial x^2}+\frac{\partial^2 U}{\partial z^2}+\frac{\partial^2 U}{\partial y^2}\right]$$

$$\rho\left[\frac{\partial W}{\partial t}+U\frac{\partial W}{\partial x}+W\frac{\partial W}{\partial z}+V\frac{\partial W}{\partial y}\right]=Z-\frac{\partial P}{\partial z}+\mu\left[\frac{\partial^2 W}{\partial x^2}+\frac{\partial^2 W}{\partial z^2}+\frac{\partial^2 W}{\partial y^2}\right]$$

$$\rho\left[\frac{\partial V}{\partial t}+U\frac{\partial V}{\partial x}+W\frac{\partial V}{\partial z}+V\frac{\partial V}{\partial y}\right]=Y-\frac{\partial P}{\partial y}+\mu\left[\frac{\partial^2 V}{\partial x^2}+\frac{\partial^2 V}{\partial z^2}+\frac{\partial^2 V}{\partial y^2}\right] \qquad (2.1)$$

These equations were first derived independently by Navier and Stokes; hence they are commonly known as Navier-Stokes equations. Here ρ and μ are the mass density and the dynamic viscosity of the fluid, respectively. U,W, *and* V are the components of the velocity in x, z, and y directions, respectively. P is the pressure and X, Z, Y are the components of body force per unit volume in the three directions shown in figure 2.1. The term in the bracket on the left hand side represents the total acceleration in a given direction, which consists of local acceleration ($\frac{\partial U}{\partial t}$ etc.) due to unsteadiness of the flow, and the convective acceleration ($U\frac{\partial U}{\partial x}+W\frac{\partial U}{\partial z}+V\frac{\partial U}{\partial y}$,etc) which is due to the non-uniformity of flow. On the right hand side, the last term in the bracket represents the viscous forces per unit volume arising out of the components of shear stresses and additional normal stresses induced due to the presence of viscosity.

Considering two dimensional boundary layer flows of an incompressible fluid over a flat plate with a streamwise pressure gradient (i.e. free stream velocity Uo changing in the direction of flow), Prandtl showed that the terms $\mu\frac{\partial^2 U}{\partial x^2}, U\frac{\partial W}{\partial x}, \frac{\partial W}{\partial t}, \frac{\partial W}{\partial z}, \mu\frac{\partial^2 W}{\partial x^2}$ *and* $\mu\frac{\partial^2 W}{\partial z^2}$ are much smaller than the other terms in Eq. 2.1 and, hence they can be neglected. The resulting equations known as boundary layer equations are

$$\rho\left(\frac{\partial U}{\partial t}+U\frac{\partial U}{\partial x}+W\frac{\partial U}{\partial z}\right)=-\frac{\partial P}{\partial x}+\mu\frac{\partial^2 U}{\partial z^2} \tag{2.2}$$

$$0=-\frac{\partial P}{\partial z} \tag{2.3}$$

The corresponding form of the Continuity equation is

$$\frac{\partial U}{\partial x}+\frac{\partial W}{\partial z}=0 \tag{2.4}$$

With the retention of the term $\mu\frac{\partial^2 U}{\partial z^2}$, the order of the differential equation is not changed and, hence, for two dimensional flow the boundary conditions $U = W = 0$ *at* $z = 0$ will be satisfied. The other boundary condition is that, when $z = \infty, u = U_o$

Considering Navier Stokes equations and the continuity equation for two dimensional steady flow of an incompressible fluid, and substituting $U = u + u', W = w + w', V = v'$, and $P = p + p'$, the boundary layer equations obtained are

$$u\frac{\partial u}{\partial x} + w\frac{\partial u}{\partial z} + \frac{\partial \overline{u'^2}}{\partial x} + \frac{\partial \overline{u'w'}}{\partial z} = -\frac{1}{\rho}\frac{\partial p}{\partial x} + \upsilon\frac{\partial^2 u}{\partial z^2} \tag{2.5}$$

$$\frac{\partial \overline{w'^2}}{\partial z} = -\frac{1}{\rho}\frac{\partial p}{\partial z} \tag{2.6}$$

$$\frac{\partial u}{\partial x} + \frac{\partial w}{dz} = 0 \tag{2.7}$$

The boundary conditions to be satisfied are

$$at\ z = 0,\ u = w = 0,\ u' = w' = v' = 0$$

$$at\ z \to D,\ u = U_o(x) \tag{2.8}$$

where D is the depth of flow and U_o is the free stream velocity which varies with x in the presence of $\partial\overline{p}/\partial x$. Integration of Eq. 2.6 yields

$$\overline{w'^2} = -\frac{\overline{p}}{\rho} + C_1$$

where the constant of integration C_1 can be obtained from the condition that at $z \geq \delta, \overline{w'^2} = 0$ and , hence p is equal to the outside pressure p_o.

Therefore,

$$\frac{p}{\rho}=\frac{p_o}{\rho}-\overline{w'^2} \tag{2.9}$$

Obtaining $\partial p/\partial x$ from Eq. 2.9 and substituting it in Eq.2.5 gives

$$u\frac{\partial u}{\partial x}+w\frac{\partial u}{\partial z}=-\frac{1}{\rho}\frac{\partial p_o}{\partial x}+\frac{\partial}{\partial z}(-\overline{u'w'}+\upsilon\frac{\partial u}{\partial z})-\frac{\partial}{\partial x}(\overline{w'^2}-\overline{u'^2}) \tag{2.10}$$

This equation can be compared with Eq. 2.2 for a laminar boundary layer. They differ in the additional terms involving derivatives of Reynolds stresses $\overline{u'w'}, \overline{w'^2}$ *and* $\overline{u'^2}$. It can be seen from Equ. 2.10 that total effective mean shear stress (τ) and boundary shear stress (τ_o) are given by

$$\frac{\tau}{\rho}=(-\overline{u'w'}+\upsilon\frac{\partial u}{\partial z})=\frac{\tau_o}{\rho}(1-z/D) \tag{2.11}$$

At the boundary i.e. z=0, Eq. (2.11) gives:

$$\tau_o=\mu(\frac{\partial u}{\partial z})_{z=0} \tag{2.12}$$

The boundary shear stress can be determined by Eq. 2.11 and 2.12 with the help of sufficiently accurate measurement techniques. The boundary shear stresses in the present experiments are determined by Eq.(2.11). The total stress Equ. (2.11) can also help in comparing the general shape of the mean velocity profile in a laminar and turbulent boundary layer. Turbulent boundary layers will contribute large Reynolds stresses in comparison to the laminar boundary layer. As a consequence the velocity gradient will be small compared with its value in a laminar flow of the same boundary stress.

The viscous stress component $\mu\frac{du}{dz}$ represents the shear stress due to molecular transfer of momentum across planes parallel to the bed and the additional term $-\rho\overline{u'w'}$ represents the Reynolds shear stress introduced by the momentum transfer due to the

mixing action of the turbulence across the shear layer. The Reynolds stress is of major importance in turbulent flow, since work is done by the mean flow to shear the fluid against its retarding action. The work rate, (locally expressed as $-\rho\overline{u'w'}(\frac{du}{dz})$ is the primary source of the energy required to sustain the process of turbulence generation.

From Eq. 2.11, the shear stress can be expressed as;

$$\tau = \tau_o(1-(z/D)) \tag{2.13}$$

Eq. 2.13 gives an approximate but direct relationship between the total effective shear stress τ, bed shear stress τ_o, and Reynolds stress $\overline{u'w'}$. Therefore, the bed shear stress is an important parameter in the scaling of turbulent flow. This can be expressed in terms of bed shear velocity, u_τ, as follows;

$$u_\tau = \sqrt{\frac{\tau_o}{\rho}} \tag{2.14}$$

NOTE: This parameter u_τ is not a physically real velocity. It has the dimensions of velocity, but its magnitude is determined by the wall shear stress. u_τ shows the coupling relationship between the flow and surface roughness.

Since the time of Boussinesq (1877) attempts have been made to obtain additional equations which, together with the Reynolds equation of motion in their original or simplified form, would allow calculation of mean turbulent flows. Prandtl (1925) simulated momentum exchange on a macro scale in a way equivalent to that of molecular motion of a gas in an effort to explain the mixing phenomenon induced by turbulence in water, and thus he established the mixing length theory for turbulent flow. The theory assumes the fluid to consist of discrete elements which can move through a short distance termed the mixing length, l, while conserving their original momentum.

The theory however does rely on some basic assumptions which tend to be physically unrealistic.

Since the turbulent fluid motion has a great ability for diffusion, it can transport with it any quantity associated with the turbulent fluid motion, such as momentum, vorticity, heat, suspended matter. etc. These transport processes were modelled by Karman, Taylor and Reichardt. Essentially these studies provided a relationship which is empirical between the mean flow characteristics such as velocity gradient and turbulent stresses. These theories are known as phenomenological or semi-empirical theories of turbulence, and do not necessarily describe the mechanism underlying the transport process correctly. However, since some of them give useful and practical empirical relations their importance cannot be underestimated.

Another approach which can possibly be employed is based upon dimensional reasoning, flow similarity and scaling. The turbulent motion is governed by velocity scales which are based on the determination of the scales of length and time. An upper limit on the scale of turbulence is imposed by the physical dimensions of the flow conduit within which the fluid is contained, whereas the lower limit is imposed by the molecular diffusion effect of viscosity.

Townsend's (1976) 'Principle of Reynolds Number Similarity' essentially states that for geometrically similar turbulent flows, the large scale and structure of the turbulence is dynamically similar, provided that the Reynolds number is sufficiently high for the flow to be fully turbulent. Flow immediately adjacent to a solid boundary will be dominated by viscosity and, therefore, Reynolds number dependent. Townsend (1976) argued that influence of the wall on the outer flow is limited to the transfer of shear stress from the wall. Then the relative motion in the fully turbulent region of the flow depends on the wall stresses (irrespective of how they are generated) and on the geometry of the flow

conduit. For simple flow geometries, it can therefore be deduced that the properties of the turbulent motion at a point in space and time are generally determined by local environmental conditions. The time scales of the turbulent motion must be small compared to the time scale of any environmental change such as boundary layer. Tennekes and Lumley (1972) point out, however, that for flows in parallel wall conduits (e.g. pipes and water flumes) boundary layer growth is limited by the geometry of the conduit. Flow in a long conduit becomes fully developed, after which the velocity distribution becomes independent of the downstream distance as was the case in the present investigation.

For a wide open channel flow the appropriate boundary conditions which control and scale the large scale structures in the outer flow regions are defined by the flow geometry. It is characterised by the depth D, and by work by the mean flow against the wall shear stress which represents turbulence energy generation process. The wall shear stress is defined in terms of the shear velocity, u_τ.

Townsend (13) has used the Reynolds number similarity principle to formulate expressions for the quantities appearing in the equations of motion (Eq. 2.5 and 2.6). These take the following form

$$U = u_t + u_o f(z/D) \tag{2.15}$$

$$\overline{u'w'} = u_o{}^2 g(z/D) \tag{2.16}$$

where u_o is the velocity scale of the motion since the flow is independent of viscosity in the outer region, u_o can be put equal to the shear velocity u_τ. The velocity u_t is an arbitrary translation velocity of the whole flow. In general its ratio to the velocity scale u_τ, is a function of Reynolds number and roughness characteristics. For pipes and closed channels u_t can be taken as the centre axis velocity, and for flat plate boundary layers as

the free stream velocity. In the case of open channel flow the maximum translation velocity U_m occurs in the vicinity of the flow surface.

From the discussion above, the standard form of the similarity velocity distribution is therefore

$$U = U_m + u_\tau f(z/D) \tag{2.17}$$

The function f(z/D) is independent of boundary roughness effects. This is more commonly written in the form shown in Eq. 2.18 below and known as the "Velocity Defect Law". This law is used to correlate mean velocities in the outer region of pipe and flat plate boundary flows.

$$\frac{U - U_m}{U_\tau} = f'(z/D) \tag{2.18}$$

The expression for Reynolds stress becomes:

$$\overline{u'w'} = U_\tau{}^2 g(z/D) \tag{2.19}$$

The velocity defect law described above applies to the outer region of a turbulent flow, where the nature of the wall does not impose any direct effect upon the flow. However, as the wall is approached the boundary layer has significant influence on the flow. Townsend's (1976) argues that:

"In channel flow and indeed in most turbulent flows with solid boundaries, there is a region adjacent to the wall within which the total shear stress is nearly constant and whose motion is determined to a considerable extent by the shear stresses and by the nature of the wall".

The presence of the wall influences the scale of turbulence in the near wall region. At a given wall distance, z, the length scale of typical turbulent eddies within the wall region will be of maximum order of magnitude z. As a result, the turbulent structure in this region will become independent of the outer region length scale, D, and will be

determined by local parameters. Townsend (1976) refers to this argument as the "Principle of Wall Similarity".

Townsend (1976) further explained the effect of turbulent flow in reducing the mean velocity gradients over the greater part of the channel and concentrating the large velocity gradients in the region close to the wall. The wall layer (inner layer) shear stresses increased as a consequence. Within this wall layer, also referred to as the constant stress layer, the shear stresses can be closely equated to the wall stress. The wall zone also forms the principal source of turbulent energy production expressed by $-\rho\overline{u'w'}(\partial u/\partial z)$ where $-\rho\overline{u'w'}$ is the Reynolds stress and $\partial u/\partial z$ is the mean velocity gradient.

In the case of a smooth wall, the constraints acting upon the flow field are the wall shear stress characterised by the shear velocity, u_τ, the kinematic viscosity ,υ, and the wall distance, z, where:

$$z^+ = \frac{u_\tau z}{\upsilon} \tag{2.20}$$

The principle of wall similarity states that in the wall region the flow is independent of the outer flow parameters. The flow close to a smooth wall can only be dependent upon the wall shear and the wall distance, giving rise to the following relationships:

$$u = u_\tau f(z^+) \tag{2.21}$$

This is more commonly written as follows:

$$\frac{u}{u_\tau} = f(z^+) \tag{2.22}$$

This latter relationship is known as the "Law of the Wall".

In the region very close to the smooth wall, extending out to a z^+ value of approximately 6, there is a layer known as the viscous sublayer, where the viscous

stresses are totally dominant and Reynolds stresses are negligible. In this region integration of the viscous shear stress with respect to z yields the following relationship:

$$\frac{u}{u_\tau} = \frac{u_\tau z}{\upsilon} \tag{2.23}$$

This viscous sublayer was at one time described as the laminar sub-layer, but work for example by Kline et al (1967) and Grass (1971) revealed the existence of what has been termed a "streaky structure" within the sublayer. The non-laminar properties displayed by this structure consequently led to the revised description of the layer.

So far two regions of a turbulent boundary layer have been identified. The outer region, described by the velocity defect law and scaling on the flow depth, D and the wall region described by the law of the wall and scaling on the viscous length scale, υ/u_τ. At low Reynolds number these scales would converge to a similar magnitude; but, in the case of high Reynolds number flows, where wall and outer regions of the flow will scale on parameters of significantly different magnitudes. There is no sharp dividing line within the flow, where one law abruptly ceases and another begins. This overlap region is known as the logarithmic region, although Tennekes and Lumley (1972) refer to it as the "inertial sublayer" due to the characteristics of the mean velocity profile in this region.

Townsend's (1972) argument to derive the velocity distribution in the logarithmic region was based on wall similarity and balance between production and dissipation of turbulent energy. Clauser (1956) considered a simultaneous application of the outer flow defect law and the inner law of the wall. This procedure is outlined below.

Simultaneous application of equations 2.18 and 2.23 can be rewritten as follows:

$$u = u_m + u_\tau f(z/D) \tag{2.24}$$

and

$$u = u_\tau f_1(u_\tau z/\upsilon) \tag{2.25}$$

The simultaneous solution of these equations involves equivalence between a multiplicative and an additive term. Clauser therefore observed that a logarithmic function would be necessary to effect a solution i.e.

$$\frac{u-u_m}{u_\tau} = A\ln(z/D)+B \tag{2.26}$$

and

$$\frac{u}{u_\tau} = A\ln(\frac{zu_\tau}{\upsilon})+C \tag{2.27}$$

In the latter equation, applying to the wall layer, the constant, A, is conventionally expressed as $1/\kappa$ where κ is Karman's constant. The other dimensionless constant, C, defines the velocity slip in the viscous sublayer immediately adjacent to the boundary. C can be expressed as:

$$C = -\frac{1}{\kappa}\ln(\frac{z_o u_\tau}{\upsilon}) \tag{2.28}$$

Eq. 2.28 therefore becomes:

$$\frac{u}{u_\tau} = \frac{1}{\kappa}\ln(z/z_o) \tag{2.29}$$

where z_o is a characteristic length scale, which for a smooth boundary is proportional to the viscous length scale. For a rough surface z_o is a measure of how efficiently momentum can be transferred into the ground at given wind speed.

2.3 The effect of surface roughness

The existence of a rough boundary imposes a further influence on the flow in the wall region. The projection of elements of roughness into the flow give rise to form and pressure drag effects. By this mechanism the boundary shear stress can be transmitted to the flow. The flow in the wall layer becomes a function of z/k, where k is the mean

roughness element height. The magnitude of the Reynolds number which determines the scale appropriate to the wall flow is defined as Roughness Reynolds number, k^+,

$$k^+ = \frac{ku_\tau}{\upsilon} \tag{2.30}$$

Colebrook and White (1937), describing the experiments of Nikuradse, outlined three possible roughness conditions

a) The hydraulically smooth regime

The roughness elements are submerged in the viscous sublayer. The flow is therefore unable to sense any presence of the roughness effect and the boundary is described as hydrodynamically or aerodynamically smooth i.e. $k^+ < k_s^+$. Nikuradse performed experiments on sand roughened pipes and found the value for k_s^+ to be 7. Goldstein (1936) interpreted the value $k_s^+ = 7$ as the onset value of periodic vortex shedding behind the roughness elements. As we know that surface friction is dependent on the surface roughness geometry, the limit of k_s^+ was recommended as 15 for uniform sphere roughness and 2.25 for sand grain roughness.

b) The transitionally rough regime

This intermediate regime was found when roughness elements are slightly thicker than the viscous sublayer. As a result the viscous shear stress and roughness form drag both contribute to the transmission of bed shear stress i.e. $k_s^+ \le k^+ \le k_r^+$. Bandyopadhyay (1987) proposed that the upper limit for k_r^+ for which the transitional rough regime occurs is a function of the aspect ratios of the roughness elements. Stuart (1983) and Mansour (1992) reported the upper limit of $k_r^+ = 60 \, and \, 70$ respectively.

c) The rough regime

A fully rough regime was found when the viscous effects are negligible i.e. $k^+ > k_r^+$. Schlichting (1979) quotes $k_r^+ = 70$, Ligrani and Moffat (1986) recommended $k_r^+ = 90$ for sand grain roughness. The difference in the upper limits of k_r^+ is due to the roughness geometry.

Grass et al. (1991) demonstrated that vortex structures are also present in the turbulent boundary layers over rough walls and they are linked to the bursting events. 3D vortices nested together with the largest scale commensurate with the total boundary layer thickness and the smallest scale with the relevant wall length scale z_o.

Mansour (1992) investigated the effect of roughness on the spanwise distribution and scaling of bursting events in a turbulent boundary layer. Experiments were reported for four flow rates and five bed conditions, which included a smooth and four rough (ranging from transitional to fully rough). The conclusions from these tests demonstrated that spanwise flow structure adjacent to a rough boundary exhibits a well defined cross-flow wavelength reflecting the spanwise scale of the vertical structures driving the bursting process. This is directly proportional to the roughness length scale under fully rough conditions. The spanwise wavelength was also observed to increase in scale with increasing wall distance.

In this chapter an attempt has been made to explain the basic theory of the turbulent boundary layer. There are numerous questions remaining unanswered in the description of turbulence theory. The next chapter will describe the experimental programme carried during the research study to better understand turbulence behaviour in relation to effective boundary roughness and pollution dispersion.

CHAPTER 3

EXPERIMENTAL APPARATUS

The experimental programme was divided into two investigations, one carried in year 1 and the other in year 2 of the research study. The project in year 1 focussed on the characteristics of turbulence generated above a rough boundary made up of 2-d roughness elements spaced at various regular intervals; the second phase focussed on the boundary layer turbulence over various bed roughness geometries simulating an urban environment.

Experiments for both the projects were carried out in a uni-directional water flume, illustrated in Figure 3.1, in the Pat Kemp Fluid Mechanics laboratory in the Department of Civil and Environmental Engineering at University College London. The same flume was previously used by Stuart (1984) and Mansour (1992) for their tests. The flume is specifically designed to be independent of general laboratory water supply and draws water from an independent collection tank.

Figure 3.2 shows a general arrangement of the water flume. The water flume was itself 0.495m wide, and 6.2m long, and consisted of a smooth marine plywood bed with plate glass sidewalls, supported on a substantial cast iron main girder structure. The channel was supported by a pivot at the inlet end, and a scissor jack near the outlet. The slope of the channel was adjustable and therefore the connection between the turbulence damper inlet tank and the flow channel was made of a flexible rubber joint faired over by sliding brass plates. The water level in the channel was controlled by an adjustable weir at the downstream end. The weir was able to slide vertically, operated by a hand wheel. Downstream of the weir, an inclined flat plate was provided for the calm entry of water into the collection tank to avoid air entrapment.

The water was re-circulated from the $3m^3$ collection tank by a 17.5 H.P. electric pump. The flow was then passed to the $0.85m^3$ capacity constant head tank. The water level was maintained at a constant level with the aid of an adjustable weir controlled with a float. The float responded to the changes in the water level. The water for the flow channel was drawn from the constant head tank, and controlled through an orifice plate flow meter. The control valve was set to fully open to avoid the jetting effect into the inlet tank. The purpose of the turbulence damper inlet tank was to damp the large turbulent motions in the flow. It was located between the constant head tank and the flow channel. The flow from the control valve was channelled to the perforated T-shaped pipe system to avoid the development of any unnecessary turbulence. The water was passed through marbles 20mm in thickness laid across the damper tank. Finally the fine scale turbulence in the flow was filtered by four sets of stainless steel wire mesh of 0.5mm aperture. The water then entered the channel through an inlet fairing, designed to produce very low inlet turbulence intensity levels of the order of 5%.

3.1 Levelling the glass plate at the bed of flow channel

The original marine ply bed of the channel was found to have unacceptable undulations of the order of 5mm in height over the channel width. Instead, a false bed made of glass was laid down, supported by sleepers placed on the marine ply wood in such a way that its upper surface was level. Initially measurements of the bed level were taken over a grid of points, by filling the channel with water to a depth of approximately 10mm, to provide a perfectly horizontal surface. The water depth at each point was subsequently measured using a micrometer pointer gauge. The relative bed levels were mapped out and discrepancies of $\pm 3.5mm$ from the mean were observed. Using these values, bed sleepers were individually made for each point,

using sandwiches of plastic shims measured with micrometer as shown in figure 3.3. The flat glass plate, 0.495m wide and 4m long was then laid in the flume over the levelled sleepers to ensure a horizontal bed (0.5mm). Water over the flat bed was prevented from flowing down between the edge of the flat bed and the vertical walls by inserting rubber tubing, 3mm diameter, along the glass plate on both sides. The tubing was flexible and found very effective in achieving the objective.

3.2 Bed roughness

Bed roughness in the context of the current experiments is the laboratory scale elements laid on the false glass bed perpendicular to the mean flow direction, effectively spanning the width of the water flume. The interaction between surface (bed) roughness and the flow has a significant effect on the friction velocity, roughness length scale, flow pattern and the dispersion of dyes and pollutants. The present study is undertaken to investigate these effects for the two types of 2-d roughness elements described below.

3.2.1 Idealised 2-d roughness

Two-dimensional roughness elements were chosen for their simplicity and reproducibility, and because of the well documented nature of this type of roughness. (Perry and Joubert (1963), Perry et al. (1969), Stuart (1984)).

At the inlet of the channel, a specially designed brass leading edge was followed by a fairing which led to a short length (75mm) of smooth bed. In order to avoid the formation of a local separation bubble, the surface of this smooth bed section was laid flush with the crest height of the roughness elements. This arrangement is illustrated diagrammatically in figure 3.4.

The roughness elements were formed from lengths of 5mm (nominal) square brass bar. The roughness elements extended over the entire 4m length of the levelled glass

bed. The elements were systematically spaced from 2.5mm to 955mm gap distance between the elements (see Table 3.1). This gave a spacing/element height (s/k) ratio from 0.5 to 191, to identify the changes in turbulence behaviour caused by the variation in gap distance. A wide range of bed conditions was investigated starting from hydraulically smooth, transitional, rough, and back to a smooth surface with occasional roughness elements by varying s/k ratio. The boundaries (s/k) proposed by Oke (1987) to define different flow regimes were also investigated. Each series of tests started from densely packed slats. Alternate slats were then removed to produce other rough bed conditions.

A schematic of the 2-d slat type roughness geometry is shown in figure 3.5. It can be seen from the figure that three injectors were incorporated to allow dye to be introduced into the flow at specific locations and thereby to facilitate the study of dispersion. The injectors at positions *c1*, *u1* and *d1* were drilled inside the slat. The dye from injector *c1* was introduced from the centre of the top of the slat as shown in figure 3.6. The other two injectors were placed opposite to each other. Injector *d1* was drilled to release dye inside the cavity in the direction of flow at 1.5mm above the glass plate. The injector *u1* released dye against the flow direction at 1.5mm from the glass plate inside the cavity forming between the slats.

Attachment of the roughness elements to the glass plate was by means of double sided adhesive tape, and particular attention was paid to the cleanliness of the mating surfaces in order to ensure firm adhesion. A random sample of 15 elements was taken and measured using a micrometer. The precise dimensions of the roughness elements were found to be: $5.05mm$ square, $\pm.025mm$. The actual dimensions of the elements therefore showed a mean variation of $\pm 1.25\%$ over the nominal $5mm$ dimensions.

Table 3.1 Idealised 2-d bed roughness geometry (see also figure 3.5 and 3.6)

Test	Gap distance (mm) s	s/k	Remarks Roughness Geometry:
1	Smooth	∞	$k = 5mm$ and $b = 5mm$ (Fig. 3.5)
2	2.50	0.5	
3	5.00	1	
4	7.50	1.5	
5	10.00	2	
6	12.50	2.5	
7	15.00	3	
8	20.00	4	
9	25.00	5	
10	30.00	6	
11	35.00	7	
12	45.00	9	
13	55.00	11	
14	75.00	15	
15	95.00	19	
16	115.00	23	
17	155.00	31	
18	235.00	47	
19	315.00	63	
20	475.00	95	
21	955.00	191	

The thickness of the double sided tape used to secure the elements to the bed was measured as $0.20mm$. The mean effective roughness element dimensions were therefore found to be $5.05mm$ (width) × $5.20mm$ (height). For the purpose of describing ratios in round numbers, calculations were based on $5mm \times 5mm$ square section.

3.2.2 Idealised 2-d simulated urban environment

The form of roughness adoption for the present tests was first introduced by Perry et al. (1969) for his classical work on rough wall turbulent boundary layers. This simple slat type roughness placed on a flat bed, simulated the roughness of a typical prototype urban surface and, acting as a momentum sink, established a profile of Reynolds stress through the layer which in turn controlled the mean velocity profile and turbulence characteristics. In order to have a fully developed turbulent boundary

layer, spaced 100mm apart face to face. Each element was 10mm thick and 20mm high placed normal to the flow direction across the channel width as shown in figure 3.7.

The test region was set 3.38m from the channel inlet. Roughness elements made of acrylic plate, 3mm in thickness, were inserted across the flat plate. Slots were made in the flat plate for holding the 3mm thick roughness elements using a cutter (figure 3.8). The term isolated street canyon is used here to refer to a cavity formed by two roughness elements. Additional roughness elements (30mm high) upstream of the test section simulated an urban environment. The test section was tested under eight different geometries, as an isolated street canyon and in the presence of additional upstream roughness (Table 3.2). Sketches of the street canyon geometry are shown in figures 3.9 to 3.12. The legend at the test section for elements of the same height and tall elements is shown in figure 3.13.

The velocity profile in the hydraulic flume was initially measured using a propeller meter. The free stream velocity in the water channel was set to 0.156m/sec. The Reynolds number based on height of roughness element ($R_k = \frac{uH_u}{\nu}$) was 4680 based on the height of the upstream elements (30mm).

The overflow weir head was set to 171mm from the marine ply wood. The flow depth was 191mm from the top of the flat bed at the test sections. The flow velocity profile was measured from the top of the flat plate up to 155mm at test sections.

Table 3.2 Idealised 2-d local bed roughness geometry simulating an urban environment

Series	Test	Element height (mm)				Gap distances (mm)			Remarks
		B_u	B_d	H_u	H_d	P_u	P_d	s	
1	1			30	30			30	Model street canyon (Figure 3.9)
	2			30	30			45	Model street canyon (Figure 3.9)
	3			30	50			30	Model street canyon (Figure 3.10)
	4			30	50			45	Model street canyon (Figure 3.10)
2	5	30	30	30	30	60	60	30	Urban approach roughness upstream of model street canyon (Figure 3.11)
	6	30	30	30	30	60	60	45	Urban approach roughness upstream of model street canyon (Figure 3.11)
	7	30	30	30	50	60	60	30	Urban approach roughness upstream of model street canyon (Figure 3.12)
	8	30	30	30	50	60	60	45	Urban approach roughness upstream of model street canyon (Figure 3.12)

3.3 Assessment of dispersion

Flow visualization is one of the most effective tools in flow analysis. It has been crucial for improving the understanding of complex turbulent fluid flows and offers a significant insight into the phenomena occurring in such flows. A classical example is the experiments by Osborne Reynolds (1883) in which the dye injection method was used to show the transition from a laminar flow to turbulent flow in a pipe. A more recent example is the investigation by Head and Bandyophadyay (1981) in which smoke injection was used to show the existence of hairpin vortices in a turbulent boundary layer. For the present research study the techniques for flow visualisation are described below.

3.3.1 Laser light sheet

A dilute fluorescent dye solution appears almost transparent under normal lighting, but when illuminated with a laser light source of an appropriate wave length the dye fluoresces strongly. This unique property motivated us to visualize the flow pattern in the cavity between roughness elements by illuminating it with a thin sheet of laser light. Some of the common fluorescent dyes used in flow visualization include Fluorescein, Rhodamine-B and Rhodamine-6G. When illuminated with the output of an argon ion laser, fluorescein displays a green colour, while Rhodamine-B and Rhodamine-6G give dark red and yellow colours respectively.

For the present investigation we have used Rhodamine-6G for analysing the flow pattern between the cavities. The dye is introduced midway across the channel by inserting a hypodermic through the brass slat. The dye was fed from a syringe pump fixed into a mechanical device to get a consistent flow rate in the test section shown (figure 3.14).

3.3.2 Colour dye

Dye visualization is perhaps the easiest way to study the flow behaviour and interaction. The choice of colour is a matter of personal preference. The following colour dyes were used to produce better contrast to visualize the flow interaction for the simulated urban environment.

- Methyl Orange (orange) used upstream with the additional large scale roughness. The dye was introduced through a stainless steel tube, 1.5mm internal diameter, through gravity feed (figure 3.15). The probe was located at a distance of 180mm from the upstream element of the test cavity. The dye exit velocity was kept equal to the local flow velocity in order to minimize the disturbance to the flow field.

- Potassium permanganate crystals (pink) were used inside the test cavity.
- Nigrosine crystals (black), water soluble were used downstream of the test cavity.

3.3.3 Styrocell particles

A slit of light was projected from above for visualization of styrocell particles, as shown in figure 3.16. The lamp in the projector operated at 24volts and produced 250Watts power. The styrocell particles are spherical in shape. They have a specific gravity around 1.03 which is quite close to neutrally buoyant. These particles are opaque and reflect light evenly. In the present tests, styrocell particles were used to better understand the reverse flow at roof level (see figure 6.4).

3.3.4 Camera

Sony PCG-NV105 Windows based laptop was used for acquisition of video. The laptop has got 30 Gigabyte of hard disk storage. Sony TRV-80 camcorder has both the facilities to be operated on a wide angle and normal lens. The camcorder and related software were connected to the laptop to facilitate quantitative data analysis. This allowed downloading the 25fps digital video images directly on to the PC. Matlab was used for graphical and image analysis software, it was possible to manipulate and analyze the video film data frame by frame to obtain data for visualization.

3.4 Laser Doppler velocimetry

3.4.1 General information

Laser Doppler velocimetry (LDV) is a non-intrusive technique which permits local instantaneous measurement of the velocity at a point in the flow. The LDV principle utilises the Doppler effect, e.g as waves from a given source proceed towards a certain point, they do so with increased frequency and alternatively as waves are moving away from that point, their frequency decreases. Laser Doppler velocimetry uses an extension

of this principle. Two or more light beams are intersected, so that interference fringes are formed. As a particle crosses these fringes, the intensity of light scattered varies at a rate directly proportional to the velocity of the particle. If the particles (seeding) are of the correct diameter so as not to interfere with the fringes, the right shape (spherical) and the right specific gravity, it is assumed that they follow the flow path of the local fluid and therefore represent the time varying local fluid velocity and acceleration.

A two-component TSI laser Doppler anemometer (LDA) was employed for quantitative measurements (figure 3.17). The system consisted of the laser head probe mounted on a fully automated traverse mechanism and linked to an INNOVA 70C-5 Watt Argon-ion laser through the optical unit and an optical fibre cable. The traverse could automatically move the laser probe to any position within a 800 mm x 800 mm x 800 mm measurement domain to a high degree of accuracy (±0.01mm). Two pairs of beams were emitted (green and blue). The LDA operated in backscatter mode and the signals were processed by a TSI IFA-655 signal processor with FIND software.

3.4.2 Laser probe

The probe was held by a special mounting device. Its vertical position was fixed, but the mount design allowed the probe to rotate in the vertical (z) axis in both directions. A PC-controlled traversing system, which was connected to the LDV PC software via the traversing system control box, was used to move the laser head to any point within the traverse's range. The PC-controlled traverse was mounted on a specially designed trolley which could be moved to any point of interest.

The wave length of laser incident light was 514.5nm. The lens of the probe was having a focal length of 363mm. For this lens beam-crossing half angle kappa was 3.97 degree. In this way the measurement volume diameter in streamwise direction was 90.5micron and length in horizontal direction was 1.31mm.

3.4.3 LDV signal processing

The IFA-655 is a digital signal processor that analyses the signals provided by the receiving optics of the LDA system. The signals produced by a laser Doppler anemometer occur in short bursts, at random time intervals (see TSI laser manual). As a particle passes through the centre of the laser measurement volume, the signal fluctuations become larger and then decay again. These fluctuations are not centred about zero because you cannot have a negative light intensity. As a consequence the fluctuating signal can be split into the following three components:

i) a high frequency part which contains the Doppler signal whose frequency is proportional to the fluid velocity being measured,

ii) a low frequency part called the pedestal, and

iii) wide-band noise.

The signal processor distinguishes the signal burst from the noise, based purely on signal-to-noise ratio (SNR). To measure the Doppler frequency accurately, bandpass filters are used in order to separate the pedestal from the Doppler signal and reduce the background noise as much as possible. A high-pass filter eliminates the pedestal while a low-pass filter reduces the amplitude of the wide-band or background noise. The signal is then passed through a fixed gain amplifier to amplify the signal and is then fed into a burst detector and sampler. The burst detector detects the signal bursts based on signal-to-noise ratio and also provides approximate frequency and start and end of burst information. The sampler samples and stores the bursts with 256 samples per burst. An autocorrelation is then performed on the stored burst which extracts Doppler frequency information. The velocity is then calculated and displayed using the FIND data analysis software which is provided with the LDV system.

3.4.4 Colorlink operation and Shift frequency

For low velocity and reversing flows, accurate LDV results can only be obtained by frequency shifting one of the two laser beams used to measure the flow velocity. The frequency shift was set to 100KHz to measure flow reversal between roughness elements in the water channel tests.

3.4.5 Laser Noise

Laser noise is an inherent problem in most LDV systems. As high a signal-to-noise ratio (SNR) as possible is generally sought and this can normally be achieved by ensuring that: adequate seeding is used; the laser is aligned properly and all lenses are clean; and that the correct shift frequencies and filter settings are chosen. A number of quick preliminary tests were, therefore, carried out to check what effect the above factors had on LDV noise and SNR.

The seeding used to improve signal quality and allow the LDV to take data readings was white-coloured "Titanium (IV) dioxide". It is insoluble in water and has a specific gravity of between 3.9 and 4.2. The reason for this variation is that the material comes in two different crystalline forms: Rutile (the more stable and dense) and Anatase. The manufacturer was uncertain to tell us form of crystal was used. The specific gravity of the optimally seeded fluid sample taken from the test section and that of drinking water was similar. Therefore seeding has negligible effect on the specific gravity of water.

The capacity of the uni-directional water flume and tanks was 5800 litres. The optimum performance in terms of data reading by LDV was observed when 8100 mg of Titanium (IV) dioxide were mixed with 21 litres of water in the seeding tank and gradually released at the channel inlet at the rate of free stream velocity (0.1m/sec) before LDV measurements.

An oscilloscope was utilised when using the LDV was used to monitor the amount of seeding passing through (and thus being read by) the vertical and horizontal beams of the LDV system. As long as the signal on the oscilloscope gave two crisp sinusoidal waves (one for the horizontal and one for the vertical beams), it could be assumed that the LDV was working correctly.

Additional noise may be caused by light scattered from small impurities collecting on the optical surfaces and channel walls. Cleaning the LDV lenses and the channel walls regularly helped to reduce this source of noise.

Laser Doppler velocimetry was used to measure a number of flow parameters (in 2-d only) including: the flow velocity (in the horizontal and vertical directions), the turbulence fluctuations (in the horizontal and vertical directions), and Reynolds stresses.

3.4.6 FIND settings

The TSI IFA655 processors were operated in "coincident mode" with time stamp to ensure that measurements of both velocities were made on the same particle. The data were sampled for 200 seconds duration at each point in the velocity profile. For spectrum analysis the time between each data point was set equal to the sampling interval of 10,000 microseconds, and 1800 seconds of data was recorded at each point. For all experiments, the frequency range was set from 30 KHz to 300 KHz on u and w components of the velocity. The random scatter due to experimental error was of the order of 4%.

3.4.7 Possible errors

The laser had to be inclined, at approximately 6°, on its stand in order to ensure readings could be made from the channel bed and that the laser beams could go inside the cavity between the roughness elements. This inevitably gave readings that were

not as accurate as those which would be given if the laser was set horizontally on its stand. However, such a small angle was regarded as having a negligible effect on the velocity readings taken by the LDV.

To determine the exact position of the channel bed, a knife edge spacer block of 26mm height was prepared. This allowed the recalibration of the laser control volume to the known bed level. However the final position was also checked with the oscilloscope by setting the LDV bursts at the critical location. This location was then confirmed by eye, wearing specially designed filtered goggles to check the control volume is away from the wall by its radius.

In this chapter two configurations of 2-d roughness have been described. These have been selected to help understand the turbulence behaviour and its effects on diffusion. The next chapter will focus on the different length scales chosen to provide an understanding of the turbulence and its effect on dispersion.

Figure.3.1 Photographic View of the turbulent flow channel and computer controlled 3-d laser traverse mounted on specially designed trolley

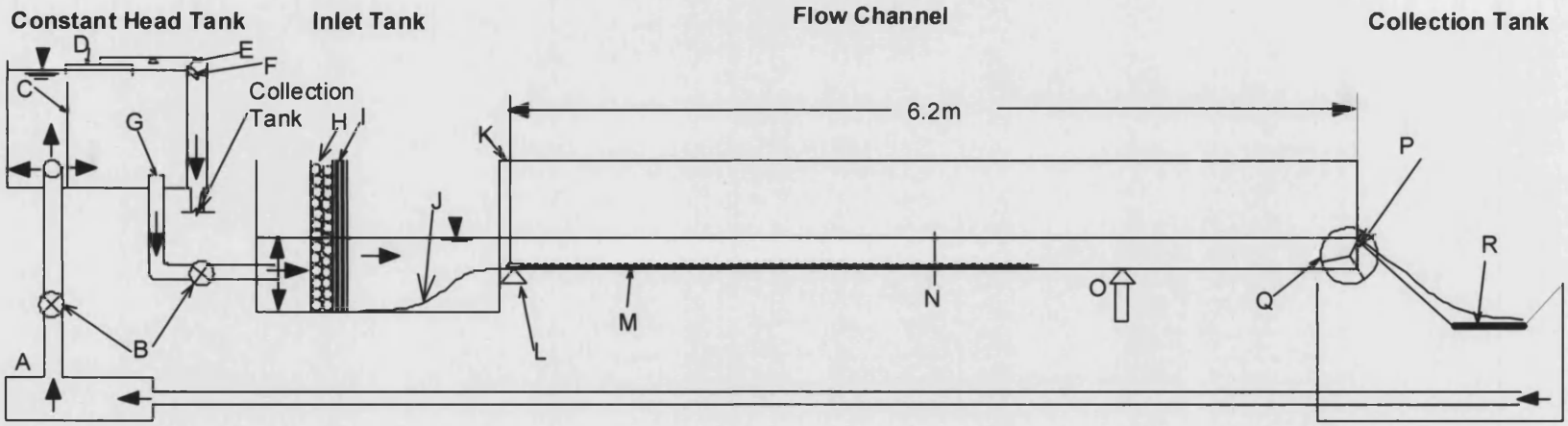

A Pump	G Orifice plate	M Bed roughness
B Control valves	H Marbles	N Test Section
C Wire gauze	I Wire screen	O Scissor Jack Pivot
D Float	J Inlet Fairing	P Discharge over weir
E Pivot	K Flexible Connection	Q Weir wheel
F Overflow	L Pivot	R Horsehair matting

Figure 3.2 General arrangement of flow channel

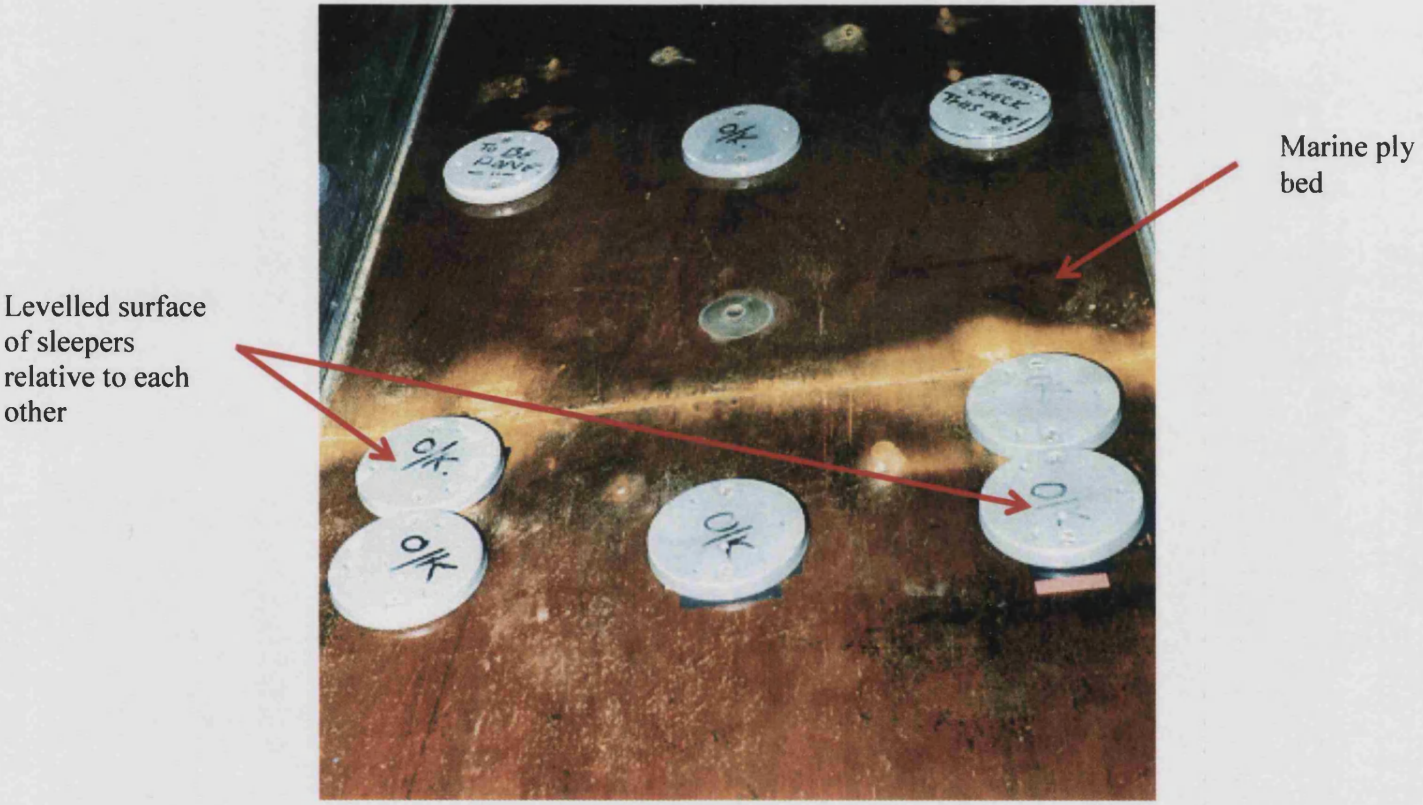

Figure 3.3 Sleepers over the marine ply bed to support flat glass plate

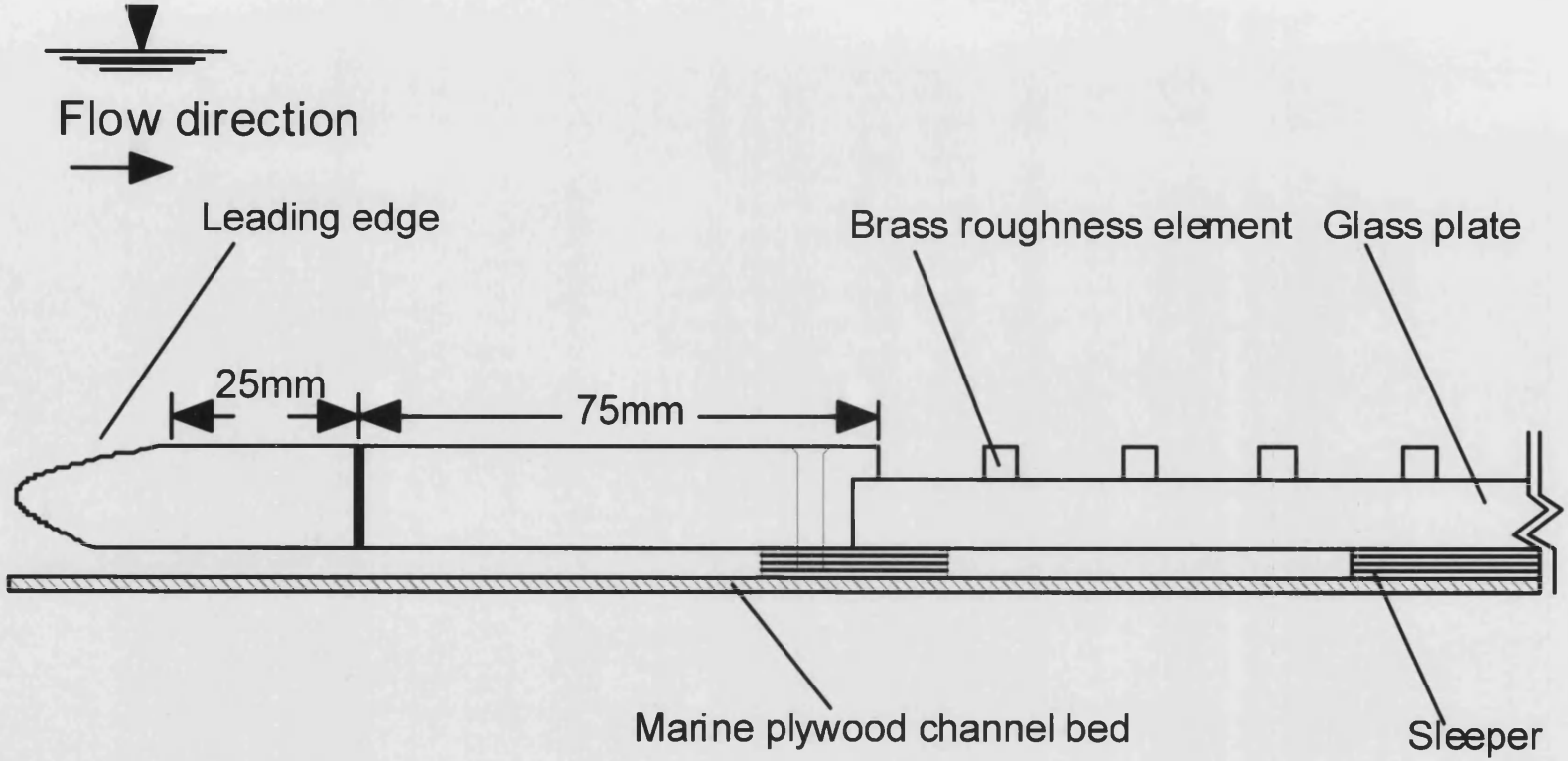

Figure 3.4 Leading edge

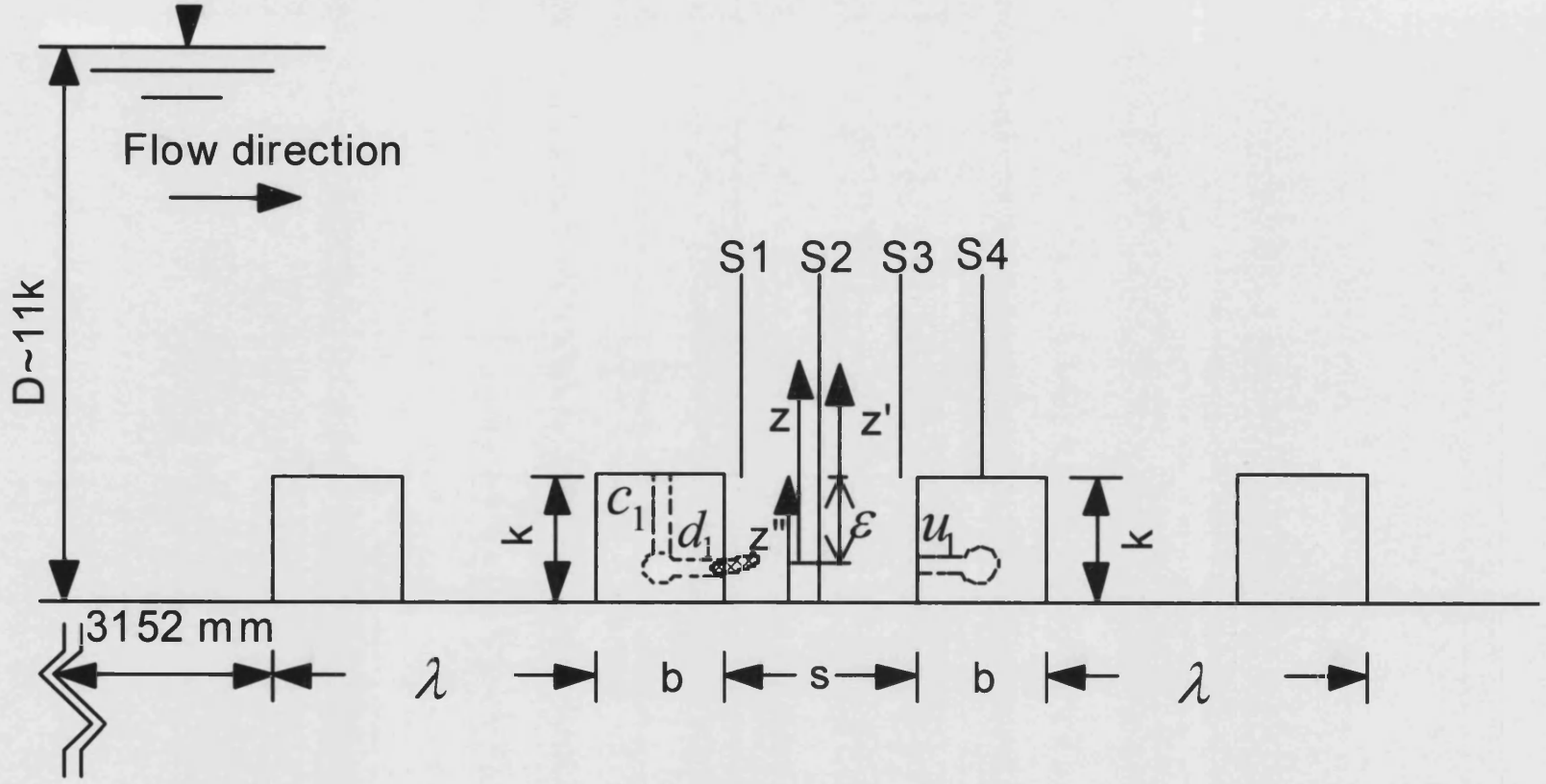

Figure 3.5 A schematic of the 2-d slat type roughness geometry showing the dye injection positions. S1 to S4 indicate velocity measurement locations

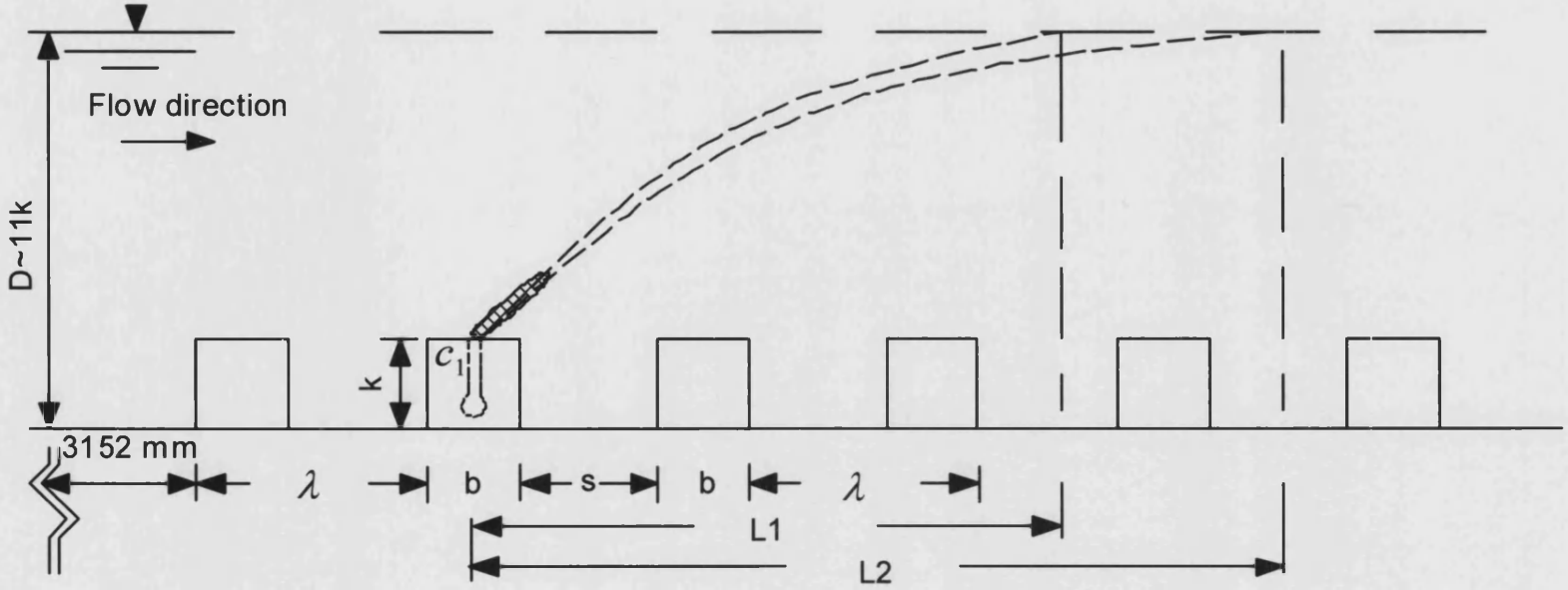

Figure 3.6 Plume growth rate in x-z (streamwise-vertical) plan from injector c1 at top of roughness

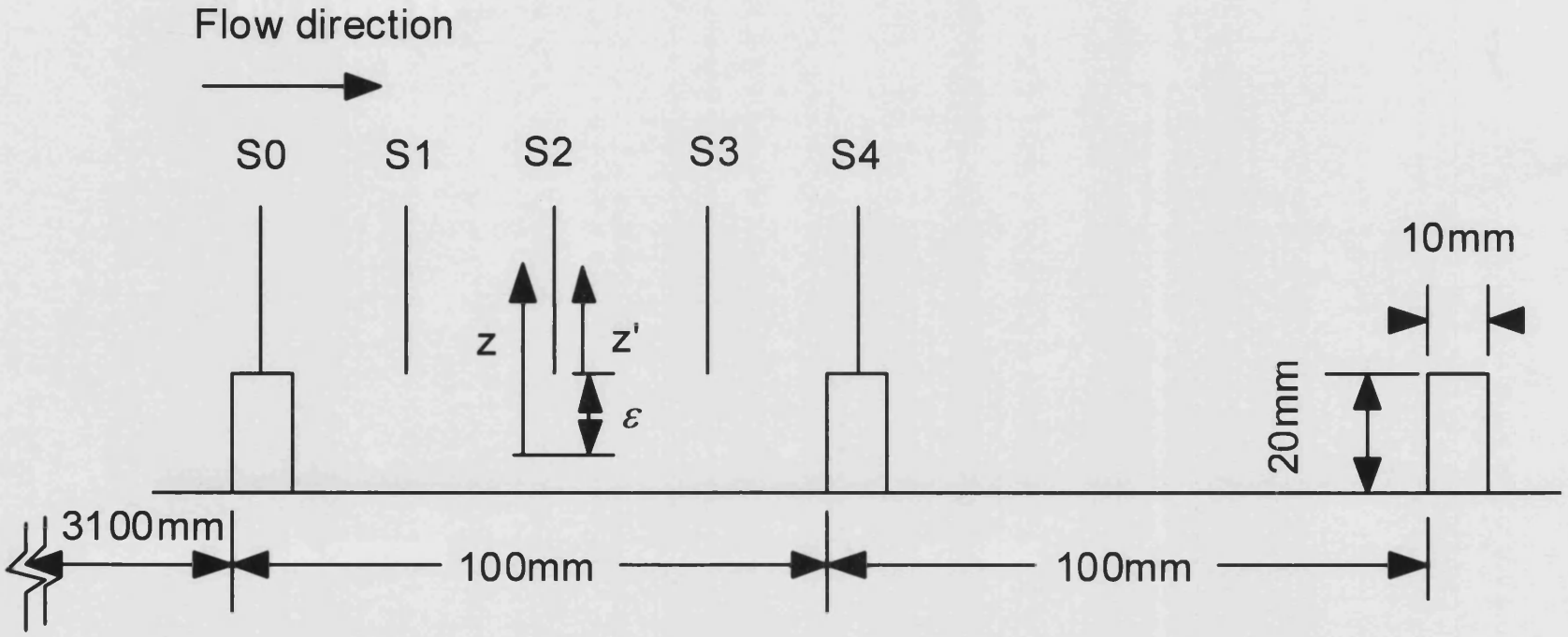

Figure 3.7 Uniform approach bed roughness placed upstream for all tests: S0 to S4 indicate the location of velocity profile measurements

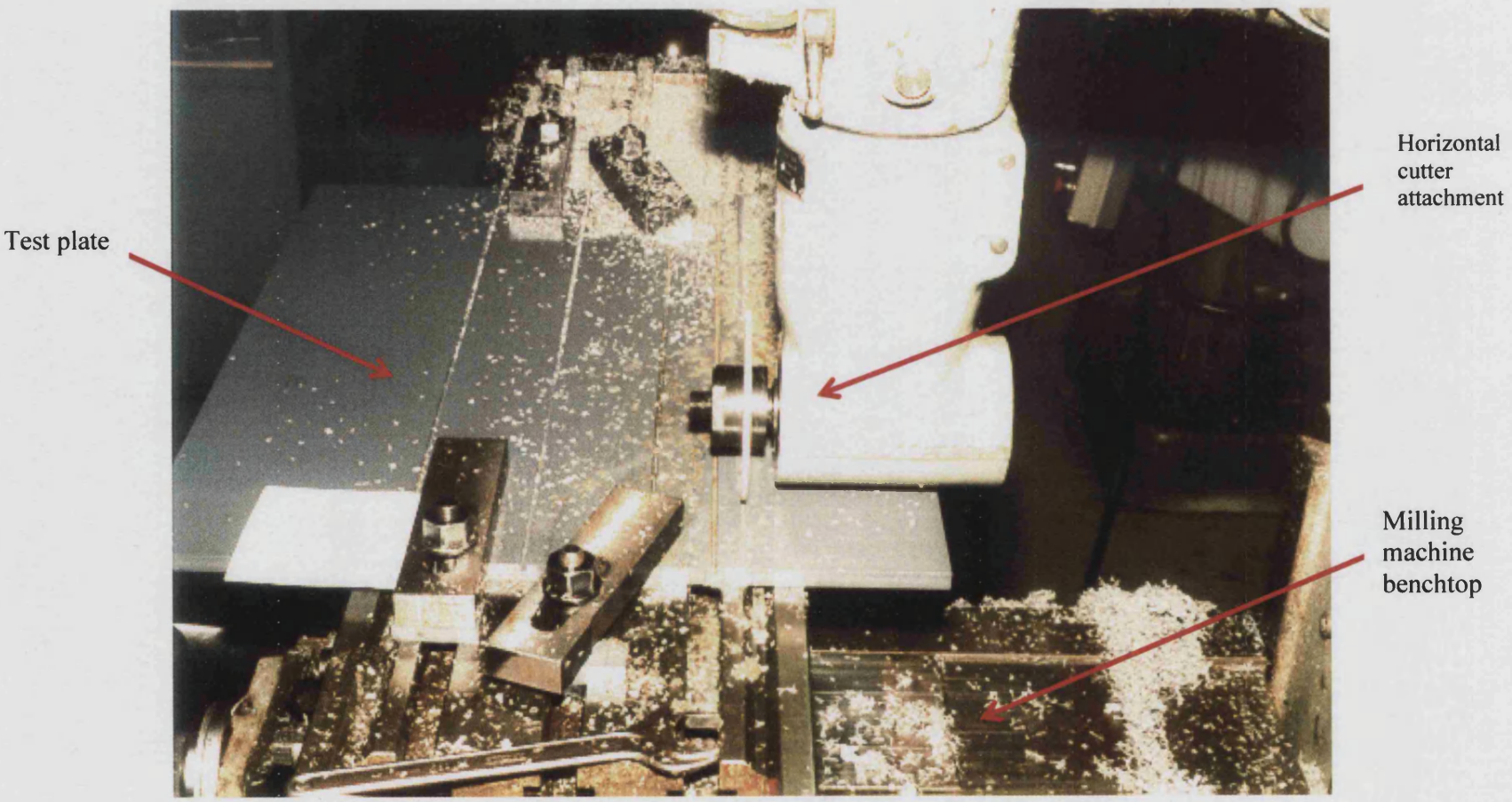

Figure 3.8 Slots cuts on flat plate for holding roughness elements

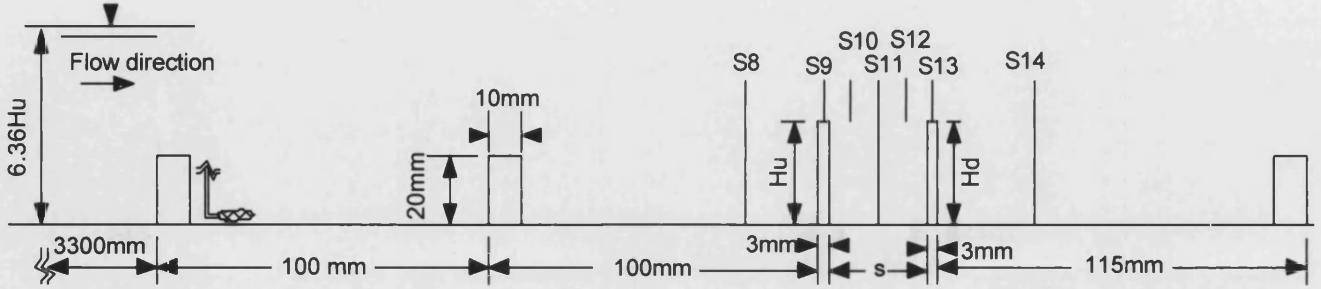

Figure 3.9 Model street canyon (Hu-s-Hd) geometry with uniform approach bed roughness upstream, S8 to S14 indicate velocity measurement locations, Tests 1 and 2

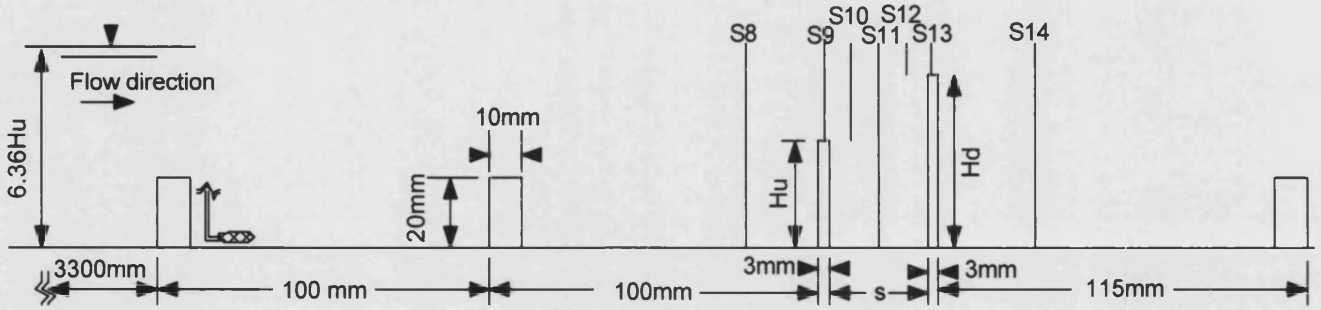

Figure 3.10 Model street canyon (Hu-s-Hd) geometry with uniform approach bed roughness upstream, S8 to S14 indicate velocity measurement locations, Tests 3 and 4

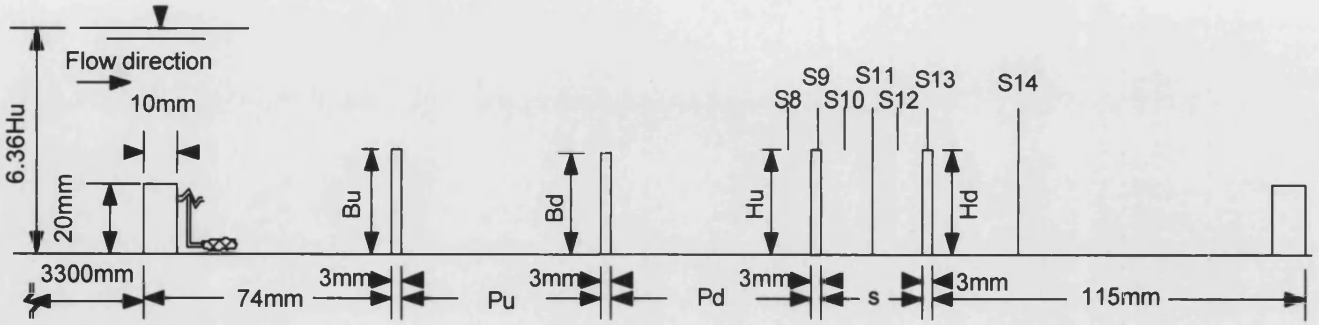

Figure 3.11 Uniform approach bed roughness with large scale roughness (Bu, Bd) immediately upstream of model street canyon, S8 to S14 indicate velocity measurement locations, Tests 5 and 6

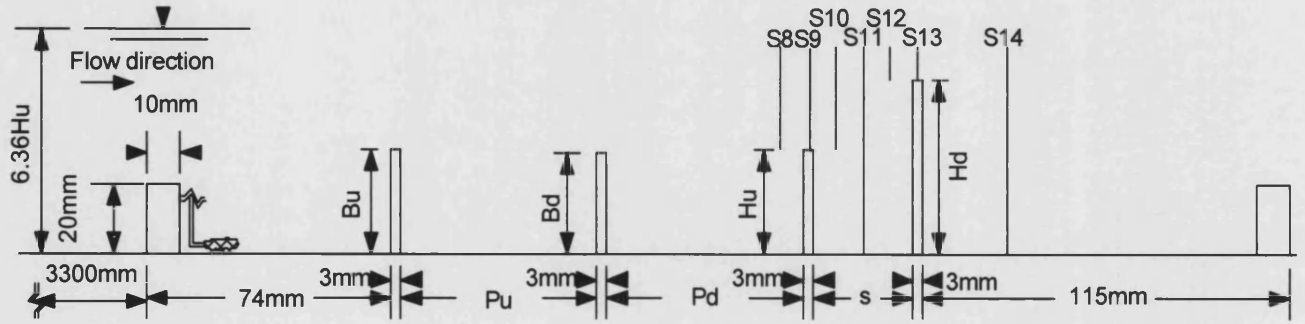

Figure 3.12 Uniform approach bed roughness with large scale roughness (Bu, Bd) immediately upstream of model street canyon with tall slat, S8 to S14 indicate velocity measurement locations, Tests 7 and 8

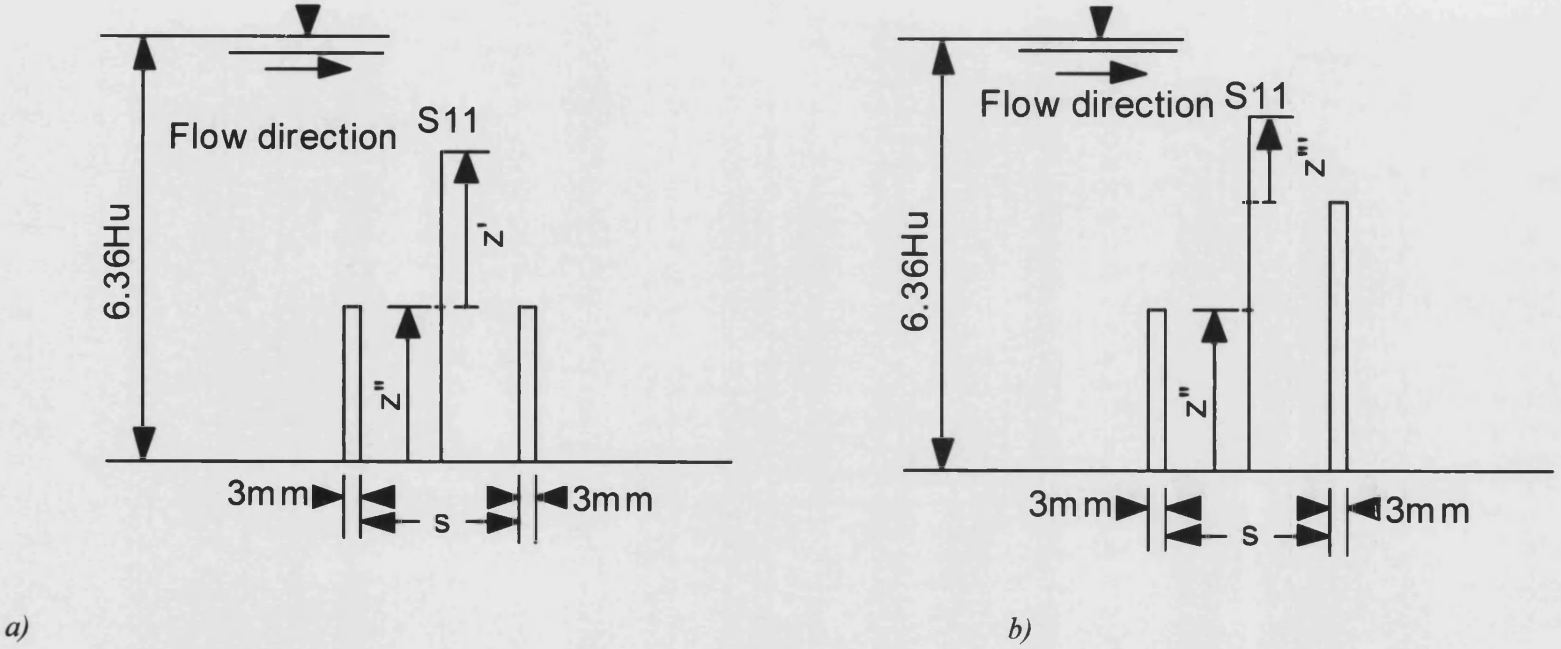

a) *b)*

Figure 3.13 Test section legend a) equal height b) tall slat

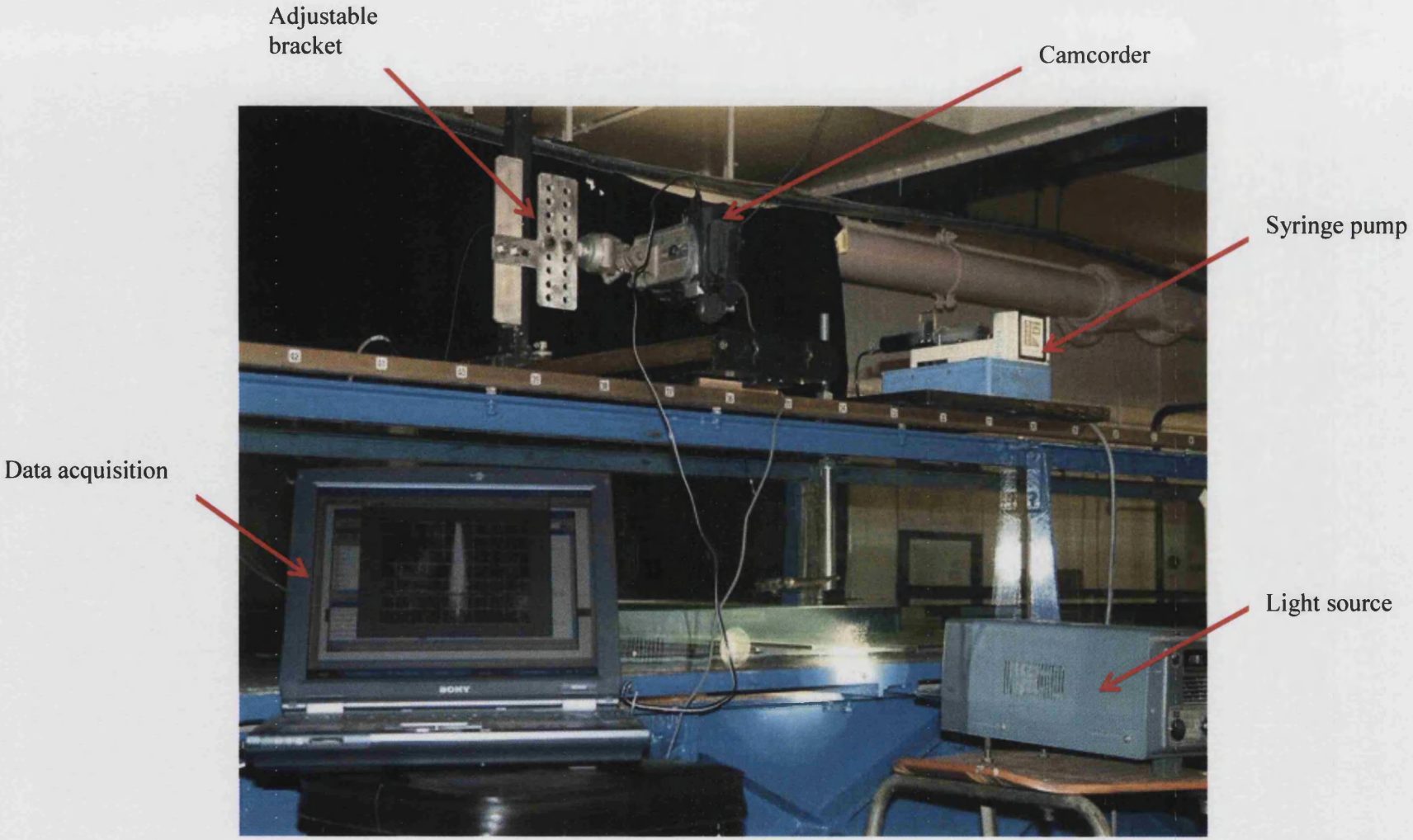

Figure 3.14 Data acquisition and controlled dye injection using mechanically driven syringe pump for systematically varied wall roughness

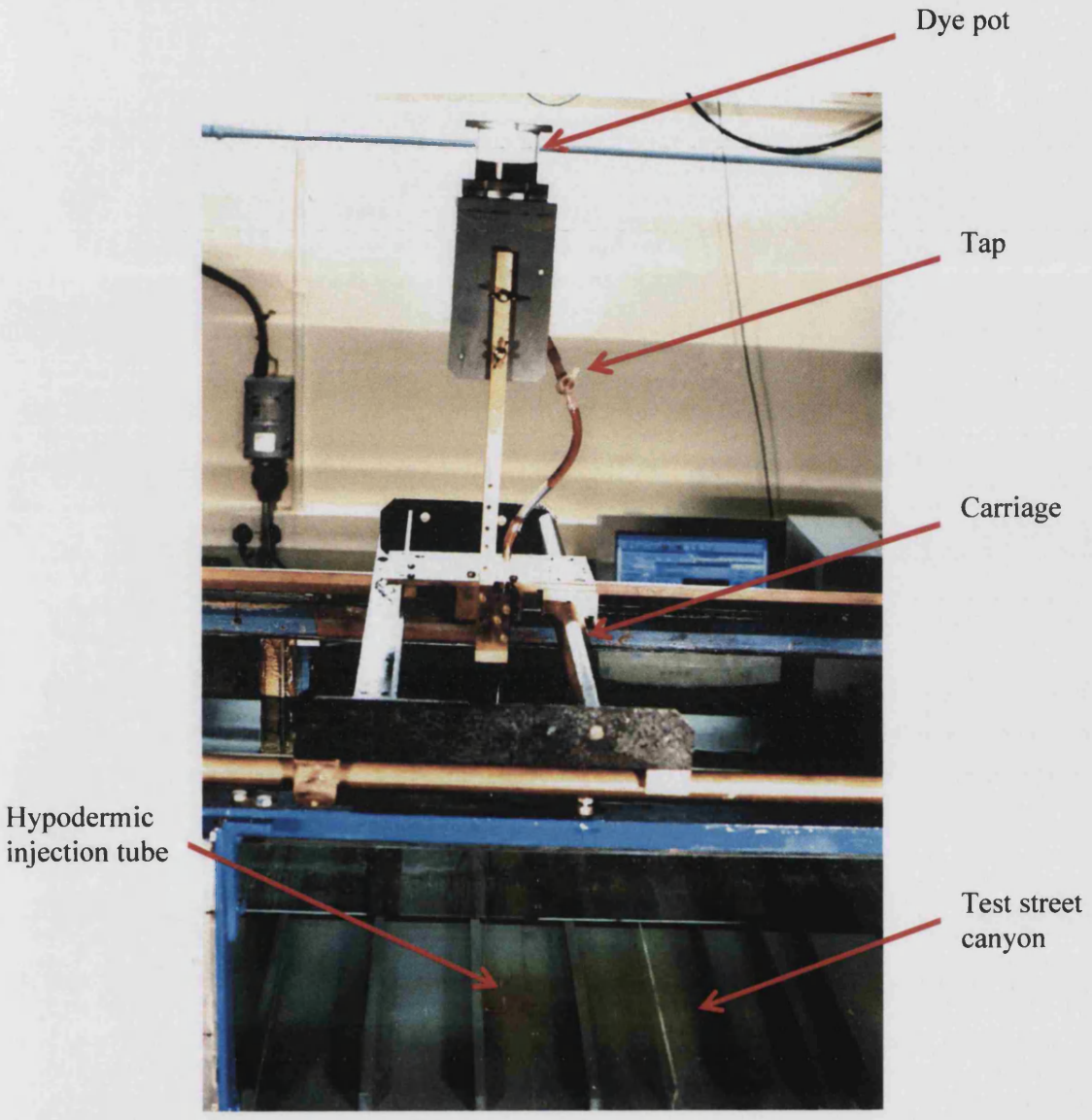

Figure 3.15 Dye injection gravity feed system (upstream of test street canyon) with sudden change in bed roughness geometry

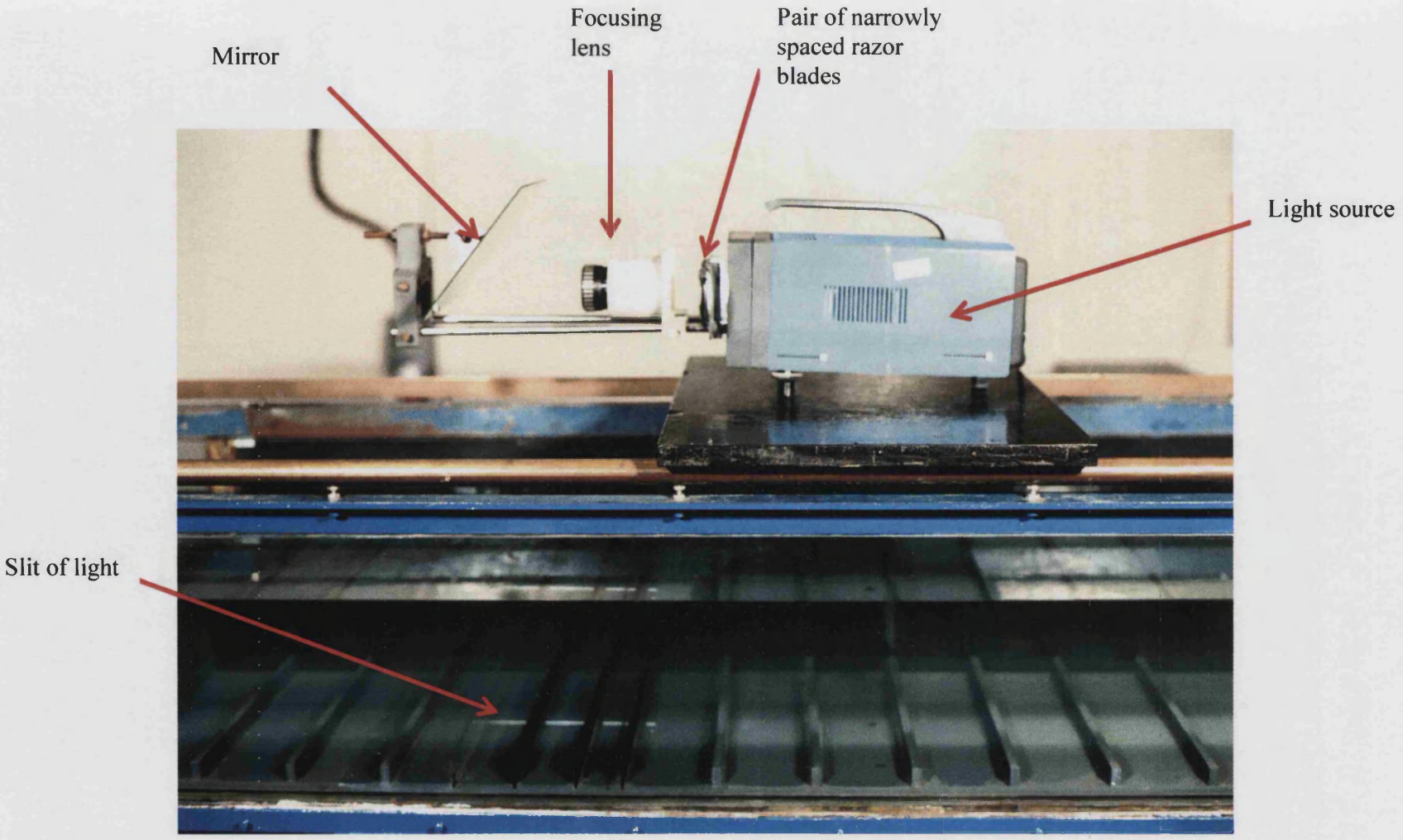

Figure 3.16 Light source designed to project a slit of light in x-z plane for styrocell particles visualisation

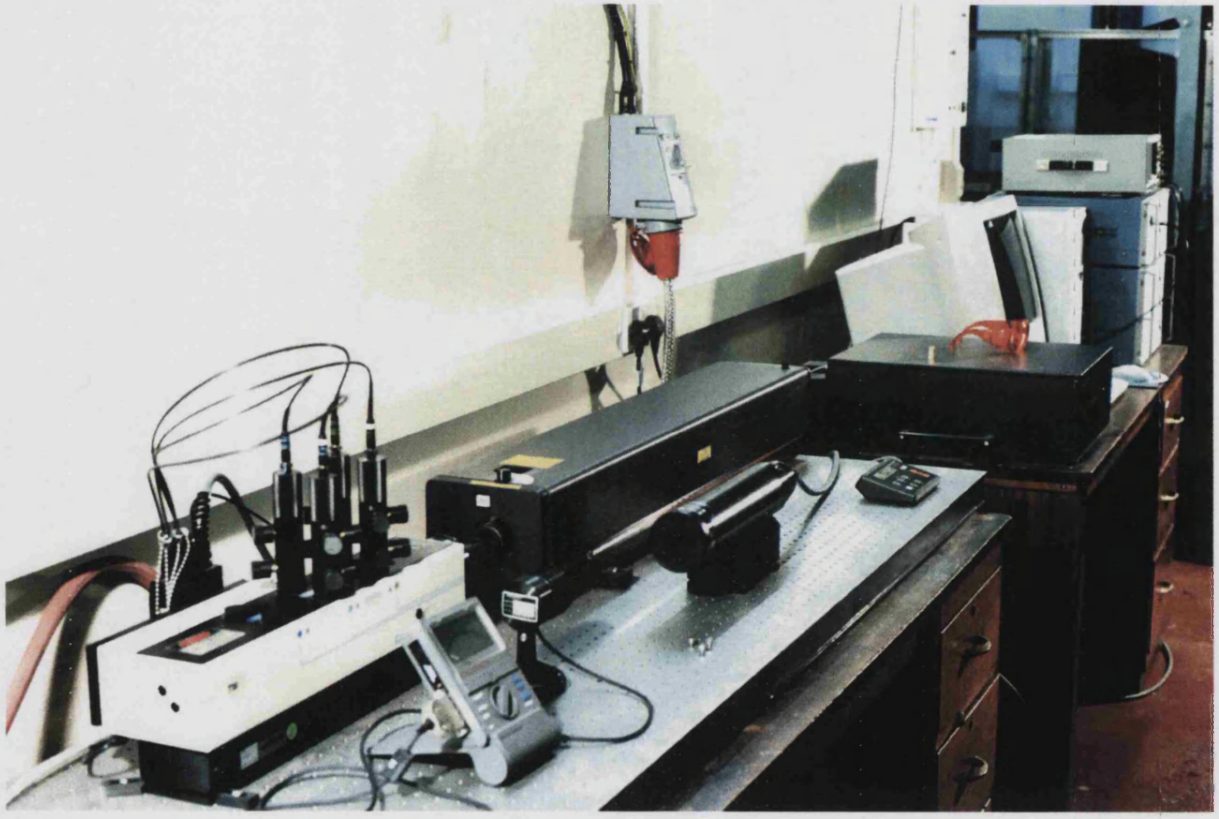

Figure 3.17 Argon-ion laser and PC control system

CHAPTER 4

EXPERIMENTAL PROCEDURES

This chapter is focused on the channel performance to achieve the desired objectives discussed in chapter 1. Before commencing the tests it was important to have fully developed two dimensional flow. From the measurement point of view it was important to identify the exact location of the laser control volume on the slat surface for accurate measurement of the velocity gradient. A standard procedure was adopted to locate the origin of the mean velocity profile of the flow over rough surface.

4.1 Secondary currents in open channel

The channel's performance in order to support the validity of the results needs to ensure the absence of arbitrary or non-general flow phenomena. The production of a uniform, two-dimensional flow has always been a problem in laboratory channels because of the existence of side walls. These side walls generate secondary flow superimposed on the primary flow.

The evidence for cellular structured secondary flow can be seen in the investigations on flows in closed rectangular ducts by Brundrett and Baines (1964) and Melling and Whitelaw (1976). These secondary flows result from gradients in the normal component of the Reynolds stress tensor. These Reynolds stress gradients produce small changes and gradients in the mean pressure field of the flow cross section in the corner regions of the flow, and exist in all turbulent flows of non-axi-symmetric cross section. Knight et al. (1982) proposed possible secondary flow cell patterns which can account for the variations in the flow field observed in open channel flows. Raven (1977) in his study considered the width to depth aspect ratio of 5 in his fully developed rectangular open

channel flume, and demonstrated a type of non-uniformity by measuring the cross channel velocity profiles. Stuart (1984) found that increasing the width to depth ratio from 5 to 10, has a significant impact on the uniformity of flow. Mansour (1992) reported flow patterns very similar to those discussed by Stuart (1984) in his assessment of the extent of the secondary flows in the same channel. Stuart concluded that the three-dimensionality of the flow was due to the corner generated secondary flow. To reach this conclusion, he measured the inlet flow in detail in order to eliminate the possibility of non-uniformity being caused by disturbances convecting through from the inlet of the channel. Inlet velocity profiles were measured indicating close uniformity except for very near the side wall sections. Stuart however reported that, from a comparison of the velocity profiles at the test section, the velocity field within 5-10 cm of the side walls is strongly influenced by those walls. With a large aspect ratio, the central region of the channel is sufficiently well-removed from the influence of the corners.

The present study used the same facility as Stuart (1984) and Mansour (1992) with channel width of 500mm as discussed in chapter 3. The flow depth was chosen to be approximately 55mm in order to keep a relatively low depth-to-width aspect ratio (9) and thereby reduce secondary flow. The previous directly relevant experience was invaluable in designing the present experimental investigation.

4.2 Development of turbulent boundary layer

In this study it was important to consider a fully developed turbulent boundary layer. It was therefore a requirement that the flow development in the channel was completed at a point well upstream of the test section. This ensured that the turbulence structure convecting through the test section had been produced within a fully developed turbulent

region. Balachandar et al. (2001) reported that the turbulent boundary layer is expected to be fully developed at a distance of about 50-70 depths from the leading edge of the flat plate. The development length in term of hydraulic radius (R) is recommended to be 100R but not less than 50R. Stuart (1984) over a similar roughness cross section and Mansour (1992) over a sand roughned bed measured the velocity profile at the inlet (x=0.0m) and up to the test section (x=2.0m). From their results it can be seen that the flow becomes fully developed within the first meter of the channel, and that the velocity profiles thereafter remain unchanged. It can therefore be assumed that the present test section 3 metres downstream from the inlet gave a satisfactory fully developed and reasonably steady channel flow.

4.3 Wall distance origin for LDV control volume

Laser Doppler velocimetry has been used to obtain the velocity measurements during this research study. In this method there is an inherent problem with the exact location of the control volume position.

To exactly determine the position of the laser control volume on the 2-d slat roughness a razor blade was positioned vertically 1mm with respect to a fixed datum. The beams were raised with the computer controlled traverse box and the control volume was positioned just to touch the sharp edge of the blade. A second reading was taken at the point when the beams became totally eclipsed by the razor blade, thereby locating the bottom of the control volume. It was thus possible to locate the centre of the control volume relative to the glass datum by taking the means of the two reference levels.

4.4 Bed shear stress determination

For flow over a smooth surface the bed shear stress, τ_o, could be obtained using two independent methods, both employing the experimental measurements. The two results were then compared to assess their reliability.

From equation 2.11 it is known that;

$$\tau = \tau_o(1-(z/D)) \tag{4.1}$$

$$\frac{\tau}{\rho} = (-\overline{u'w'} + \upsilon\frac{\partial u}{\partial z}) \tag{4.2}$$

Near the smooth boundary in the viscous region $\overline{u'w'}$ tends to zero as, z, tends to zero, therefore;

$$\tau_o = \mu(\frac{\partial u}{\partial z})_{z=0} \tag{4.3}$$

In case of flow over a smooth surface, $du/dz_{z\to o}$ can be deduced from the near wall velocity. For the same experiment a set of Reynolds stress $\overline{u'w'}$ results was also obtained. At each measurement point the velocity gradient was obtained from the measured velocity profile. Hence the total stress, τ/ρ, was plotted against the position above the bed, z, for the smooth surface test, as in figure 4.1. Reynolds stresses were also plotted on the same graph. It can be seen that the Reynolds stress makes the major contribution to the total stress, and that except for a thin region adjacent to the wall, Reynolds stress is almost equal to the total stress for the majority of the boundary layer.

For a rectangular open channel flow over smooth wall, the streamwise velocity, u, could be expressed by Karman-Prandtl's Log-law.

$$\frac{u}{u_\tau} = \frac{1}{\kappa}\ln(\frac{zu_\tau}{\upsilon}) + A_1 \tag{4.4}$$

Where u_τ =shear velocity at channel bed, defined as $\sqrt{\frac{\tau_o}{\rho}}$; τ_o bed shear stress; ρ = the mass density of the fluid; κ = Karman constant; A_1 = integral constant; z is normal distance from the bottom and υ is kinematic viscosity of the fluid. The smooth surface length scale for the flow was estimated from the logarithmic region of the mean velocity profile shown in figure 4.2. The distribution of the mean velocity normalized by friction velocity u_τ, (u/u_τ) shown against the dimensionless wall unit z^+, (zu_τ/υ) in figure 4.3. Laufer (1951), Grass (1967), Rajaratnam (1969), Steffler et al. (1985) , Cardoso et al. (1989), Nezu and Rodi (1986) and Dong et al. (1990) from their experimental work over smooth wall test recommended the value for the Karman constant and the integral constant A_1. It was found from their experiments that the value of the Karman constant κ varied from 0.33 to 0.42, and that of the integral constant varied from 4.5 to 7. The best fit to the measured profile as recommended by Stuart (1984) for the current smooth wall test gave values in good agreement with the values above (see figure 4.3). However it suggests a value of κ (Karman constant) of 0.34 would be in better agreement with the present data. This is in line with similar experiments conducted in same laboratory.

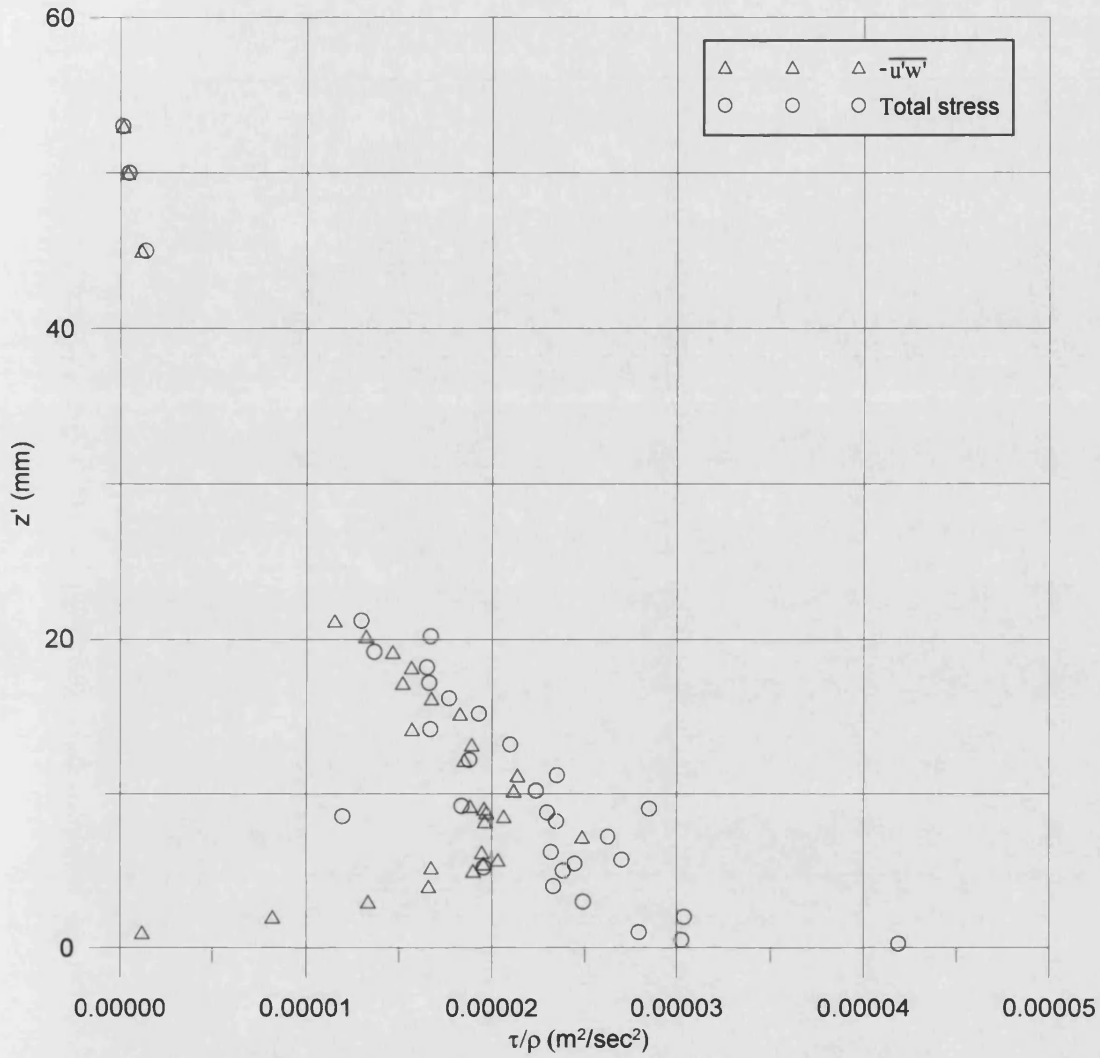

Fig. 4.1 Reynolds stress and total stress distribution for the smooth surface bed

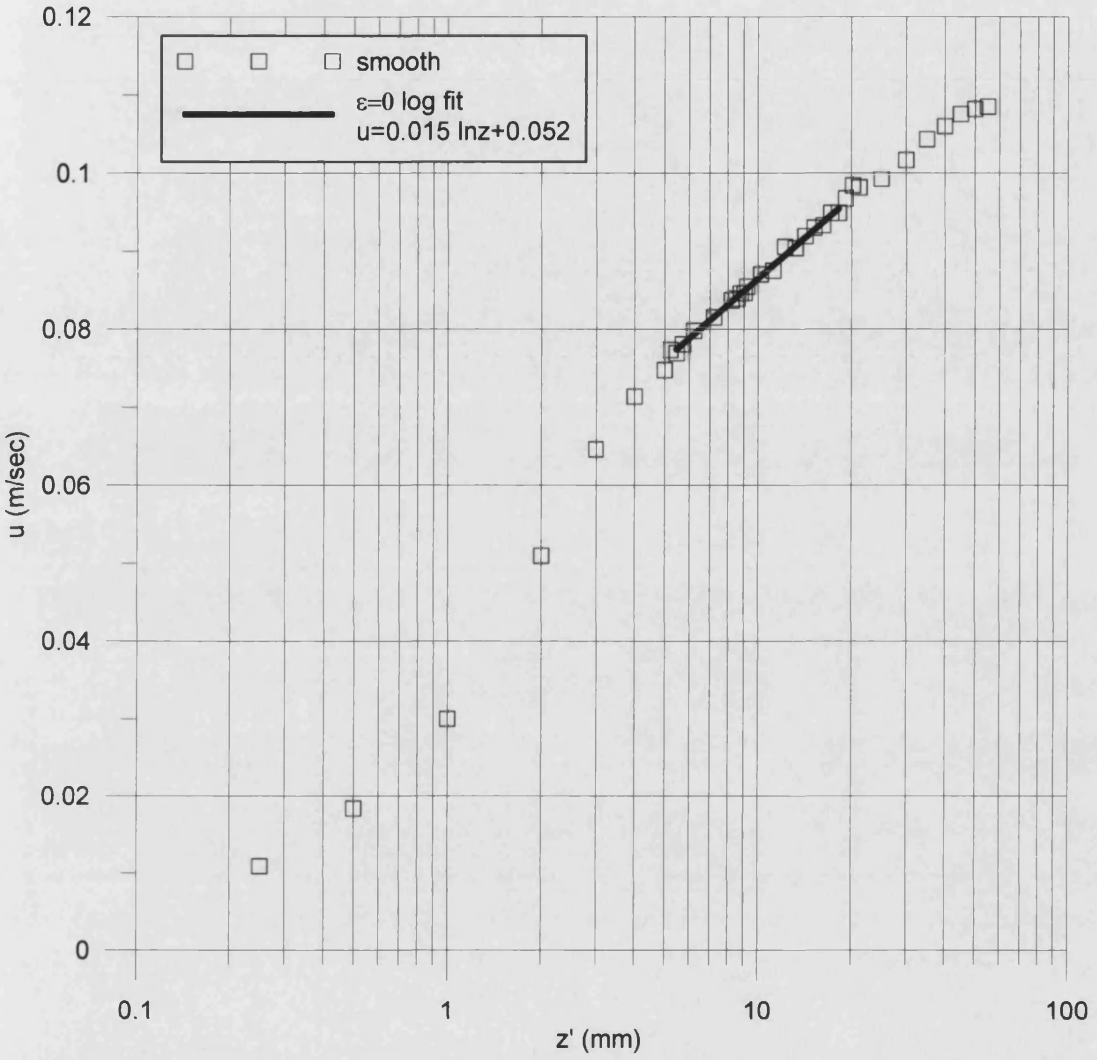

Figure. 4.2 Roughness length scale for the smooth surface bed

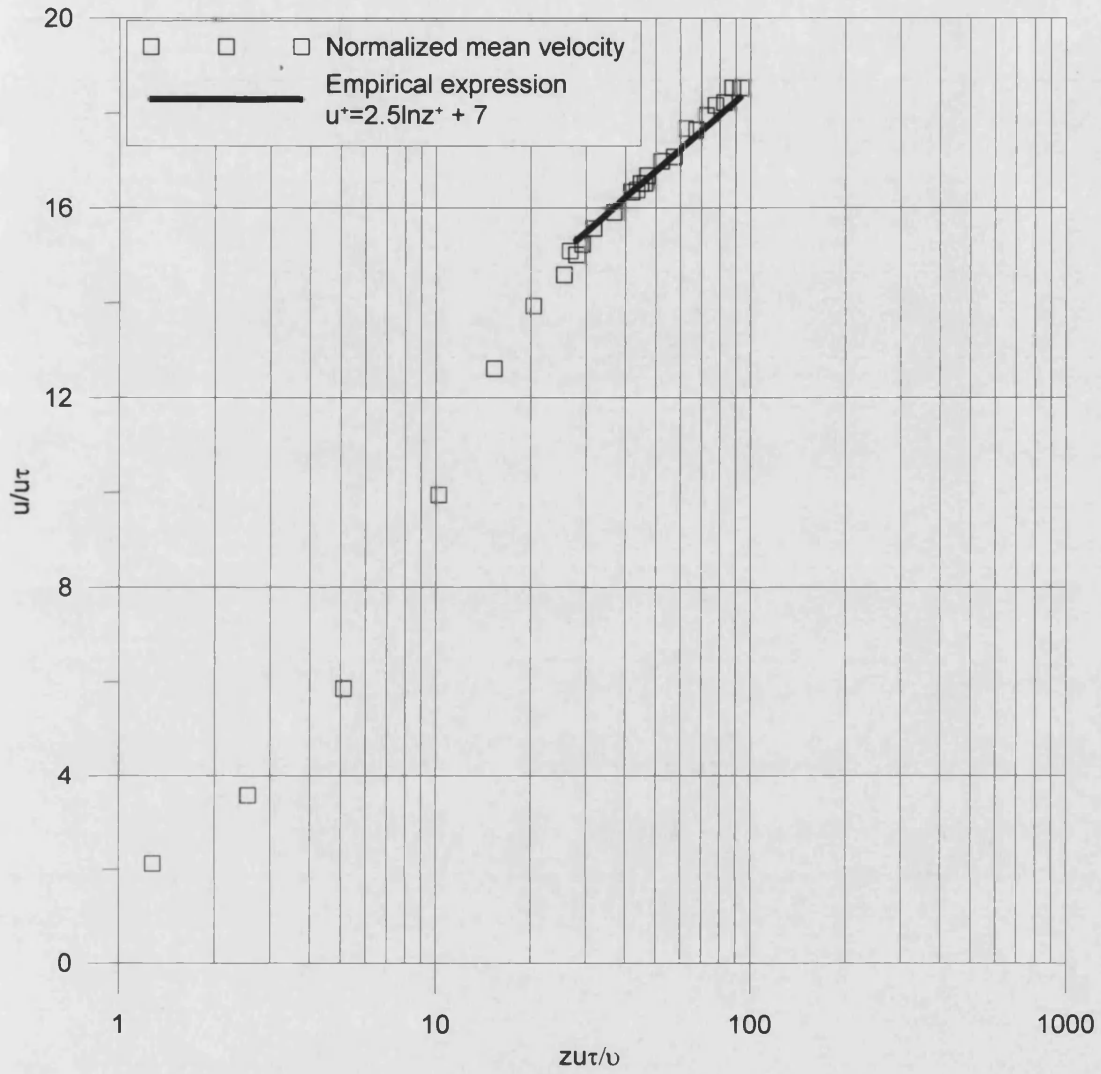

Figure 4.3 Mean velocity profile over smooth wall

4.5 Considerations for the rough wall tests

When a turbulent boundary layer comes in contact with a rough surface the question arise concerning the definition of an effective z-origin. To overcome the arbitrary nature of the origin in the rough boundary test for each experiment, the procedure suggested by Clauser (1954), was used. Clauser's method was also used by Stuart (1984) and Mansour (1992). Clauser (1954) observed that a constant shift in z, due to change of the origin, would cause the straight line logarithmic portion of the velocity profile to become distorted into a curve.

He suggested, therefore, that the z origin should be shifted until the curved logarithmic region, resulting from the use of an arbitrary z datum, was transformed back into the appearance of a straight line on a semi log plot. Clauser's procedure, which is used widely in the analysis of rough boundary flows, has the advantage of consistency since it utilises the properties of the flow, rather than trying to categorise details of the roughness geometry.

The Clauser method is only valid when applied to the logarithmic region of the velocity profile. Therefore the correct determination of the upper and lower limits of the logarithmic region is very important. It is generally accepted that the upper limit of the log-layer is approximately 0.2δ above the wall, where δ is the boundary layer thickness. In order to decide on the upper limit of each test, the actual individual log linear plots were examined, and the upper limit was selected to be where a noticeable deviation from the straight line appears to occur.

From the above discussion it is important to take a good account of the lower limit and upper limit of the log region. One can by simple physical reasoning argue that, inside the roughness sublayer immediately adjacent to the rough bed, the flow can be influenced by the localized geometry and individual roughness excrescences of the rough bed. Reynolds (1974) mentions a roughness 'layer', extending for approximately one roughness height above the roughness tops, in which the flow is strongly influenced by the local geometry. Townsend (1976) and Perry and Joubert (1963) also describe such an effect, without quantifying the extent of the region. The approach used by Stuart (1984) was adopted in the present study to give an indication of the lower limit of the log layer in the current tests. Details of the tests carried out covering a range of roughness with a systematic variation in gap distance were shown earlier in Table 3.1. In the example shown here a

20mm gap distance between the slats is considered. The lower limit of the log region is identified by the comparison of the velocity profiles measured at different horizontal locations above the roughness, directly above the element (S4) and above the centre of the trough (S2) between the roughness elements (figure 3.5). Typical profiles are shown in figure 4.4. The fixing of the lower limit cannot be made independent of the upper limit of the logarithmic region. It was found that at about 6mm above the roughness tops the two profiles merged, thus demonstrating the height at which local velocity influences cease to affect the flow. However, it is clear that the extent of the roughness sublayer is strongly dependent upon the shape of the roughness elements and in particular the roughness configuration in each test (Table 3.1).

Having established the limits of the log layer for each test, it was possible to apply the Clauser method to locate the position of the origin. The Clauser method was applied using a technique suggested by Perry and Joubert (1963) and also used successfully by Stuart (1984) and Mansour (1992). The velocity profile in the logarithmic region was plotted against z (vertical distance from the datum) on a semi log plot. A large value of the origin correction shift, ε, was then added to the z coordinates of the experimental points, now locating the z origin well below the roughness crest height, and these shifted points were plotted. This shift brought the points closer together and enabled a curve to be faired in by eye through the data points. Working back from the faired-in curve,

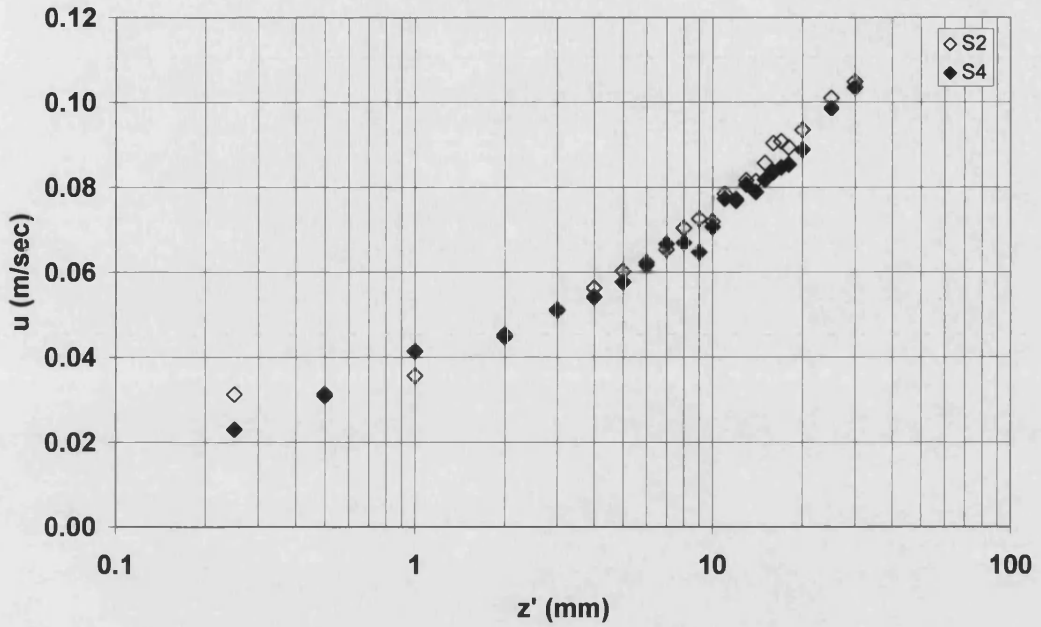

Figure 4.4 Logarithmic region identification from the mean velocity profiles for gap distance s=20mm between brass slats

small increments were successively subtracted, giving a family of curves corresponding to various values or origin correction shift, ε, from the datum shown in figure 3.5. This process was carried out for every rough surface. The origin correction, ε, which resulted in the best straight line velocity profile in the logarithmic region was chosen.

As noted by Perry and Joubert (1963), this method did not give the precise value of ε, but located it within a relatively narrow range. Stuart and Mansour reported that attempts were made to narrow this range by using a computer regression analysis routine. In view of the presence of random scatter due to experimental error of the order of 4%, the calculated regression coefficients differed significantly and were of no practical use. The selected value of ε, therefore, had to be identified subjectively. Individual graphs for each different increment were plotted to enable better subjective judgment of the best

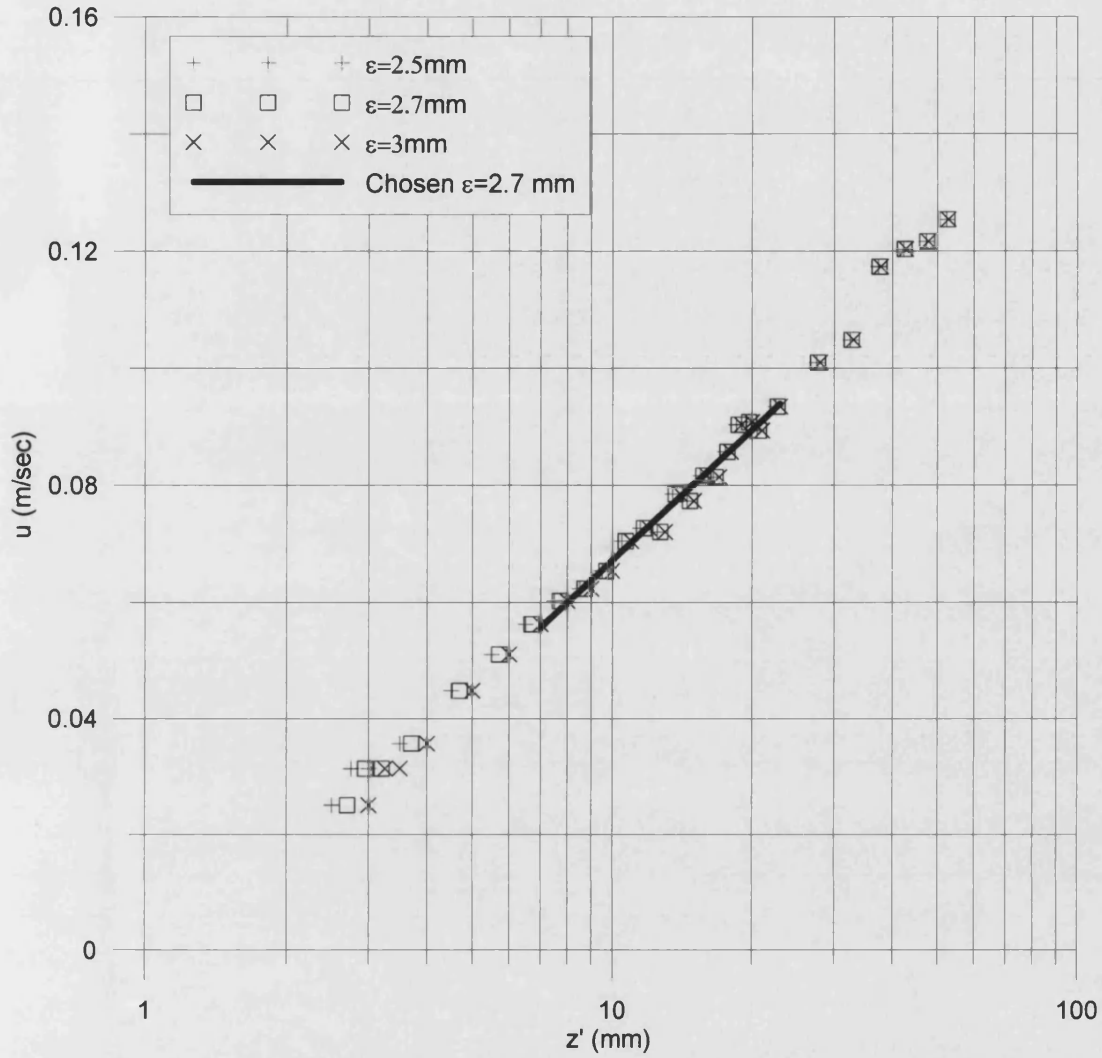

Figure 4.5 Approximate origin location plot for gap distance s=20mm between brass slats

agreement between the data points and the fitted straight line. Change in ε led to consequential changes in κ and u_τ, and the final choice of ε was made with a view to optimizing the values of these three parameters.

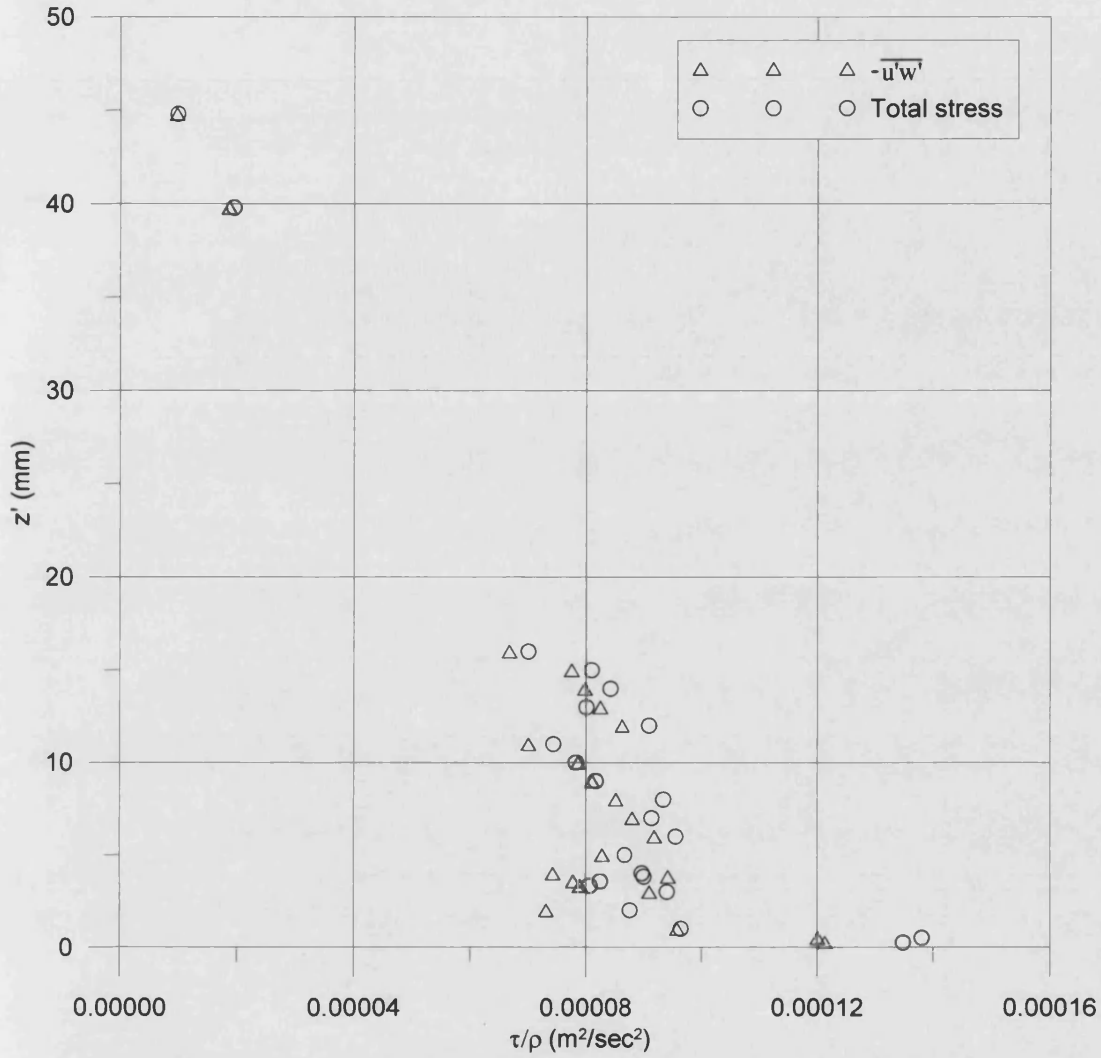

Figure 4.6 Total stress and Reynolds stress distribution for gap distance s=20mm between brass slats

4.6 Bed shear stress for rough surface tests

For the rough surface, the total stress measurements were used to obtain the bed shear stress accurately. Using the experimental results, graphs of τ / ρ against z were plotted for each array of roughness density as shown in figure 4.6. The Reynolds stresses are also plotted on these graphs, demonstrating the major contribution of Reynolds stress to the total stress.

4.7 Results of channel centre line measurements

The mean velocity profile can be described by the Eq. 2.29 is given below

$$\frac{u}{u_\tau} = \frac{1}{\kappa}\ln(z/z_o) \tag{4.5}$$

This equation can be rewritten as follows;

$$u = \frac{u_\tau}{\kappa}\ln z - \frac{u_\tau}{\kappa}\ln z_o \tag{4.6}$$

which correspond to a straight line of the form

$$u = A\ln z + B \tag{4.7}$$

where:

$$A = \frac{u_\tau}{\kappa}$$

$$B = -\frac{u_\tau}{\kappa}\ln z_o$$

The values of A and B in Equ.4.7 had already been evaluated during the origin correction procedure described in section 4.5. From these values, the roughness length scale z_o could be determined. Since u_τ is independently derived, it was possible to calculate a value for Karman's constant, κ. The values calculated for the various wall roughness conditions are tabulated in Table 4.1. Error bars due to random scatter in the experiments were analysed and shown in the following chapters.

In this chapter the relevant length scale z_o for the flow in the near wall region is estimated by dimensional analysis as being proportional to the physical dimension of the roughness elements on the wall. This was derived from the law of the wall logarithmic

Table 4.1 Surface roughness length scales

Gap distance s (mm)	Friction velocity u_τ (mm/sec)	Roughness origin shift ε (mm)	Roughness length scale z_o (mm)	Kappa κ
Smooth	5.123	0	.0312	.3415
2.50	6.123	.05	.0820	.3560
5.00	6.199	.40	.0849	.3874
7.50	7.202	.50	.1137	.3674
10.00	7.416	.50	.2468	.3401
12.50	8.062	1.00	.3729	.3649
15.00	8.139	1.50	.5667	.3349
20.00	10.606	2.70	1.2069	.3324
25.00	10.124	3.00	1.2879	.3086
30.00	10.839	3.50	1.3657	.3345
35.00	10.723	3.10	1.2004	.3320
45.00	11.401	3.20	1.2353	.3596
55.00	10.723	3.90	1.0285	.3775
75.00	9.486	3.50	1.0970	.3141
95.00	10.488	3.50	.7547	.3987
115.00	10.000	4.50	.7494	.3846
155.00	7.5000	5.20	.5537	.3330
235.00	7.664	4.90	.2380	.3971
315.00	6.708	5.20	.1386	.4115
475.00	6.324	5.00	.1116	.3928
955.00	5.123	5.20	.0476	.3795

velocity profile relationship in turn derived from the inner wall law and the outer layer velocity defect law overlap argument. The next chapter focuses on the flow pattern formed inside the cavity between the roughness elements and its effect on the diffusion behavior in the turbulent boundary layer.

CHAPTER 5

EXPERIMENTAL RESULTS AND DISCUSSIONS

The primary purpose of this chapter is to discuss and interpret the experimental measurements and observations. These are of particular relevance to turbulent diffusion of pollutants in water and flow over systematically varying rough boundaries. The rough boundaries under consideration have been chosen to simulate a city centre with closely spaced buildings and narrow streets, flow over open countryside roughness, and flow over smaller towns with relatively wide streets. The dispersion of pollutant has been observed for a range of bed roughness with systematically varied roughness spacing.

5.1 Flow pattern classification

The flow pattern between and above the roughness cavities can be classified as skimming, wake interference or isolated roughness flow for definitions (see section 1.4). In this section the boundaries between these regimes are determined from flow visualization and from mean flow patterns obtained with the laser Doppler velocimeter. In skimming flow the roughness elements are relatively closely spaced, the bulk of the mean flow does not enter the cavity (or canyon) and a stable vortex is established in the cavity, as shown in figure 5.1, 5.2, 5.3a. Wake interference flow is found when the roughness elements are more distant, the downwind roughness element disturbs the circulation vortex before adjustment can take place and interaction between the two vortices is possible as shown in figure 5.1, 5.2, 5.3b. Isolated roughness flow occurs when the roughness elements are well apart. Multiple horizontal vortices form between the roughness elements. A low pressure recirculation vortex is formed behind the upwind roughness element due to flow

separation from the roughness top edge; a high pressure vortex due to flow separation on the downwind roughness element is also formed as shown in figure 5.1, 5.2, 5.3c. The boundaries between these three flow regimes (skimming, wake interference and isolated roughness flow) over square section slat type bed roughness are not well established and the next section of this chapter looks closely at this issue. The test plan was presented earlier in figure 3.5 and in Table 3.1.

5.1.1 Skimming flow

The skimming flow regime has been identified with the help of flow visualization. The flow visualisation results (figure 5.1a) using a laser light sheet showed an organised single vortex flow in the cavity. This formation of the vortex inside the cavity between the roughness elements is confirmed by the LDV measurements shown in figure 5.3a.

When the dye was introduced with the injector (*c1*) on the top face of the roughness slat (shown in figure 3.6), there was little lateral spreading in the flow. This gave a unique insight into the turbulence behaviour at roof level. Significant influence on the lateral spreading was noticed when the surface roughness was varied from closely spaced to relatively widely spaced roughness elements.

The dispersion behaviour was also confirmed by other injectors drilled into the slats, one (*d1*) introducing the dye in the direction of the mainstream flow and the other (*u1*) against the direction of flow. Both injectors were located at 1.5mm above the surface of the glass plate. The arrangement was shown in figure 3.5 in chapter 3. An interesting observation found was the lateral spreading of the dye inside the cavity formed between the roughness slats. This was termed as "Cavity Plume Width". Figure 5.4a,b demonstrates that dispersion for a skimming flow was different when the dye was introduced with injector *d1* and *u1*. The cavity plume width was found to

be more for injector *dl* than *ul*. This shows that vortex activity close to the roof level is high and disperses the pollutants effectively from downstream of the cavity in comparison to pollutant introduced on the upstream face of the cavity. The evidence to support this from the ejection to sweep ratios measurements along the roof level shown in figure 5.5a. This figure shows slightly higher ejection to sweep ratios for the flow interacting in the region of injector *ul* than that for *dl*. The measurements of cavity plume width for varying gap distances are shown in figure 5.6. On the basis of flow visualisation, it was found that a strong organized and 2d skimming flow is present for a gap to height ratio (s/k) up to a value of 1.5.

5.1.2 Wake interference flow

Wake interference flow is one in which the two vortices formed inside the cavity, one at the upstream and the other at the downstream corners, strongly interact with each other as shown in figure 5.1,5.2,5.3b. An interacting layer (figure 5.2b) was observed between the vortices inside the cavity. This layer was found to change its position across the cavity and helped the vortices to extract energy from the mean flow. The LDV measurements provided evidence for the increase in local mean streamwise velocity inside the cavity with the increase in gap distance between the roughness slats as conditions changed from skimming to wake interference flow (see figure 5.7). The increase in reverse flow has consequently increased the turbulence fluctuations and Reynolds stresses which promote mixing inside the cavity shown in figure 5.8, 5.9, and 5.10. The reverse flow at the centre of the cavity achieves a peak value and consequently increases the turbulence fluctuations between the roughness slats. On looking at the measurements of cavity plume width (figure 5.6) it is evident that the vorticity between the roughness elements is efficiently dispersing the dye from both the injectors facing in the direction of the flow and the other which faces the opposite

to flow direction. Ejection to sweep ratios (figure 5.5b) for $s/k = 4$ shows that surface roughness promotes significant sweeps in comparison to skimming flow regime at the centre of the cavity at a point corresponding to the dynamic interaction layer (figure 5.5.a). Flow visualization confirmed that the two vortices interact strongly for gap to height ratio from (s/k) 2.5 to 5.

5.1.3 Isolated roughness flow

The flow is classified as isolated roughness flow when the upstream vortex acts independently of the downstream vortex inside the cavity. The mean velocity profile provides evidence that as the flow switches from wake interference to isolated roughness the reverse flow at the centre of the cavity becomes negligible and turbulence fluctuations stay high. As the vortices change their position inside the cavity (figure 5.1, 5.2, 5.3c) they become more able to interact with the outer boundary layer. LDV measurements at the centre of the cavity show the overall behaviour of unsteadiness in the cavity. On further increasing the gap distance the turbulence fluctuations in the boundary layer and inside the cavity decrease. This is evidence that the upper boundary layer and the flow in the gap between roughness elements have interaction between them. Ejection to sweep stress ratio (figure 5.5.c) for $s/k = 9$, illustrates the presence of two active vortices, one upstream, shown by dye released at injector *dl* and the second in the downstream of the cavity shown by dye from *ul*. Both the vortices have a significant influence on the ejections and sweeps stresses at upstream and downstream locations at roof-level of the cavity. The flow pattern for gap to height ratio (s/k) greater than 9 was found to behave as isolated roughness flow.

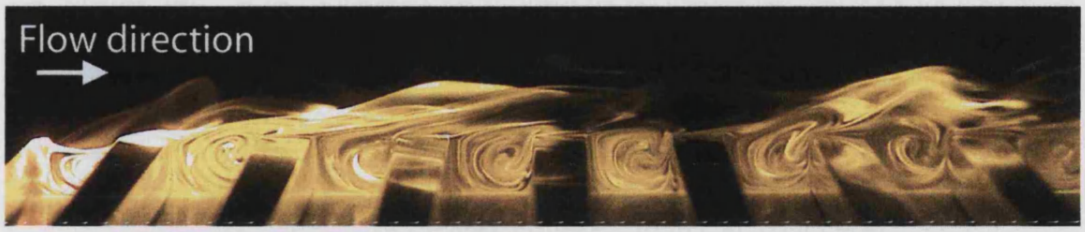

a) Skimming flow visualisation for gap distance s/k=1.5 between slats

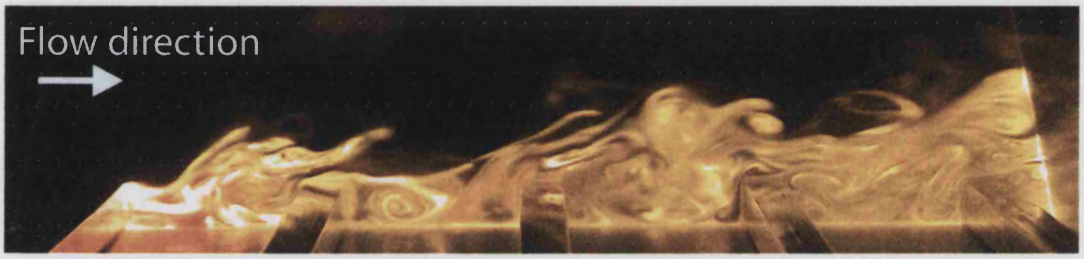

b) Wake interference flow visualisation for gap distance s/k=4 between slats

c) Isolated roughness flow visualisation for gap distance s/k=9 between slats

Figure 5.1 Flow visualisation with laser light sheet a) skimming, b) wake interference, c) isolated roughness flow

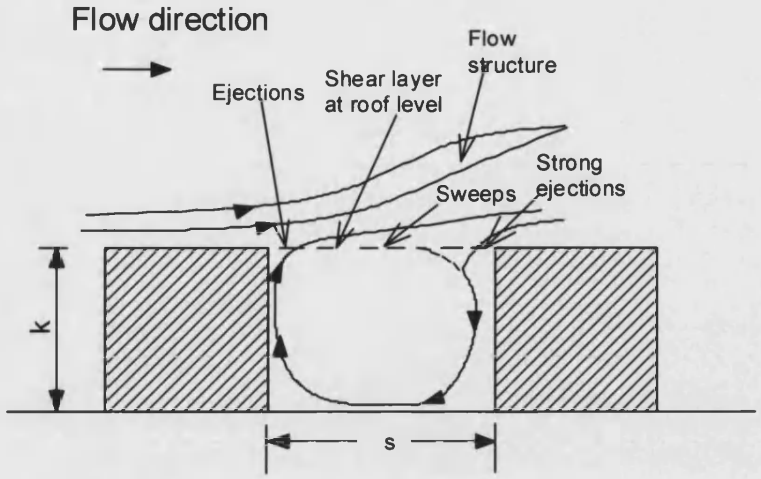

a) Skimming flow s/k<1.5

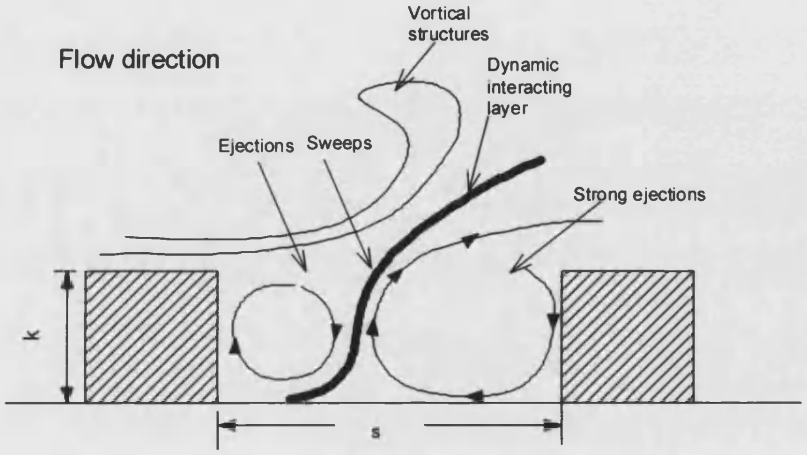

b) Wake interference flow 5>s/k>2.5

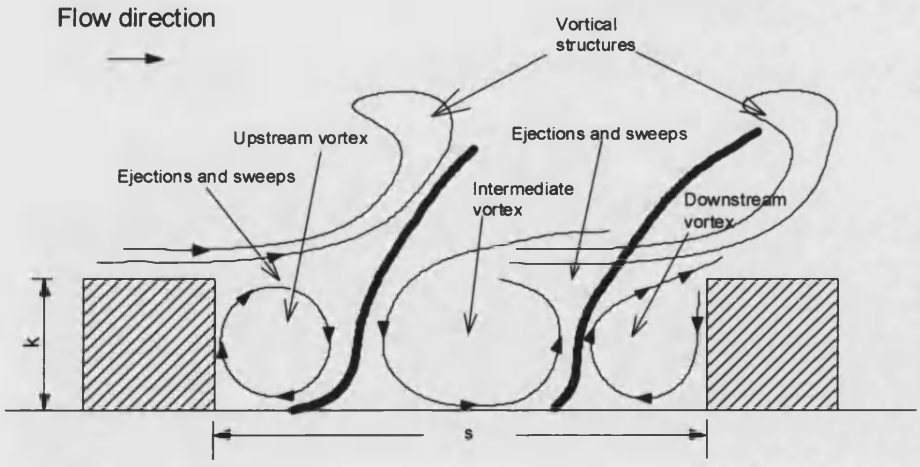

c)Isolated roughness flow s/k>9

Figure 5.2 Changing gap flow patterns for varying relative gap width between roughness elements a) skimming, b) wake interference, c) isolated roughness flow

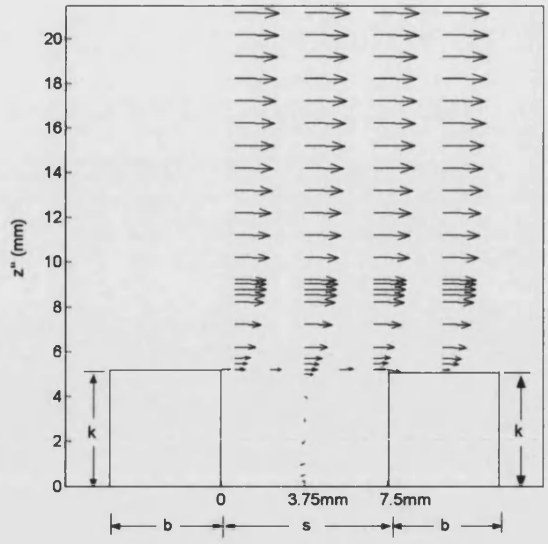

a) Flow pattern for Skimming flow over gap distance s/k=1.5 between slats

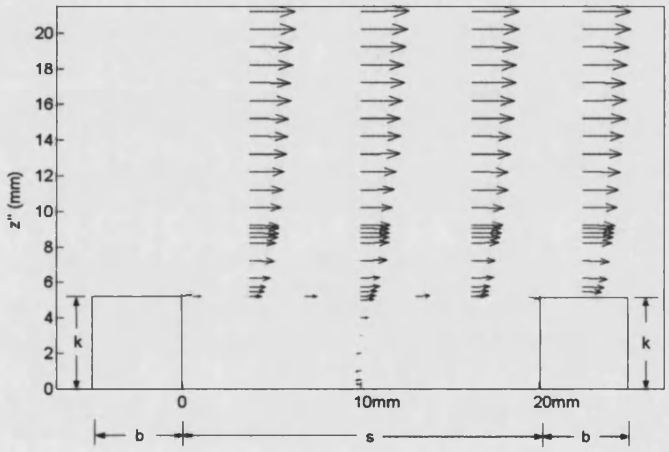

b) Flow pattern for wake interference flow over gap distance s/k=4 between slats

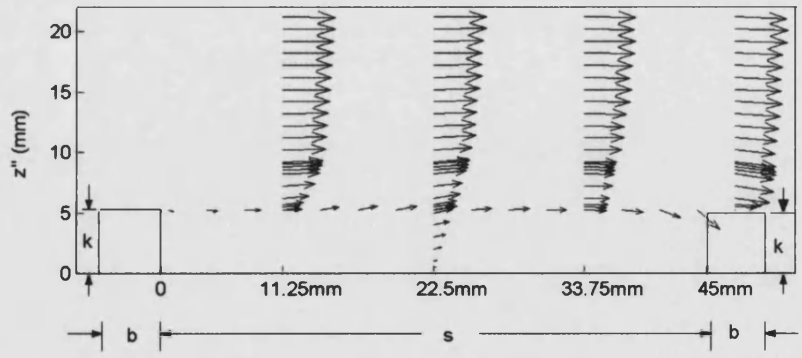

c) Flow pattern for isolated roughness flow over gap distance s/k=9 between slats

Figure 5.3 Flow pattern from local mean flow velocities measured with LDV a) skimming, b) wake interference, c) isolated roughness flow

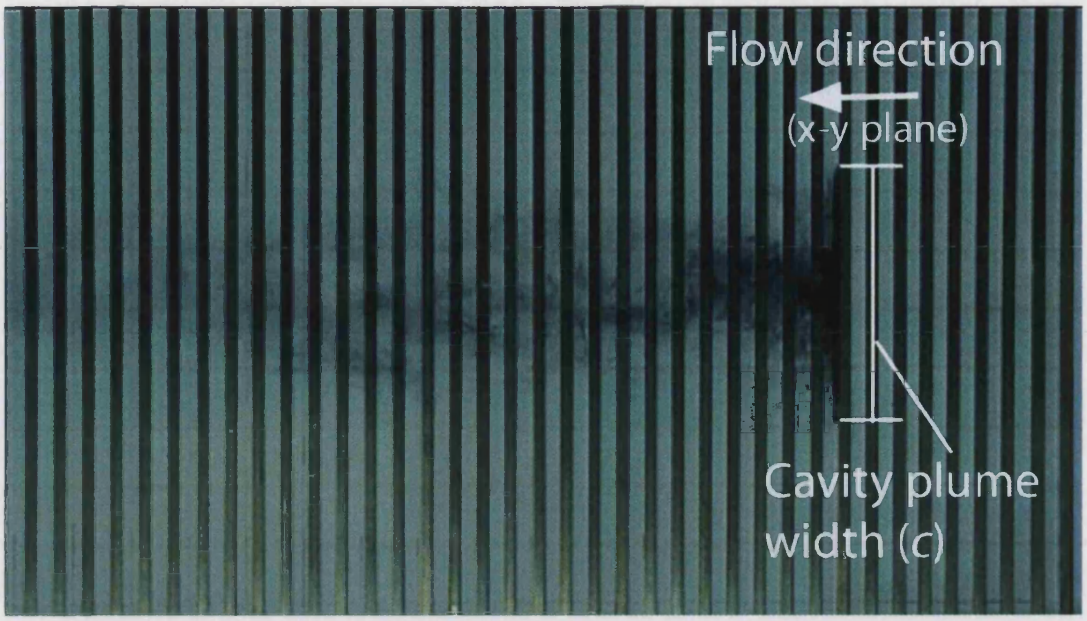

a) Injector d1 (facing downstream)

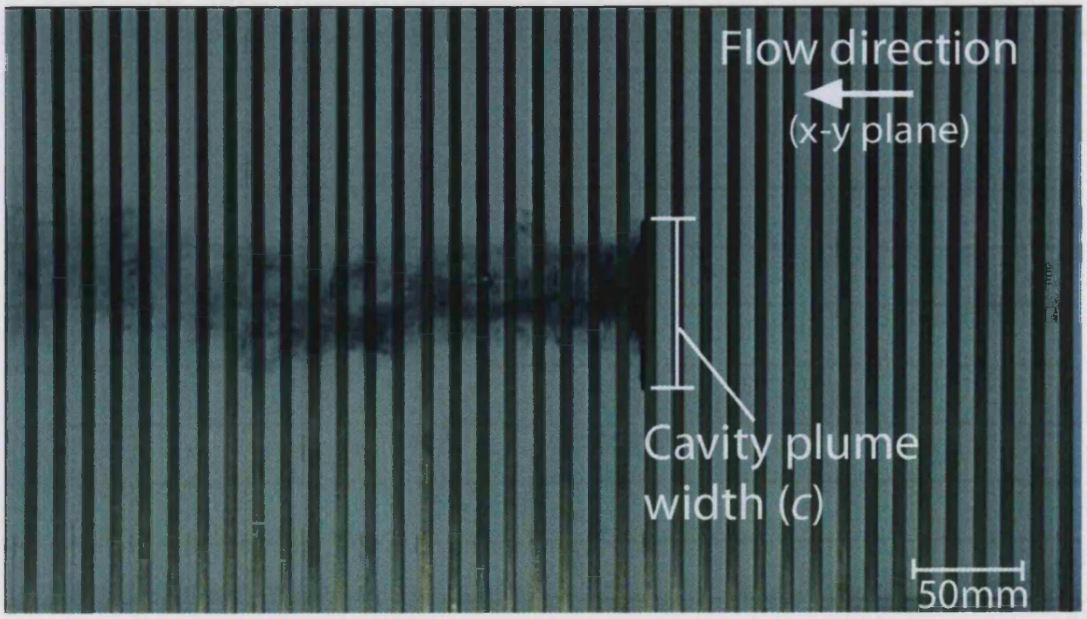

b) Injector u1 (facing upstream)

Figure 5.4 Cavity plume width for gap distance s/k=1.5 between slats a) injector d1, b) injector u1. Each image shows an area 500*mm*×275*mm.*

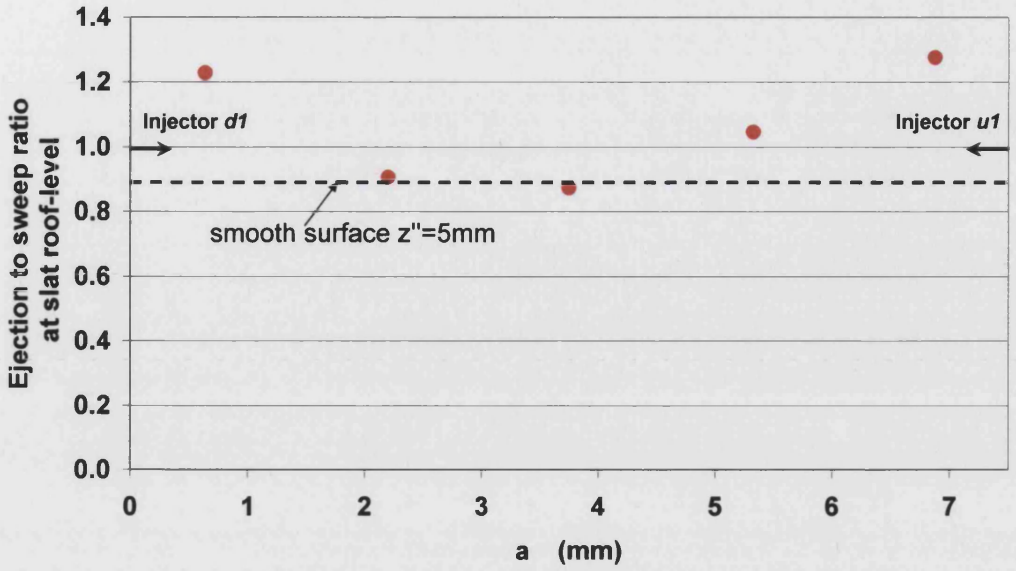

a) gap distance s=7.5mm

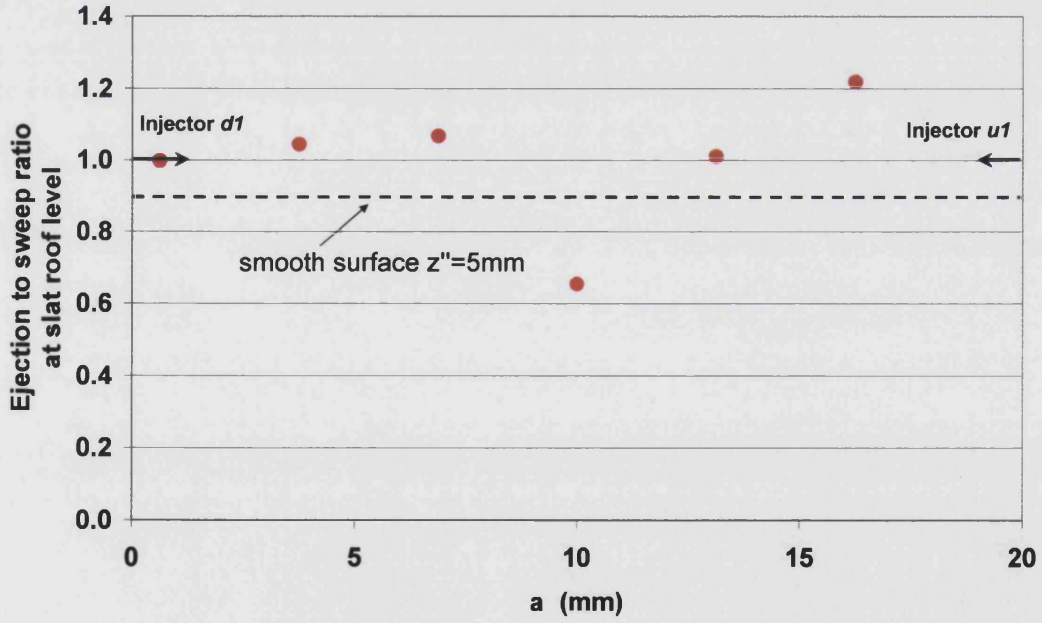

b) gap distance s=20mm

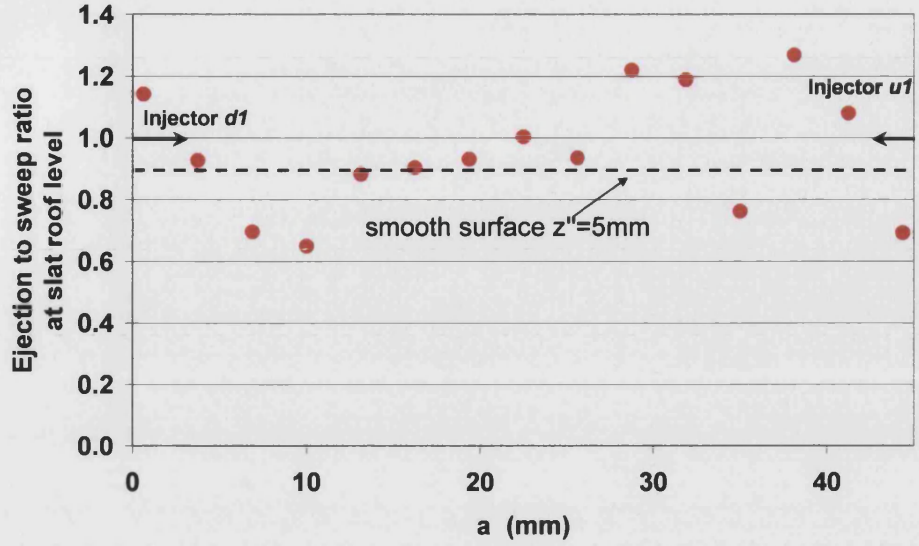

c) gap distance s=45mm

Figure 5.5 Ejection to sweep ratios at z''= 5mm along the gap between slats (H=0) a) skimming flow, b) wake interference flow, c) isolated roughness flow

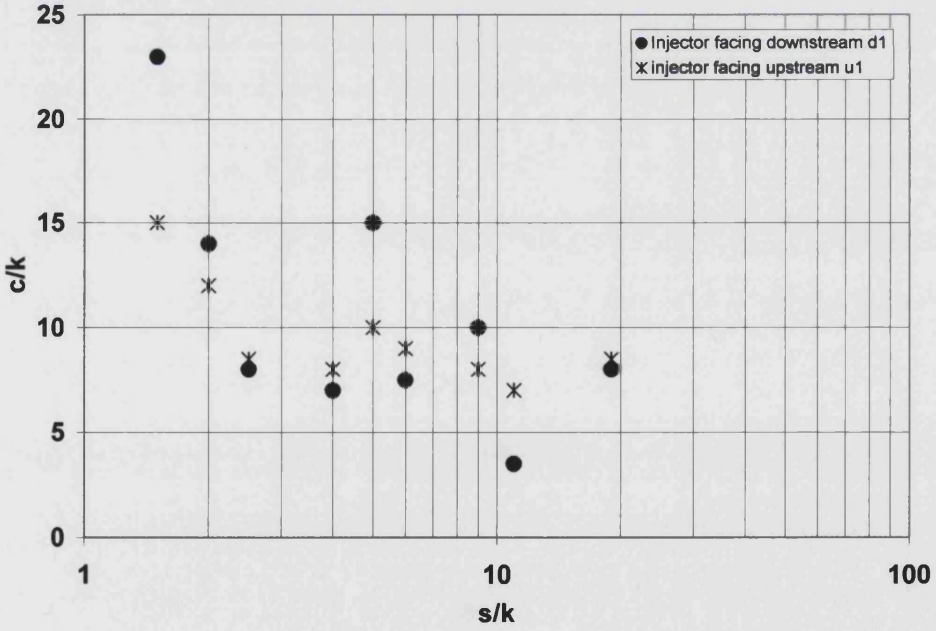

Figure 5.6 Growth in cavity plume width c in the gap between roughness elements

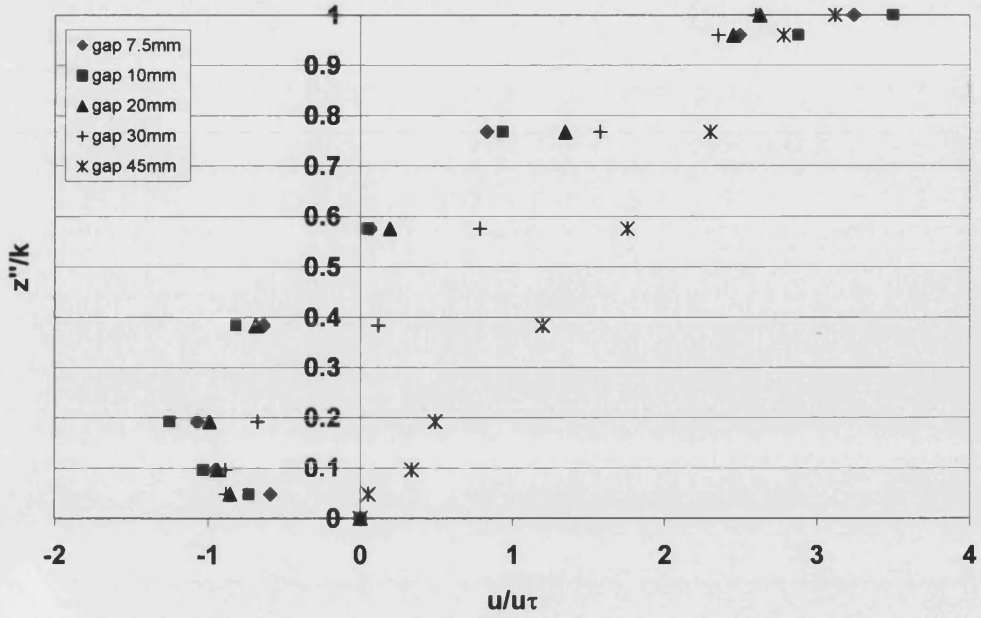

Figure 5.7 Reverse mean flow velocity in the gap between roughness elements

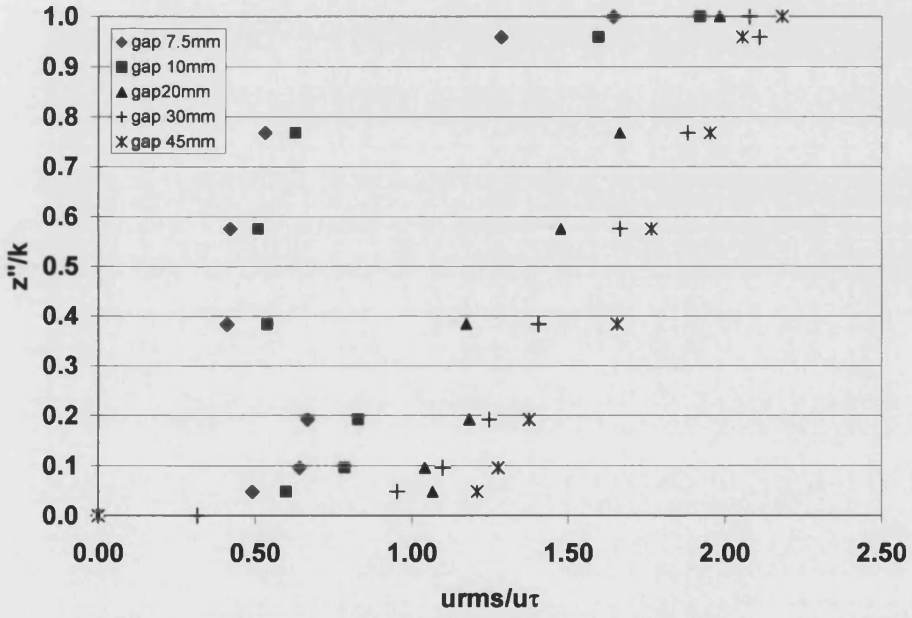

Figure 5.8 Streamwise turbulence fluctuations in the gap between roughness elements

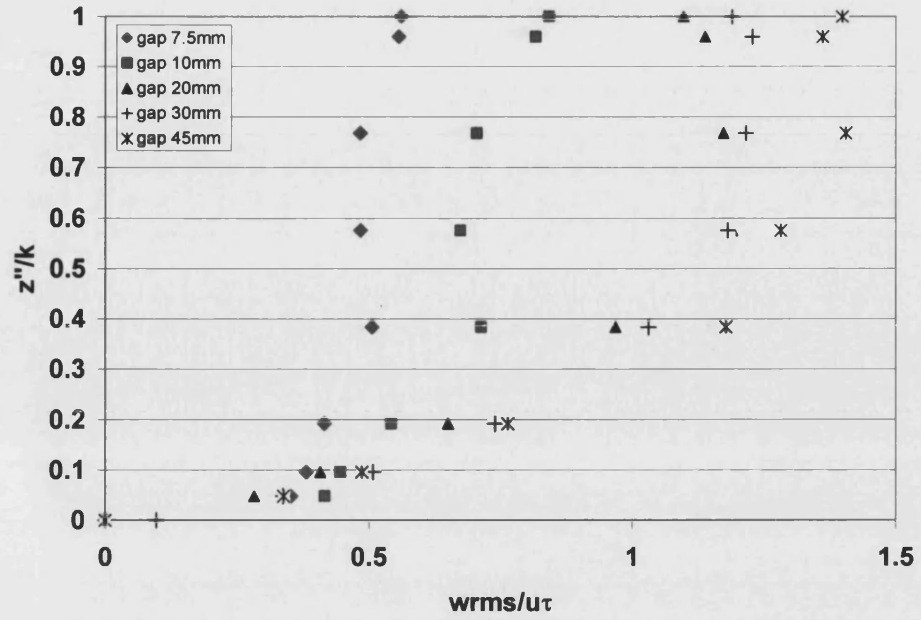

Figure 5.9 Vertical turbulence fluctuations in the gap between roughness elements

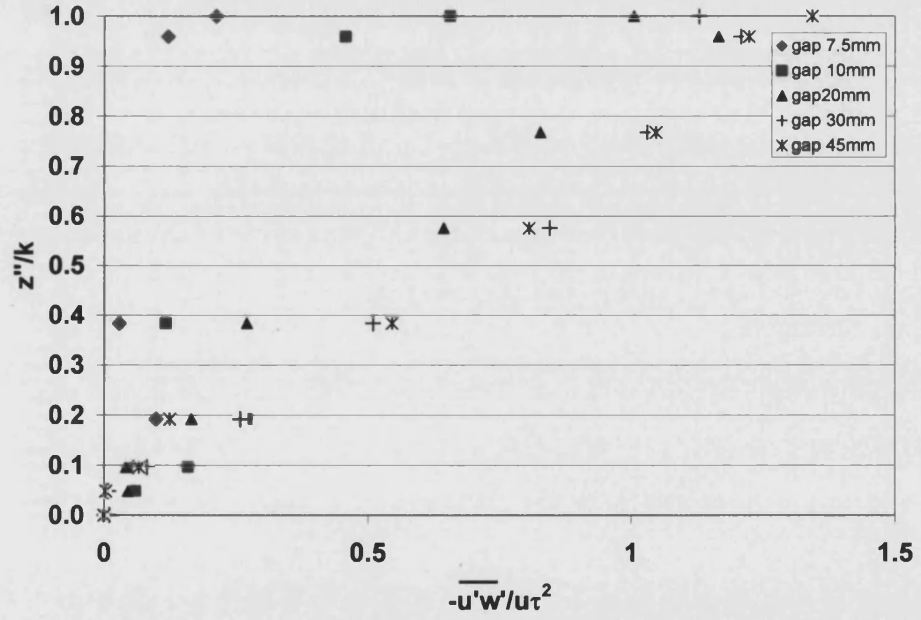

Figure 5.10 Reynolds stresses in the gap between roughness elements

5.2 Local mean velocity profiles and associated turbulence

The velocity distribution over varying wall roughness is compared with the smooth bed case in figure 5.11(a,b). Velocity profiles provide a component part of the term defining

the rate of turbulence production ($\overline{u'w'}\frac{du}{dz}$) and correlates with the dispersion behaviour of the flow.

The comparison of the velocity profile for a gap distance of 955mm with the smooth bed case is very interesting as it shows that both have attained nearly the same profile. The fluctuating velocity is one of the most important properties of turbulence and is shown here both as vertical profile of the root-mean-square values of the longitudinal (urms) and vertical (wrms) velocities, $\sqrt{\overline{u'^2}}$ and $\sqrt{\overline{w'^2}}$, and written in dimensionless form with the shear velocity u_τ as the normalizing factor (shown in figure 5.12 and 5.13). For some distance z' away from the wall, the turbulence fluctuations increases rapidly and reaches its peak value. The boundary layer flow exhibits changing levels of turbulence intensity with changing wall roughness.

Grass (1971) used the hydrogen bubble technique and high speed photography to measure profiles of urms and wrms and plotted them normalised by u_τ. These were estimated for three bed conditions, i.e. hydraulically smooth, transitional and rough, with flow characteristics closely similar to those used in the present study. Direct comparison of the current tests with the peak turbulence fluctuations values presented by Grass compares well. For example Grass found that $\text{wrms}/u_\tau = 1.125$ which agrees well with the value of $\text{wrms}/u_\tau = 1.1$ obtained in the present tests shown in figure 5.13b. Similarly Grass found the peak $\text{urms}/u_\tau = 2.750$, whereas in the current tests $\text{urms}/u_\tau = 3$ shown in figure 5.12b. From the current tests it was found that the turbulence fluctuations from the near bed region are transferred through the main flow up to the surface of the water. The rougher the bed, the less the longitudinal fluctuations urms/u_τ and more the vertical fluctuations wrms/u_τ. A similar observation was reported by Grass (1971). However,

Grass's profiles of urms$/u_\tau$ extend uniformly in the main flow. He reported that the type of boundary has no effect on the intensity of the fluctuations in the main flow region. The surface roughness was believed to have an effect only in the region close to the wall. Further Grass(1971) found that, in the main flow region, the intensity of the vertical fluctuations approaches the shear velocity, wrms$/u_\tau \approx 1$. However from the current tests it was found wrms$/u_\tau \approx 0.5$ as shown in figure 5.13b. The streamwise turbulence fluctuations have no constraint in the streamwise direction. It was found increasing in the flow till until the flow regime changed from wake to isolated roughness flow. Close to the surface of the water the streamwise turbulence fluctuations increased and then reduced on touching the water surface. The vertical turbulence fluctuations were found increasing until the isolated flow regime was achieved as shown in figure 5.13a. Close to the water surface the vertical turbulence profiles converged towards zero because of the constraint in the form of the water surface. The profiles of the Reynolds stresses are shown in figure 5.14(a, b).

Total bed shear stress profiles were estimated for each of the surface roughnesses, as shown in figure 15.15(a, b). The Reynolds stresses $(-\rho\overline{u'w'})$ were obtained directly from the measurements of longitudinal and vertical fluctuating velocities. Figure 5.14(a, b) confirms that turbulent shear stresses $(-\rho\overline{u'w'})$ are distributed linearly, that is, the shearing stress between flow layers is mainly the Reynolds stresses induced by turbulence. Flow over the smooth surface indicated that the turbulent shear stress increases rapidly away from the wall and the viscous shear stress (dominant at the wall) decreases rapidly. For flow over the rough surfaces there was no decrease in the turbulent shear stress. Thus, right up to the wall, almost the entire shear stress is transferred through turbulent shear $(-\rho\overline{u'w'})$. Similar conclusions were reported by Grass (1971).

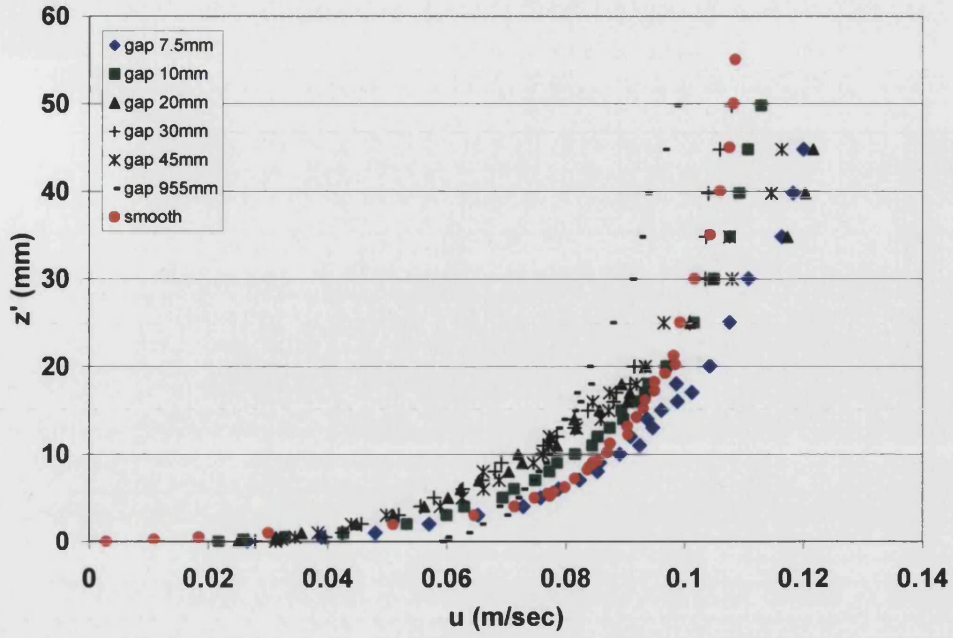

a) Local mean flow velocity profile (measured midway between roughness elements at position S2)

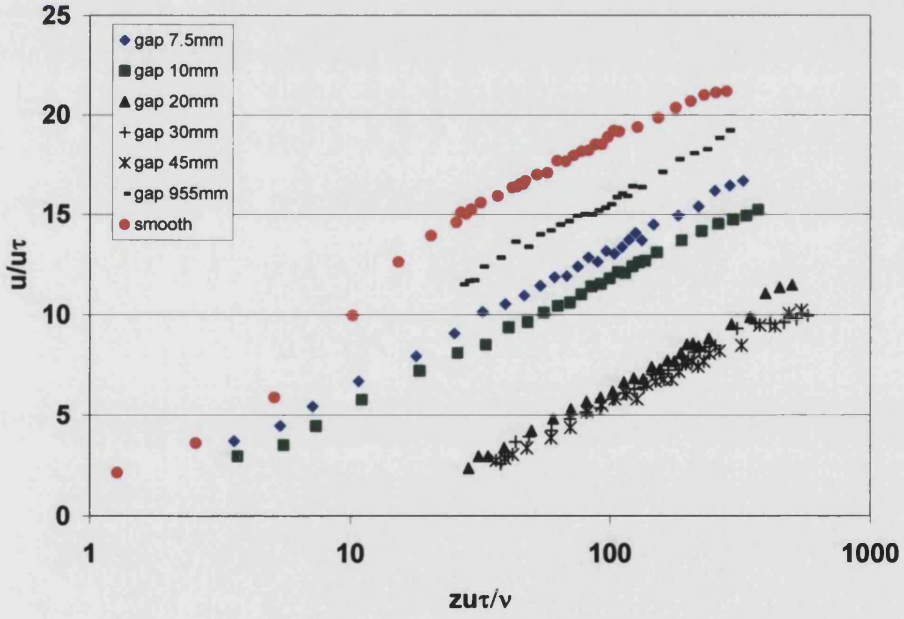

b) Local mean flow velocity profile scaled by friction velocity (measured at S2)

Figure 5.11 Streamwise local mean flow velocity profile a) dimensional b) scaled by friction velocity

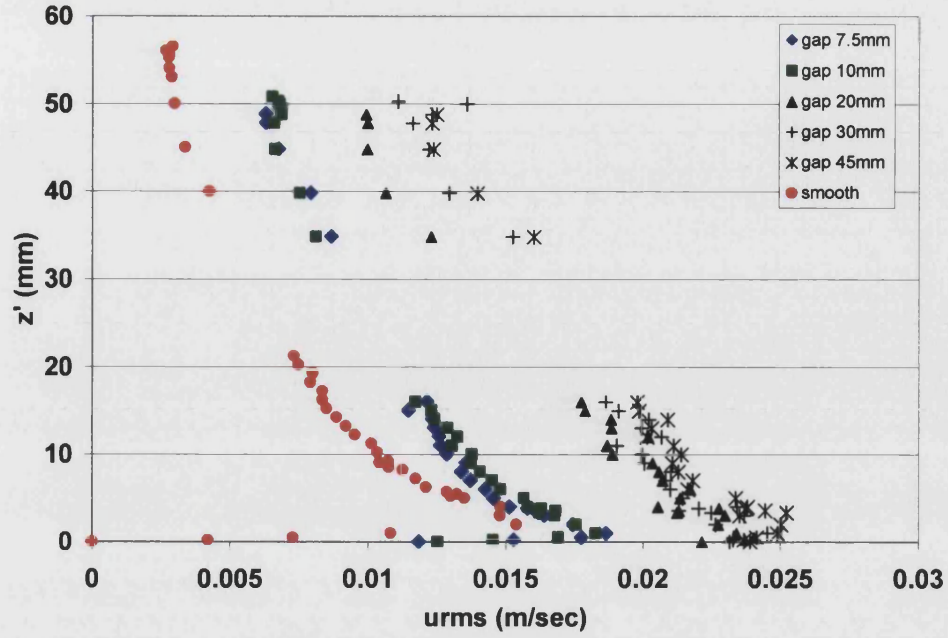

a) Streamwise turbulence profile (S2 location)

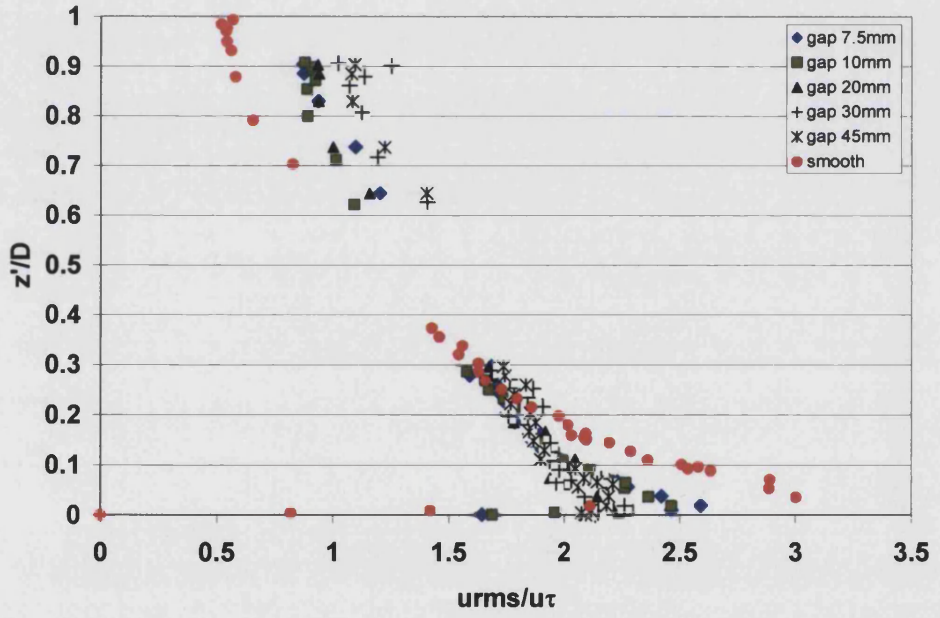

b) Streamwise turbulence profile scaled by friction velocity (S2)

Figure 5.12 Streamwise turbulence profiles a) dimensional b) scaled by friction velocity

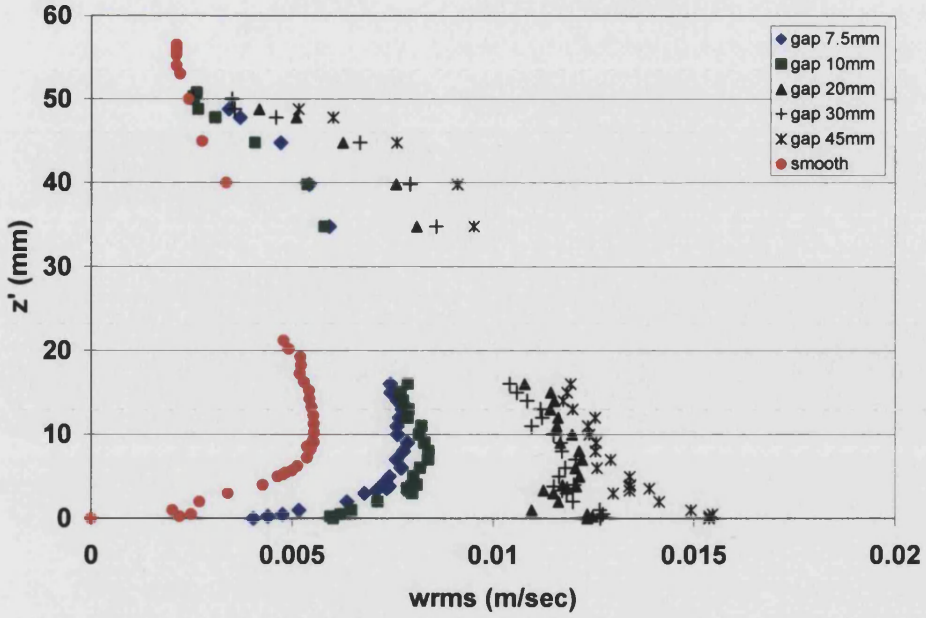

a) Vertical turbulence profile (S2 location)

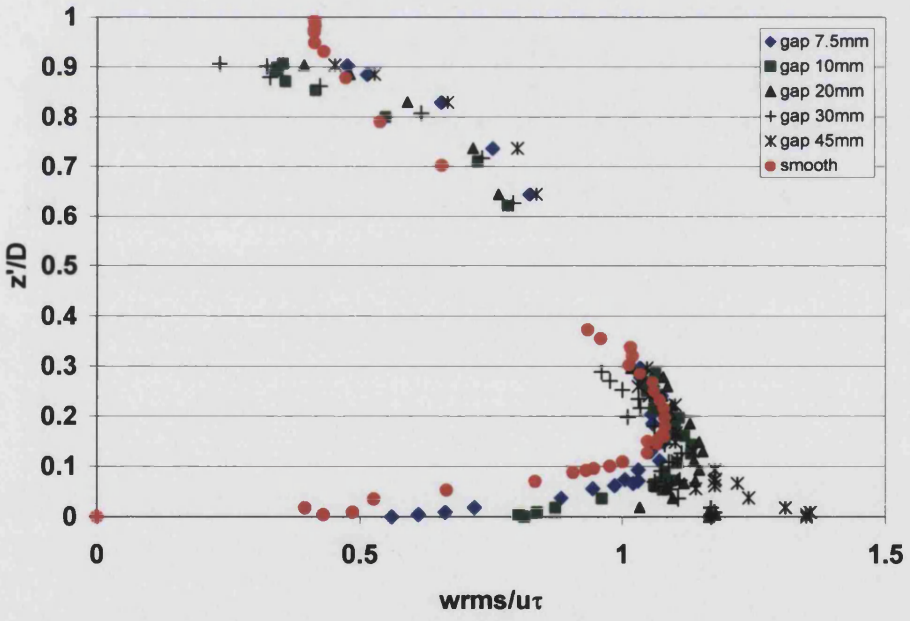

b) Vertical turbulence profile scaled by friction velocity (at S2)

Figure 5.13 Vertical turbulence profiles a) dimensional b) scaled by friction velocity

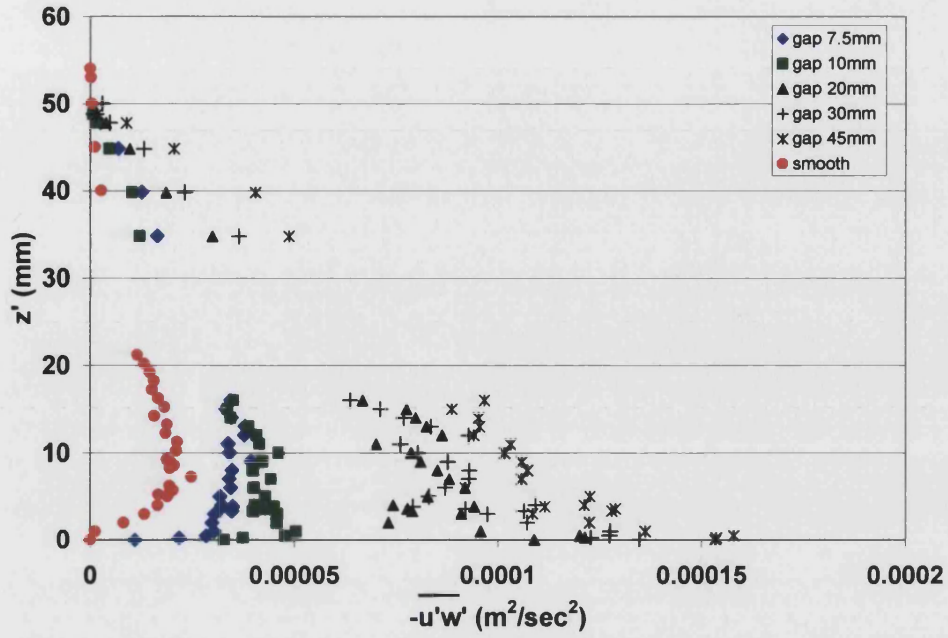

a) Reynolds stress profile (S2 location)

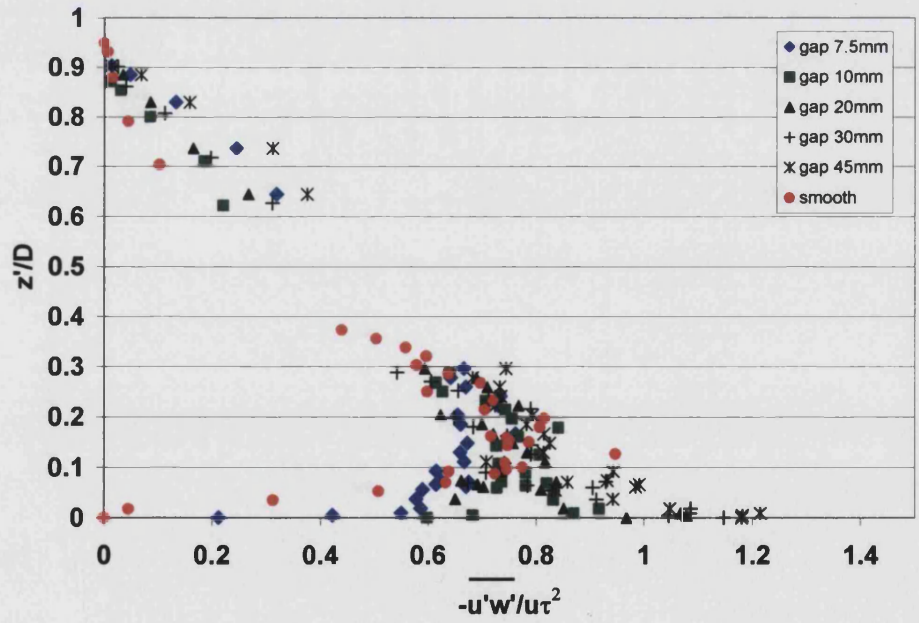

b) Reynolds stress profile scaled by friction velocity: measurements at S2 location

Figure 5.14 Reynolds stress profiles above surface roughness a) dimensional b) scaled by friction velocity

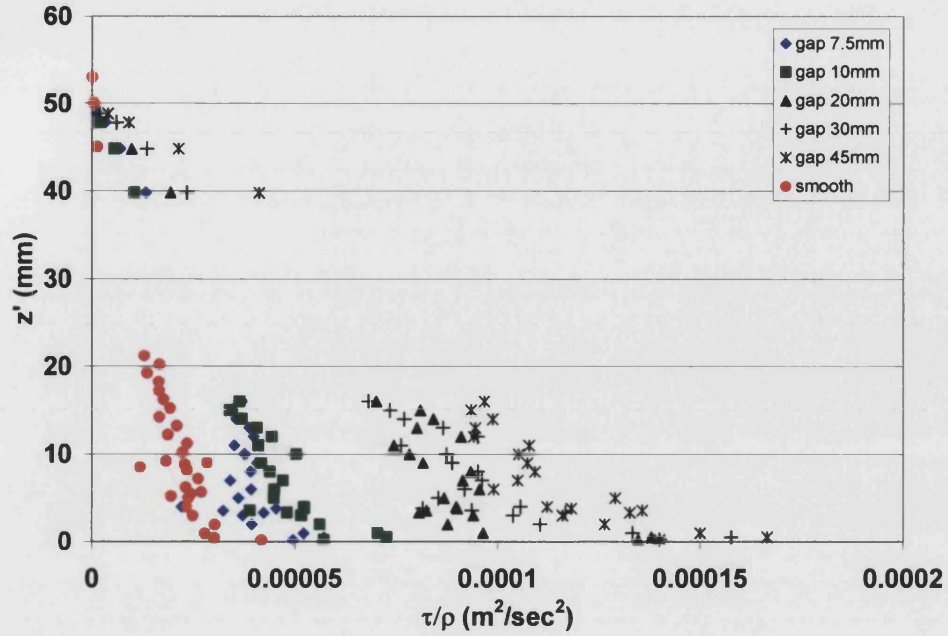

a) Bed shear stress profiles (measured midway between elements at S2)

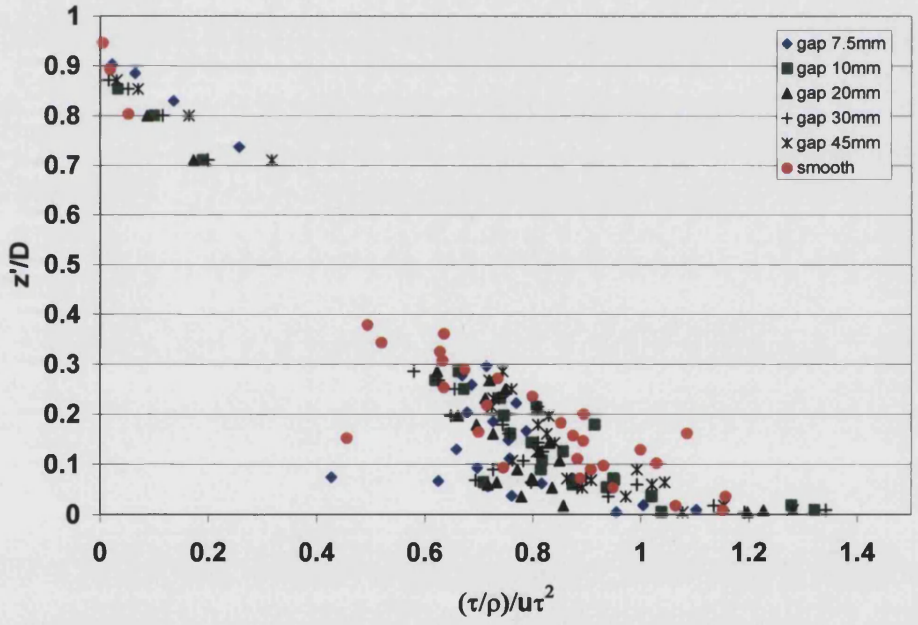

a) Bed shear stress profiles scaled by friction velocity (at S2)

Figure 5.15 Bed shear stress profiles a) dimensional b) scaled by friction velocity

5.3 Limits of the inertial sublayer

The boundary layer developed over a rough surface is comprised of an outer layer and a surface layer. The surface layer extends from the wall and constitutes of an inertial

sublayer, a roughness sublayer and a canopy layer. The inertial sublayer is the upper part of the surface layer, where both the "velocity defect law" and the "law of the wall" are simultaneously valid as was reported by Raupach et al. (1991).

The upper and lower limit of the logarithmic region (inertial sublayer) of the velocity profile depends on the type of flow and the wall roughness conditions as discussed in chapter 4. In the current tests the upper limit was identified from the outer region (velocity defect law) deviation from the logarithmic profile at the inflexion point as indicated in figure 4.4. The lower limit of the logarithmic region was established by comparison of the velocity profiles measured above the centre of a roughness element and above the centre line of the trough between two adjacent roughness elements. Stuart (1984) argued that when the two profiles appear to diverge the flow is affected by the proximity of the roughness elements. For this reason it would be incorrect to assume the existence of the standard logarithmic profile. Further away from the wall the two profiles converge at a value of z considered to be the lower limit of the inertial sublayer. Figure 5.16 shows the change in location of the inertial subrange for the different roughness conditions and thickness. The wake interference regime was associated with a relatively thicker logarithmic region at the upper limit. The reason for that is a rougher surface promotes vortex flow in the cavity between the roughness elements. The formation of subsequent vortices in the same cavity with increasing gap distance enhances its turbulence fluctuations. The lower limit of the logarithmic region was found least effected by the surface roughness.

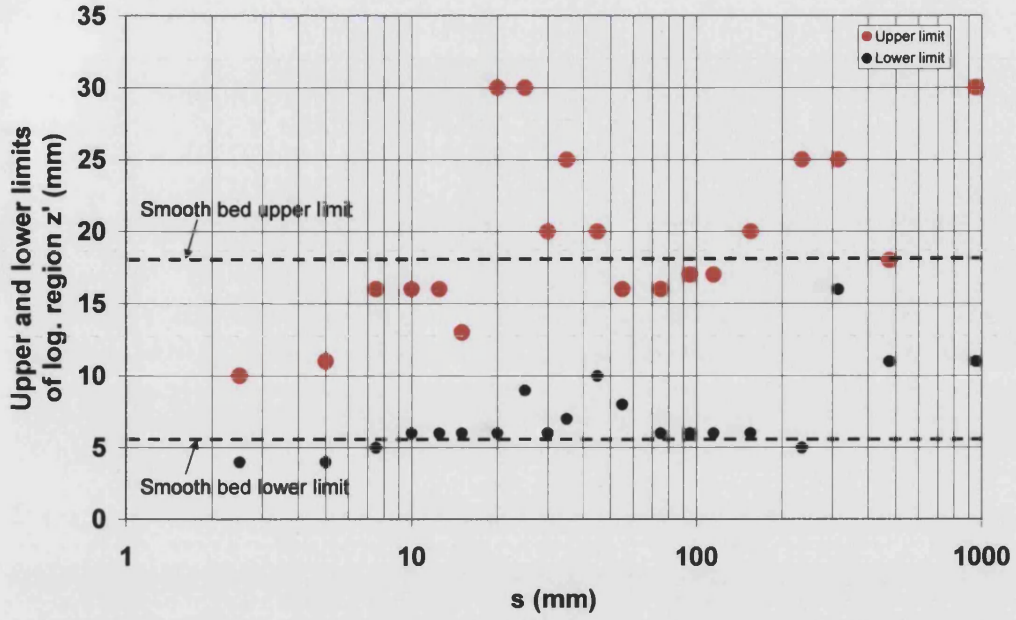

Figure 5.16 Limits of logarithmic region for profile measured at location S2

5.4 Frequency spectrum

An energy spectrum shows the distribution of total kinetic energy among eddies with different frequencies (corresponding to different scales). Results obtained for an open channel flow over roughness elements spaced at $s/k = 4$ was shown in figure 5.17a. The figure illustrates that the bulk of the turbulence energy occurs at low frequency motion (u-freq<4Hz). In the range of 2<u-freq<8, the curve has a slope of approximately -5/3. In the high frequency range, the slope is about –1/7. The peak frequencies and the associated mean velocity at the point were transformed into effective eddy length scales shown in figure 5.18. The trend from the results shows that the eddy size is higher than the flow depth and not naturally generated by the 2-d roughness but is due to the oscillation due to the pump feeding the channel.

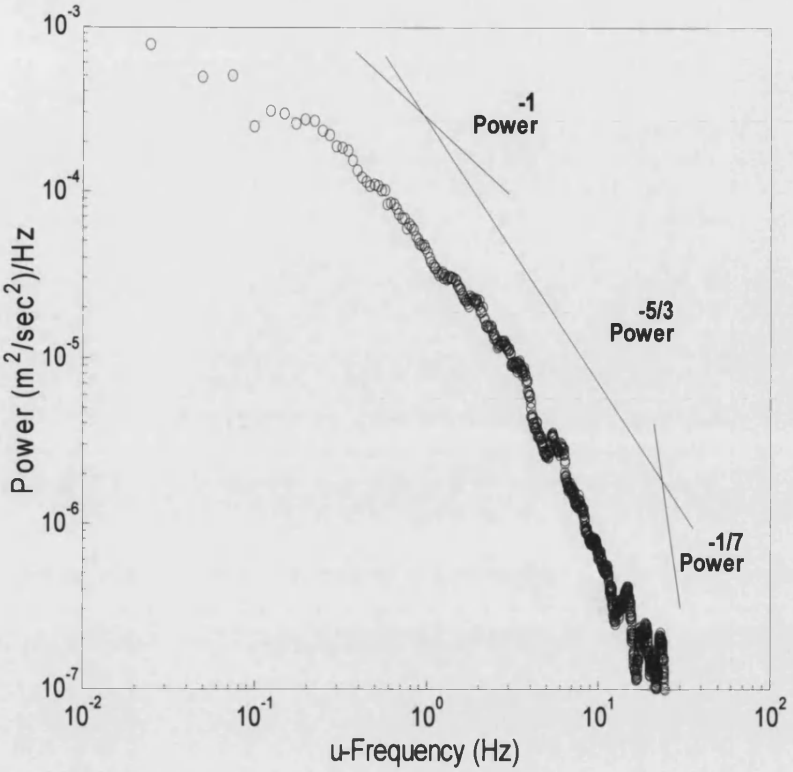

Figure 5.17 Logarithmic scale u-frequency spectra of turbulence for s/k=4 at z'=11mm from the top of slat at S2

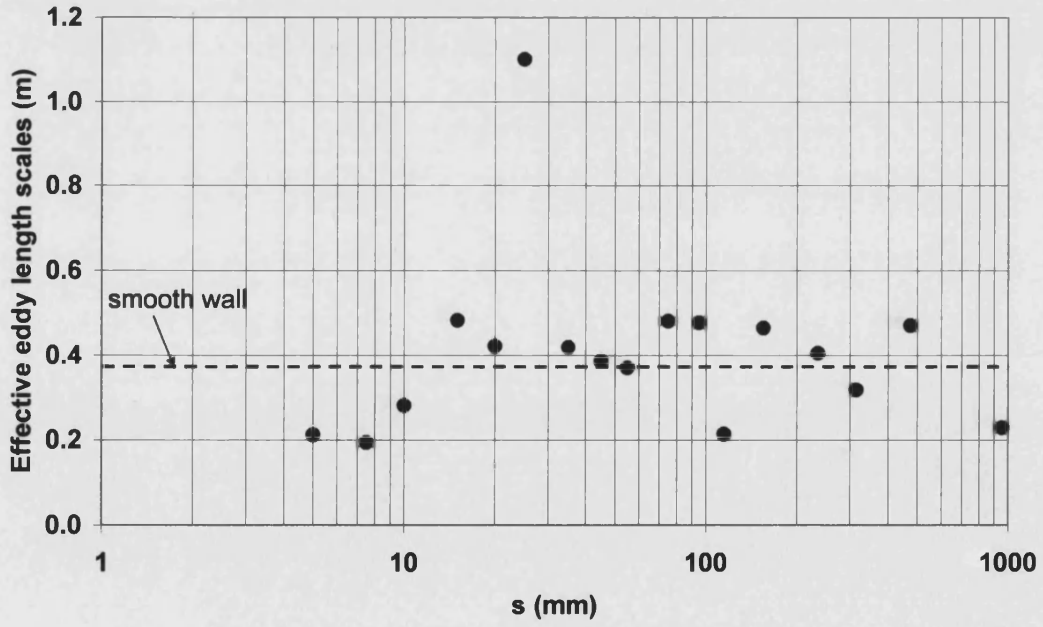

Figure 5.18. Effective eddy length scales in the logarithmic region at z'=11mm from the top of slat at S2

5.5 Turbulence fluctuations in the roughness sublayer

The turbulence fluctuations in the roughness sublayer are highly influenced by the surface roughness. The roughness sublayer is a region of spatial inhomogeneity where the different length scales of the surface geometry are important. The present experiments show that turbulence production and diffusion are significantly affected by the variation in gap distance between the roughness elements.

Jones (1968) discussed some results from field experiments in the atmospheric boundary layer and found that average turbulence intensities ($urms/u$) lie between 15 and 20 percent. He further explained that turbulence intensity is highly dependent on the surface roughness and atmospheric conditions. He reported 15% turbulence intensity for neutral conditions, whereas unstable conditions can increase turbulence levels by a factor up to five times that under neutral conditions. He further pointed out that at rougher sites this intensity can increase up to 22 percent. Owen (1964) in his field study found that turbulence intensity varied for open downland in comparison to measurements for a city. He found that turbulence intensity of 12.5 percent can occur at 15m above open downland in comparison to 33% measured on a roof 61m above a rougher urban surface.

For the present tests the turbulence intensities associated with the lower and upper limits of the roughness sublayer are shown in figure 5.19. This shows that the turbulence intensity has an increasing trend until the flow switches from wake to isolated roughness flow. The turbulence intensity at the upper end of the roughness sublayer retains a value of 20 percent of the local mean flow velocity for skimming flow. The reason for that is the bulk of the flow passes over the top of the roughness elements. When the flow starts behaving as wake interference flow, the turbulence intensity increases to 30 percent. On further increasing the spacing between the

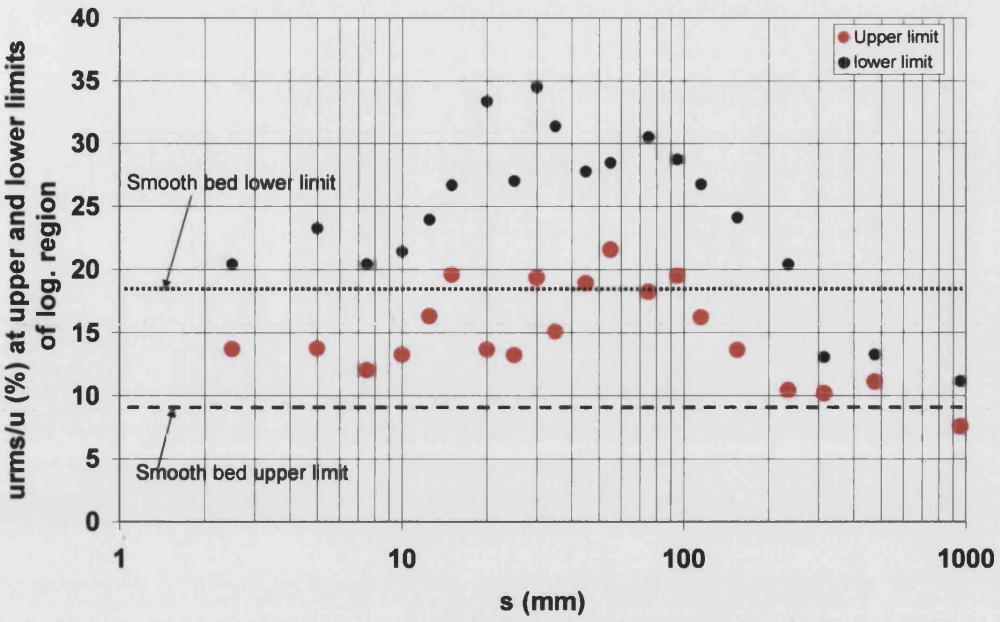

Figure 5.19 Turbulence intensity at upper and lower limits of logarithmic region

surface roughness elements, the flow moves into isolated roughness regime and the peak turbulence intensity starts decreasing.

It is quite clear from the above discussion that turbulence intensity in the roughness sublayer is affected by the violent interaction between the vortices formed in the cavity between the roughness elements and their periodic ejection and absorption of energy from the mean flow. This process extends the thickness of the logarithmic region upwards into the main flow.

5.6 Mean flow characteristics

5.6.1 Shift in logarithmic origin for profiles midway between roughness elements (S2)

The shift determined from the logarithmic origin, ε, relative to the top of the roughness elements is shown in figure 5.20. It is evident from the figure that the origin of the log profile is approximately level with the tops of the roughness elements equal to the height of the roughness element for skimming flow regime. This move

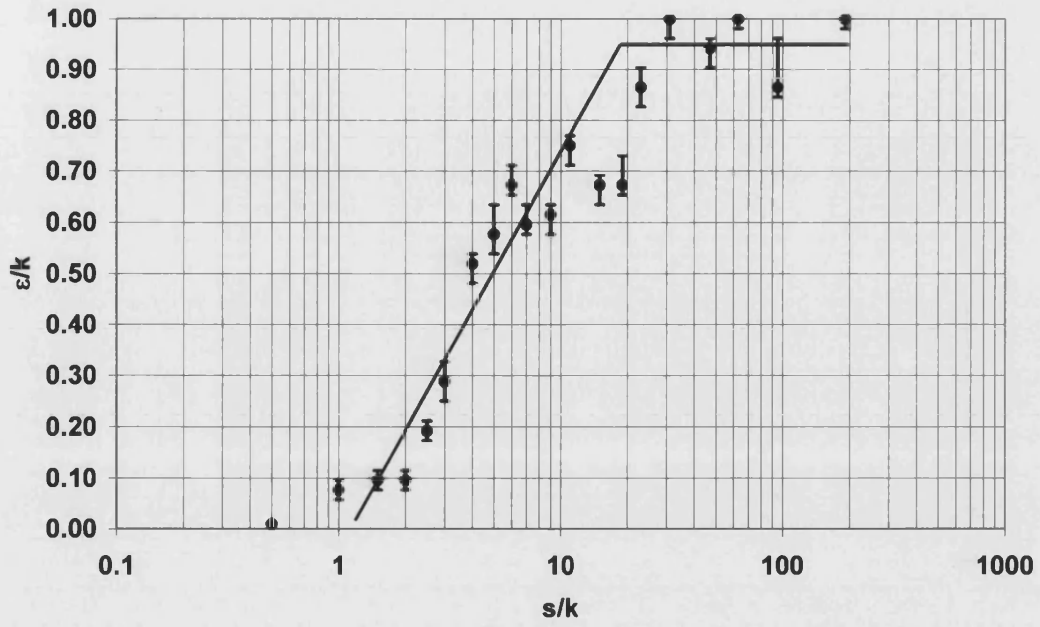

Figure 5.20 Shift in origin of logarithmic mean velocity profile (at location S2)

lower as the gap distance between the slats increases, and lies at the base of the cavity for isolated roughness.

5.6.2. Von Karman Constant

The Karman constant κ was determined from the logarithmic mean velocity profiles

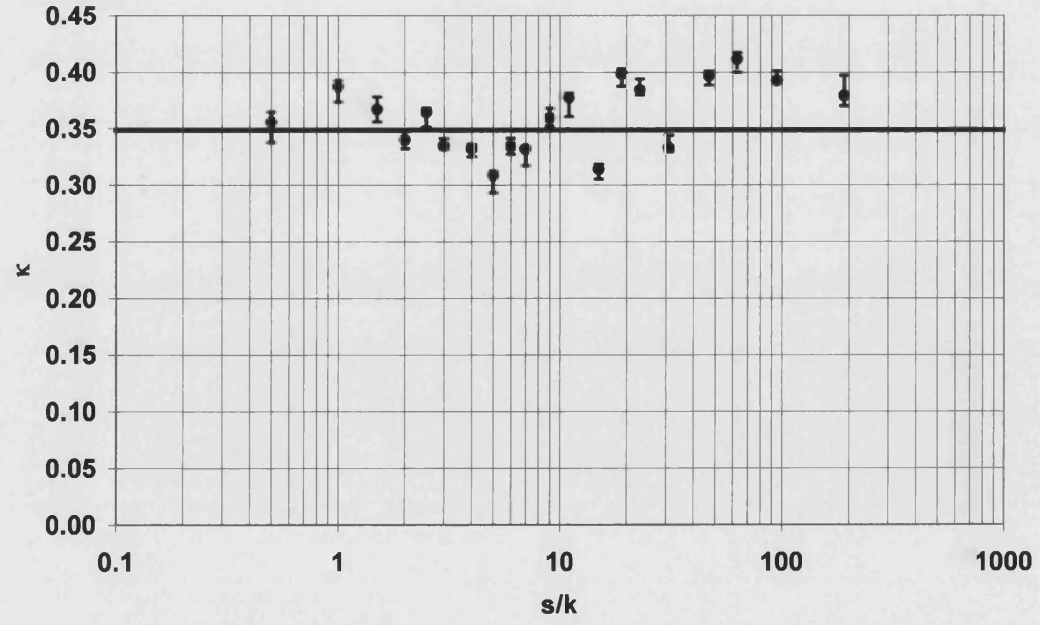

Figure 5.21 Variation of Karman constant

and found to vary randomly between 0.31 to 0.41 as shown in figure 5.20. The average value of kappa for the current tests was found to be 0.35, in good agreement with previous flume studies and close to the conventionally accepted value of approximately 0.4.

5.6.3 Roughness length Scales

The experimentally estimated roughness length scales z_0 have been plotted against the gap distance between the roughness elements in figure 5.22a, b. The boundaries for the flow regimes (skimming, wake interference flow and isolated roughness flow) discussed in section 5.1 are classified on the basis of the corresponding length scales. Townsend (1976) discussed a connection between the diffusion and the supply of energy to the turbulent motion is a fundamental characteristic of turbulent flow. The similarity between the trend shown by the roughness length scale and the rate of turbulence energy production at $z''=5mm$ is shown in figure 5.23. When the flow switches from skimming to wake interference flow there is a violent interaction between the vortices formed between the roughness elements. These vortices are periodically ejected into the mean flow where they absorb energy by vortex stretching. This all serves to promote and enhance the outward diffusion process of momentum and passive contaminants including pollutants trapped in city street canyons. This phenomenon is of great physical importance in public health engineering and in urban planning when designing street and open spaces. The comparison of the roughness length scale from current tests on 2-d slat type bed roughness (figure 5.24) with tests on 3-d cubical roughness is shown in figure 5.25. The results from Macdonald et al. (1998) compares quite well with the current tests. An attempt is made to compare the 2-d characteristics of the roughness elements with

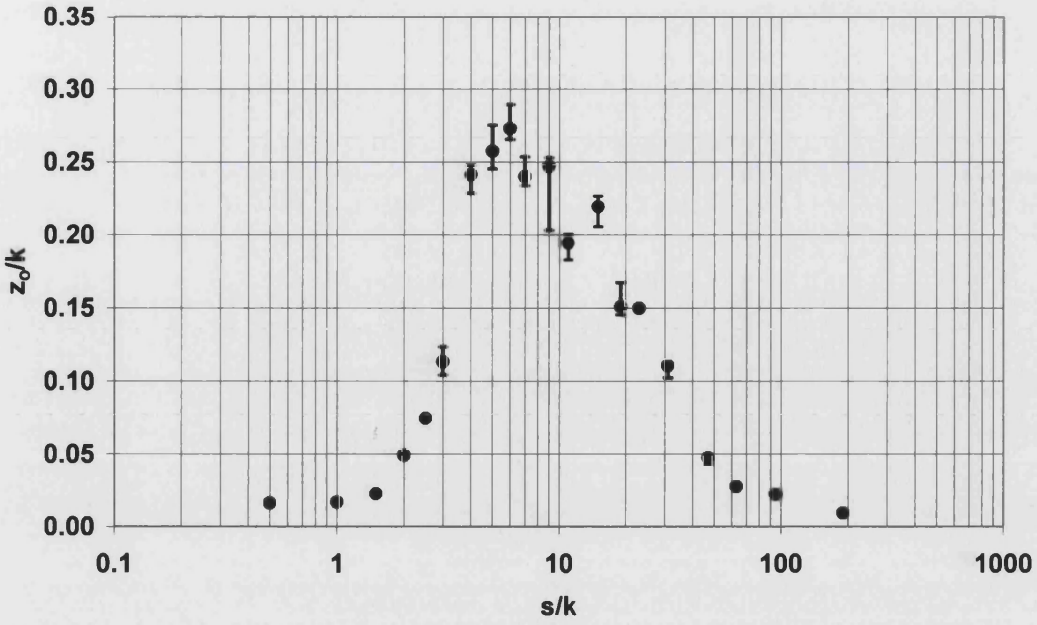

a) Variation in roughness length scale as a function of gap distance

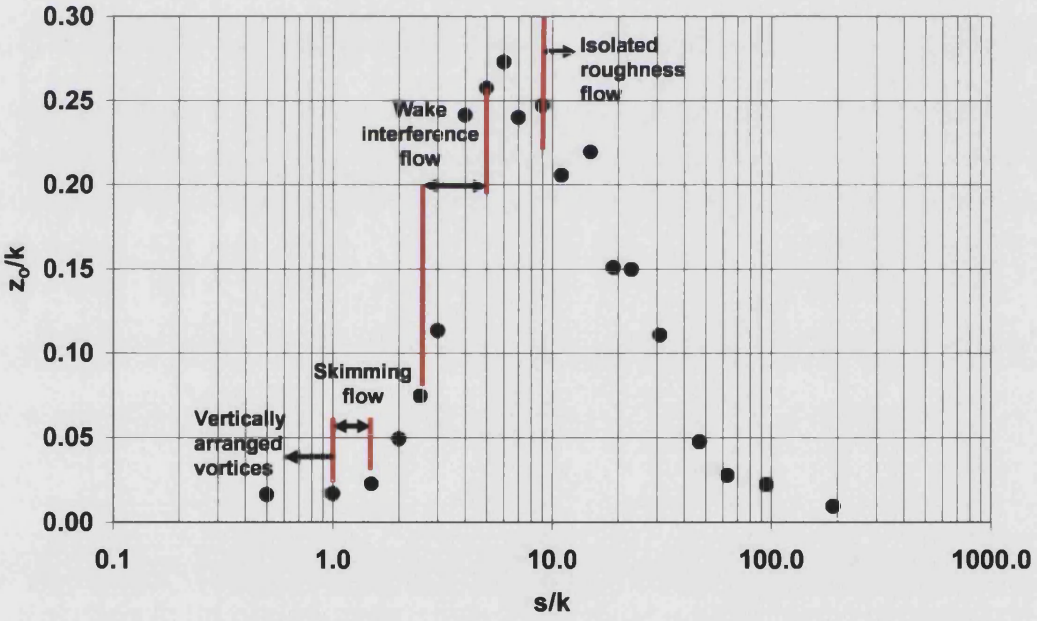

b) Variation in roughness length scales as a function of s/k

Figure 5.22 Effect of varying gap distance on roughness length scales a) dimensional b) non dimensional

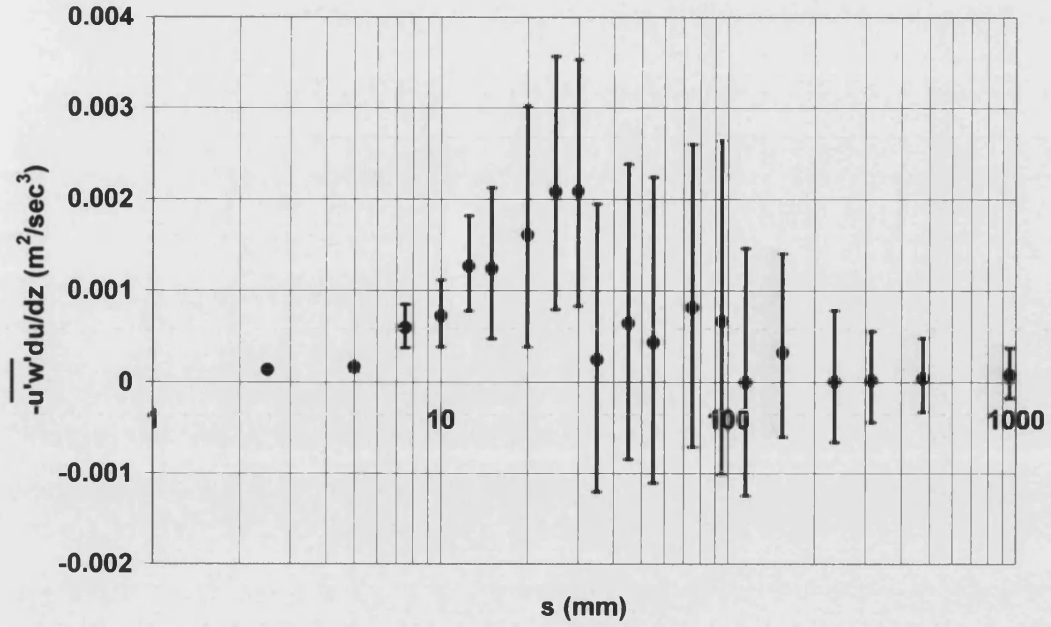

a) Variation in turbulence energy production at position S2

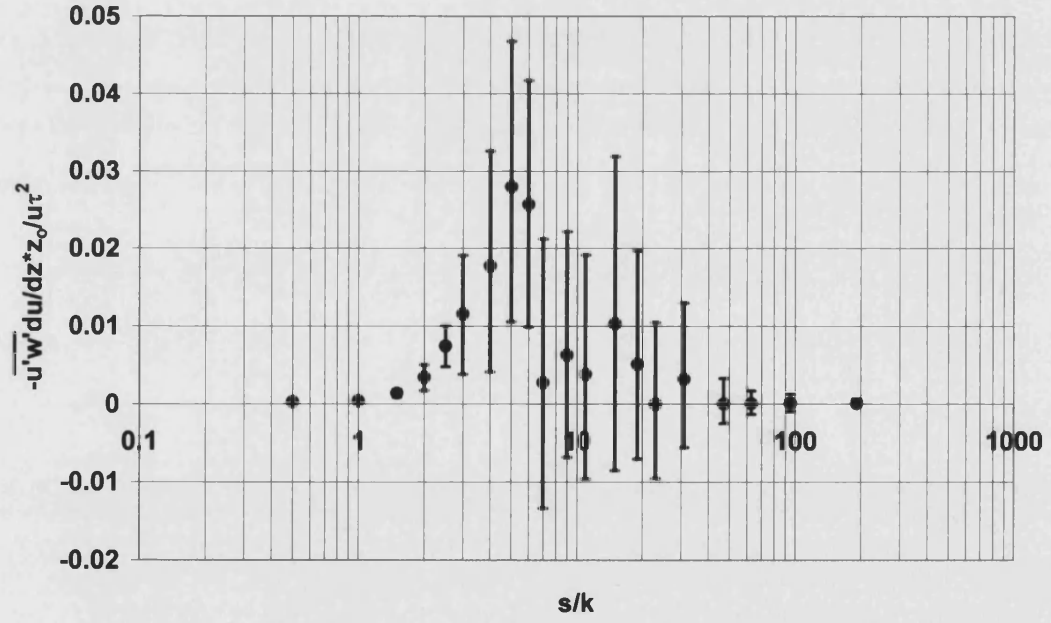

b) Variation in turbulence energy production at position S2

Figure 5.23 Turbulence production at z''= 5mm for varying gap distance between slats a) dimensional b) scaled by roughness length scale and friction velocity

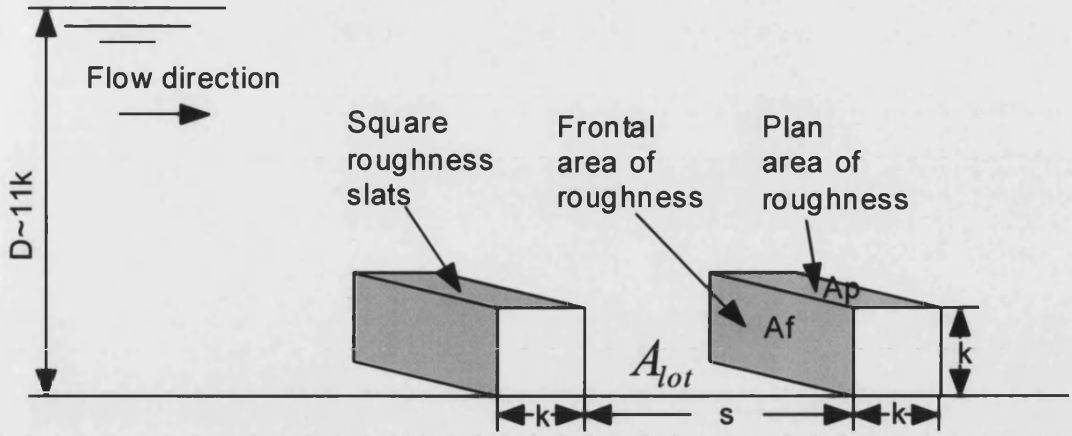

$$\lambda_d = \lambda_f = \lambda_p = \frac{k}{s+k}$$

Figure 5.24 Roughness density parameter for 2-d square slat roughness

the 3-d characteristics of London. Ratti et al. (2004) characterised the roughness of the ground for London. The surface roughness was reported to be calculated by Digital Elevation Modelling. The average height of the buildings for London was estimated as 13.6m and its ratio plan area (λ_p) and frontal area (λ_f) reported as 0.55 and 0.32 respectively. Based on this information, figure 5.26 shows the roughness length scale have obtained for London. It can be seen that corresponding roughness length scale varied from 0.26m (for λ=0.55) to 0.875m (for λ=0.32). From the comparison of the results with Ratti et al. (2004), λ_p was found a dominant parameter which gave a roughness length scale of 0.23m from 2-d roughness and compares closely with the 0.30m estimation for London. The flow pattern associated with the length scale of 0.26m is associated with a skimming flow pattern. However, if the density range is considered from λ_d=0.32 to 0.55, the flow pattern would be found in transition from skimming to wake interference flow.

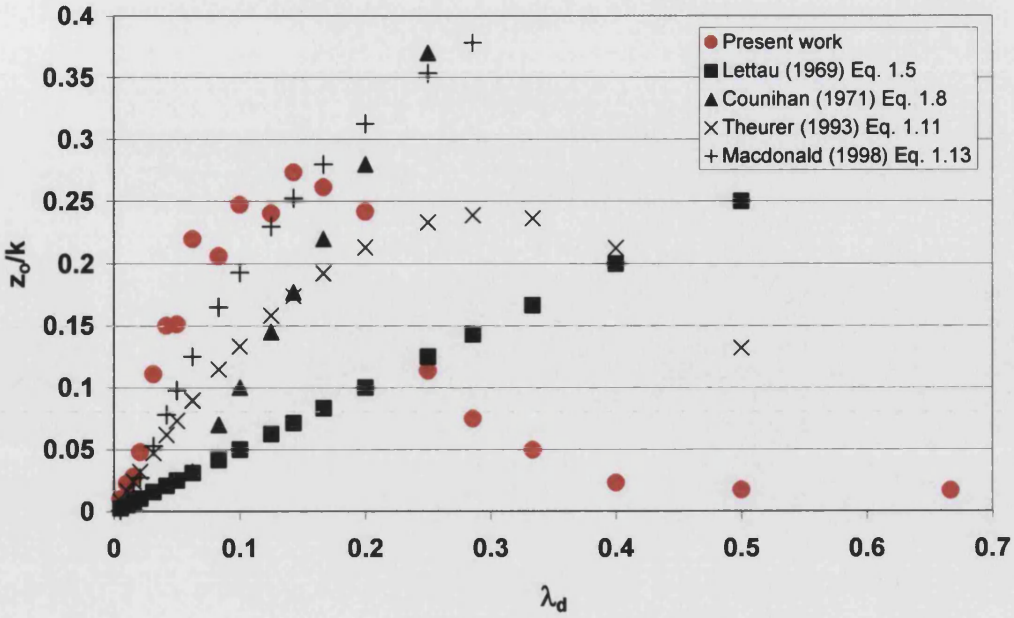

Figure 5.25 Comparison of roughness length scale with others

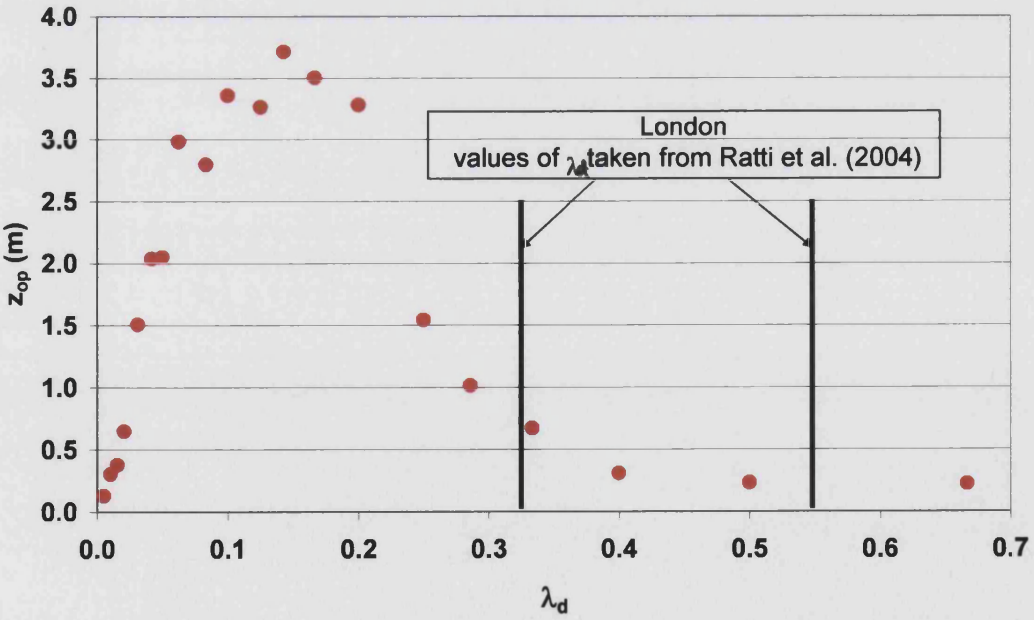

Figure 5.26 Roughness length scale for London

5.6.4 Friction velocity

Dimensional analysis shows that the friction velocity is the characteristic velocity for the mean flow and turbulence velocity fluctuations. Knowing the flow pattern between the slats for a particular gap distance, it is evident that friction velocity increases as the surface roughness increases. The flow was found to have maximum friction velocity when the bed roughness slat spacing ratio coincided with the previously identified and described isolated roughness configuration. This is illustrated in figure 5.27a.

A non-dimensional friction factor ($\frac{\tau_{wall}}{\frac{1}{2}\rho\bar{u}^2}$) has also been calculated (figure 5.27b) from the direct measurements using the depth average velocity by integrating the mean velocity profile (S2).

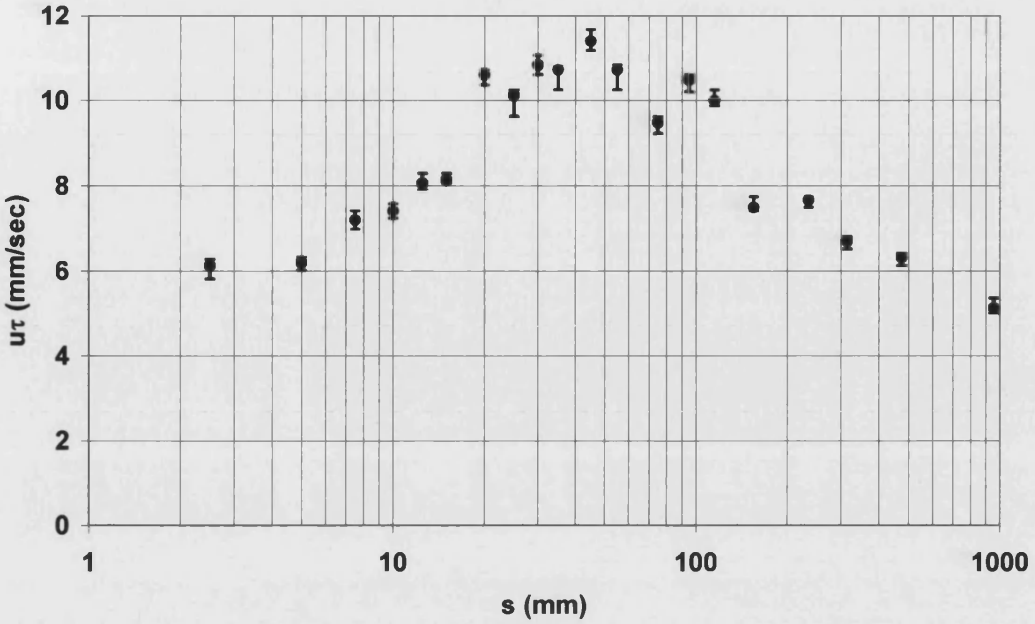

a) Friction velocity as a function of gap distance

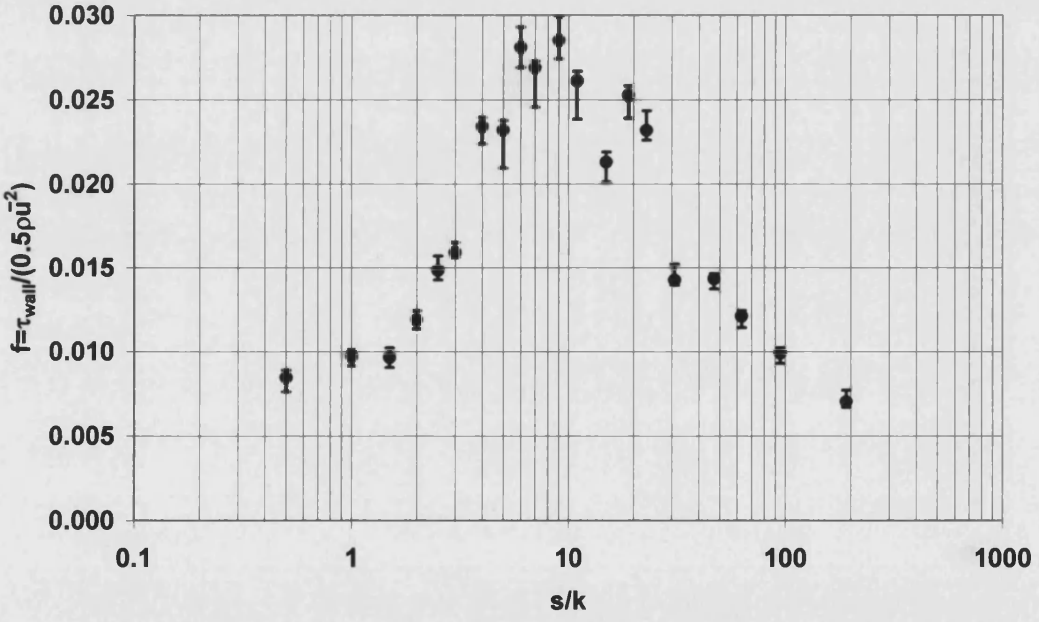

b) Friction factor as a function of s/k

Figure 5.27 Effect on friction by variation in gap distance a) friction velocity b) friction factor

5.7 Mixing length scales

5.7.1. Rate of turbulence production in boundary layer

The rate of turbulence production in the boundary layer is estimated from the Reynolds stress and the velocity gradient. It is seen in figure 5.28a, that the change in roughness spacing has an effect on the turbulence production in the boundary layer. Turbulence production is normalised by the roughness length scale and friction velocity in figure 5.28b. It is seen that maximum turbulence production was for roughness spaced $s/k = 6$.

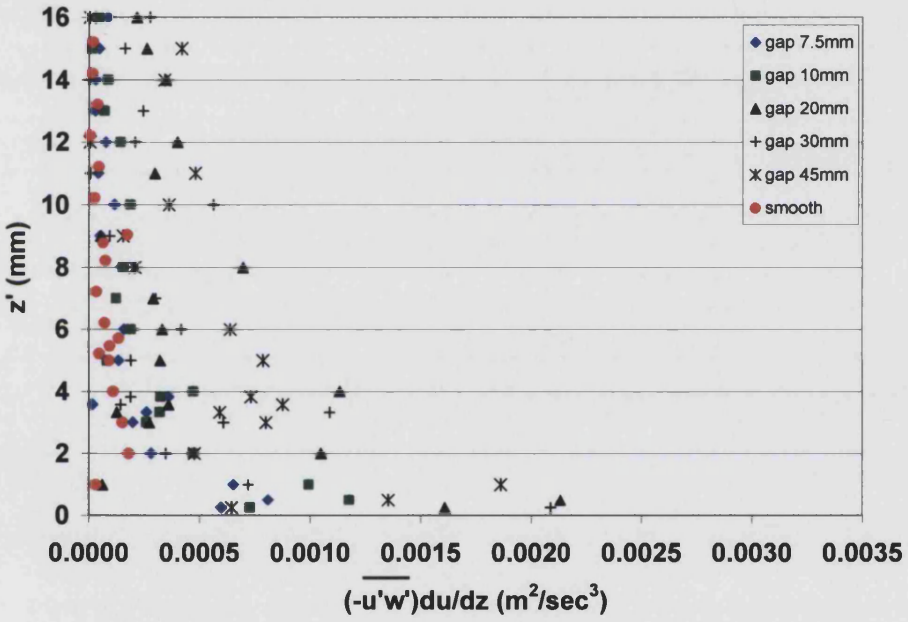

a) Turbulence production as a function of z'

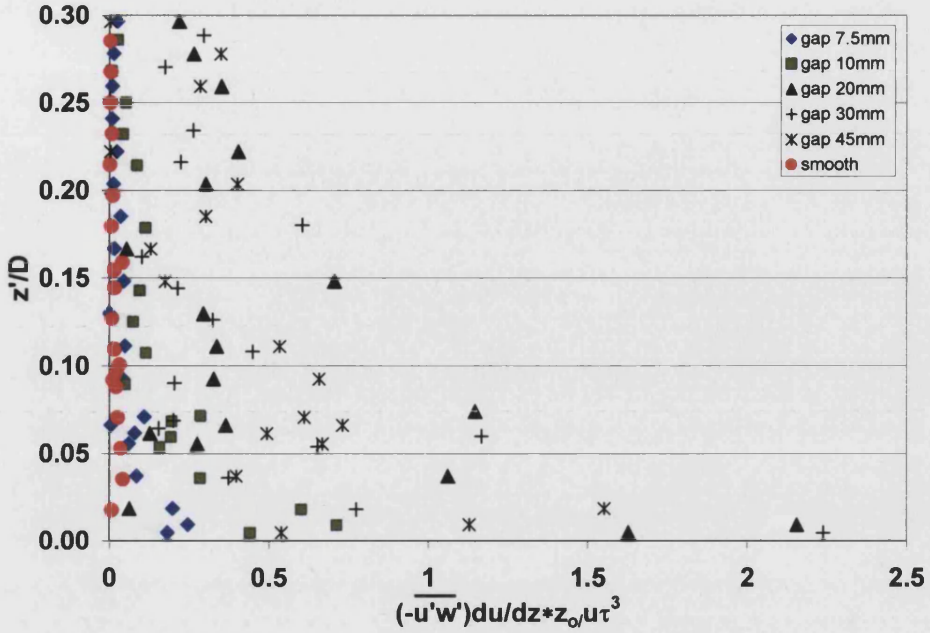

b) Turbulence production as a function of z'/D

Figure 5.28 Rate of turbulence production in the boundary layer a) dimensional b) scaled by roughness length scale and friction velocity

5.7.2 Mixing length scales and turbulence diffusion coefficient

In this section the results have been plotted in terms of Prandtl's (1925) mixing length theory (figure 5.29). From the discussion in section 5.2, it was found that the major contribution to bed shear stress comes from the Reynolds stresses. The defining equation for mixing length l is obtained by,

$$\frac{\tau_{wall}}{\rho} = l^2 (\frac{du}{dz})^2 \qquad (5.1)$$

In Prandtl theory, expressions for u' and w' are obtained in terms of a mixing length distance l and the velocity gradient $\frac{du}{dz}$, where u is the temporal mean velocity at a point and z is the distance normal to the wall.

The mixing length scales in figure 5.29 were estimated using the distance above the top face of the roughness slats. They show the changes in l for a smooth surface

through skimming flow and wake interaction to isolated roughness conditions for the 2-d slat roughness. For a smooth surface, close to the wall, turbulent shear stresses reduce and therefore the turbulence length scales are also reduced. In contrast, over the rough surface, there is no decrease in the turbulent shear stress close to the top of the roughness and the flow was found associated with increasing roughness length scale z_o. Consequently, the mixing length scales were found to increase as the surface became rougher. A straight line fit through the smooth surface length scales gives the empirical relationship, $l = 0.2z$, which appears unrealistic in comparison to the value of kappa estimated as 0.34 for the smooth surface tests. For a rough surface the length scales were widely scattered, but better described by a parabolic distribution. However, an attempt to fit a straight line for tests with gap to height ratio (*s/k*) from 4 to 9 was found to give, $l = 0.4z$, which is in reasonable agreement with the value of kappa found from the earlier analysis of mean velocities and Reynolds stresses.

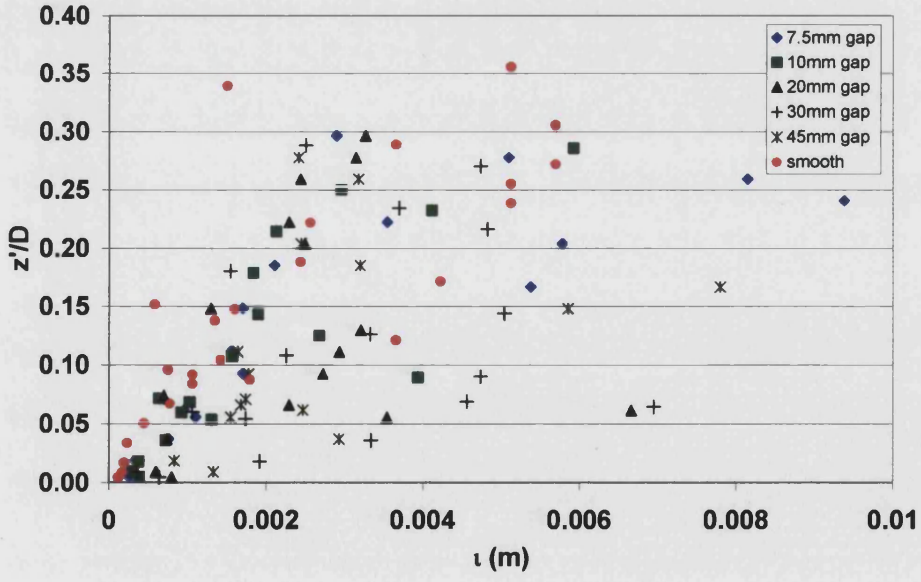

Figure 5.29. Mixing length scale for varying gap distance between slats

The turbulent diffusion coefficient "Cd" is not a material property of the fluid (unlike the coefficient of molecular diffusion) but depends upon the character of the turbulence. It can be expressed in the dimensional case as:

$$Cd = \upsilon_w + V_T \tag{5.2}$$

where υ_w is the kinematic viscosity of water and V_T is the turbulent viscosity. Sloadvik et al. (2004) reported the turbulence model which is employed for estimation of turbulent viscosity is:

$$V_T = l^2 \sqrt{(\frac{du}{dz})^2 + (\frac{dw}{dz})^2} \tag{5.3}$$

Figure 5.30 illustrates that the turbulent diffusion, Cd, near the wall increases as the surface roughness increases. Taking kinematic viscosity of water to be 1.004e-6m^2/sec, at roof level (position S2) the ratio of turbulent diffusion coefficient to molecular diffusion coefficient varied from 3 for skimming flow, to 9 for wake interference flow and 11 for isolated roughness flow regimes.

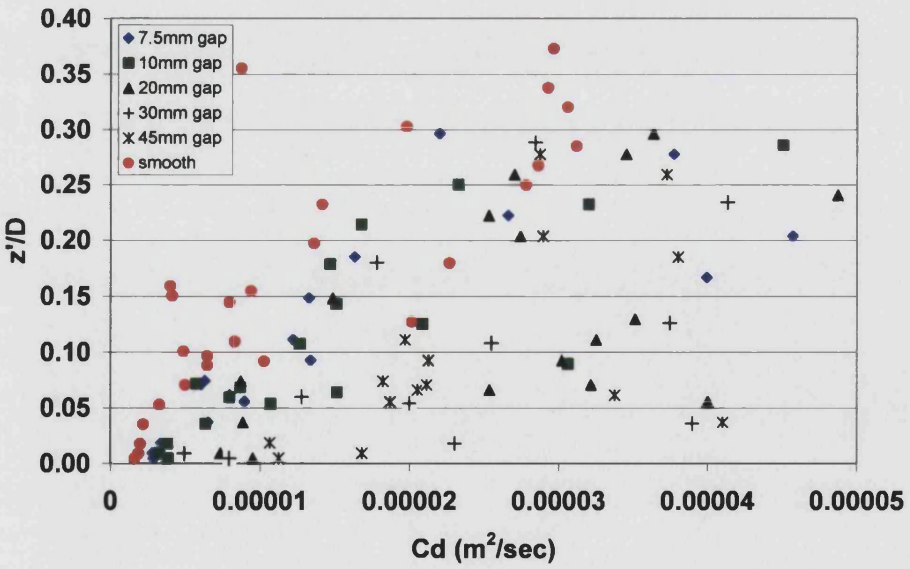

Figure 5.30 Turbulent diffusion coefficient for varying gap distance between slats at S2

5.8 Ejection to sweep ratios in the log region

In this section an attempt is made to study the turbulence in the logarithmic region at $z' = 11mm$ for the various different wall conditions. The fluctuations in the velocity were distributed in four quadrants (figure 5.31a, b) using the method introduced by Lu and Willmarth (1973). Two set of analysis were carried out, one with a hyperbolic hole H=0 and other with hyperbolic hole H=1 to estimate the ejection and sweep stresses for the rough surface compared with the smooth bed case at $z'' = 6mm$ from the wall. The ratio between ejections (quadrant 2) and sweeps (quadrant 4) was plotted in figure 5.32. It is evident from the illustration that high sweeps were observed over smooth wall case in comparison to ejections from skimming, wake interference and isolated roughness flows in the inertial layer.

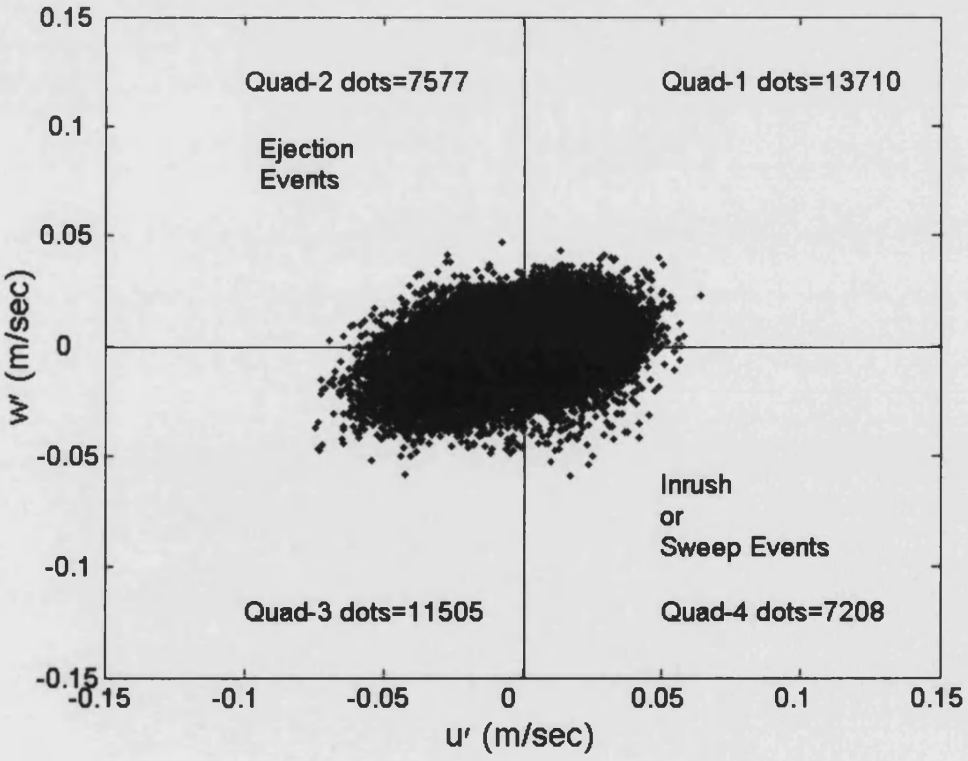

a) H=0

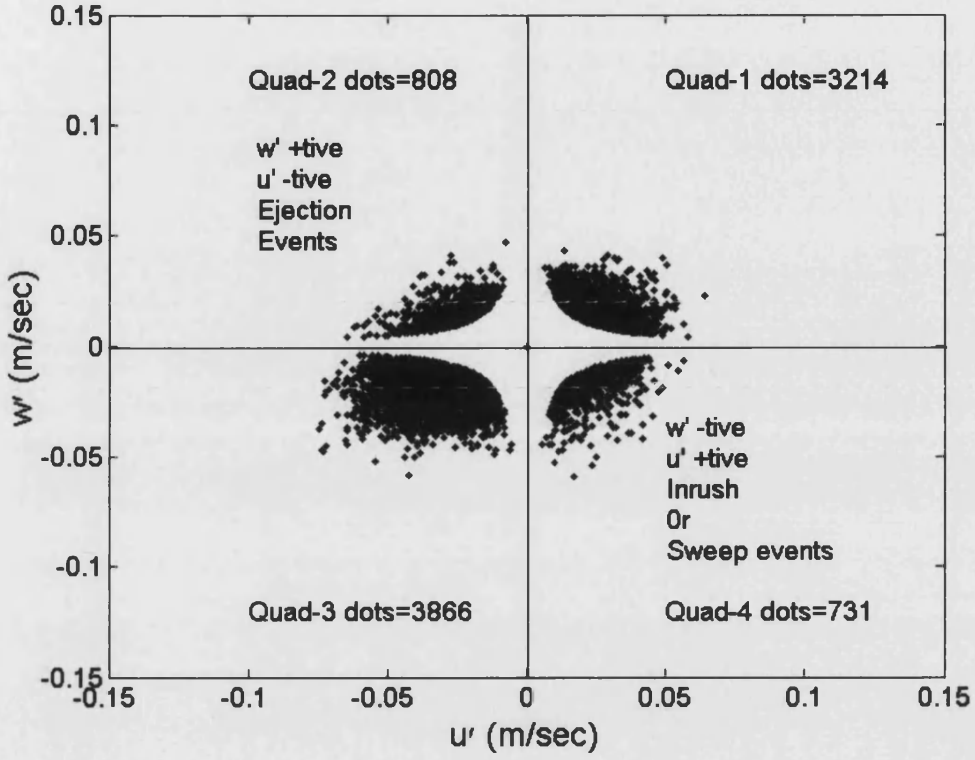

b) H=1

Figure 5.31 Quadrant decomposition of Reynolds stresses in log region at 11mm from top of roughness a) H=0 b) H=1

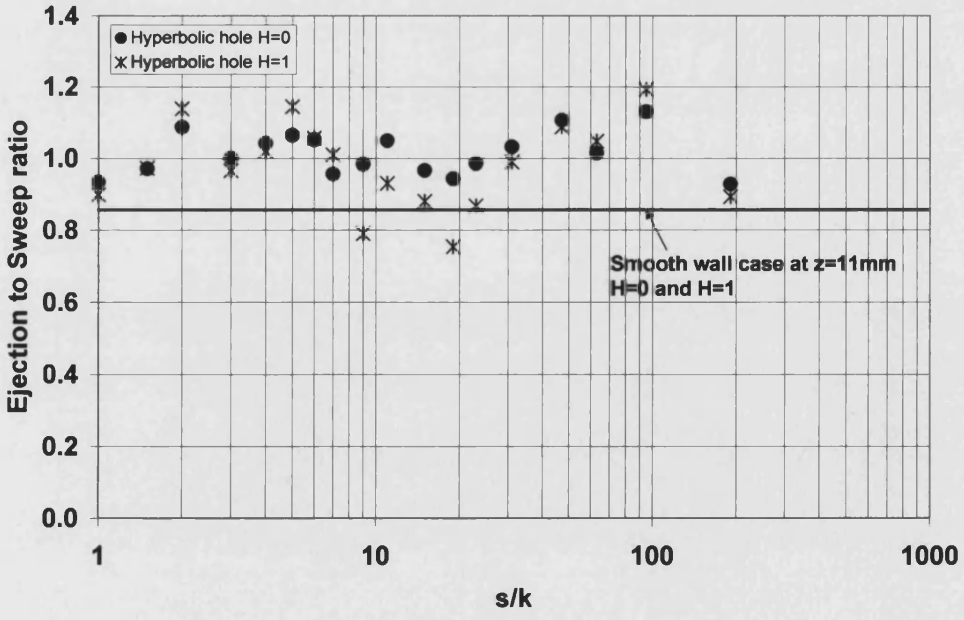

Figure 5.32 Variation in ejection to sweep ratios at $z' = 11mm$ (in the logarithmic region)

5.9 Transition between flow regimes

In this section three regions of transition are discussed, where the flow regimes switch from one to another. A comparison is made with the corresponding length scales estimated experimentally.

5.9.1 Transition from vertically arranged vortices to single vortex in gap between slats

In a city centre it is often the case that the gap distance between buildings is quite narrow. To investigate this case the flow dynamics inside a narrow cavity with $s/k = 0.5$ are illustrated in figure 5.33a, b. This is equivalent to $\lambda_d = 0.67$; London is reported to have values of λ_d in the range 0.32 to 0.55. From the flow visualization it was found that two zones are interacting inside the cavity. The lower one is relatively stagnant and the transport of dye from this region was found to be dependent on the vortex above it inside the cavity. This vortex was comparatively active, extracting energy from the mean flow and transporting it to the bed. The zero plane displacement height for this flow behaviour was found experimentally equal to the height of the roughness element.

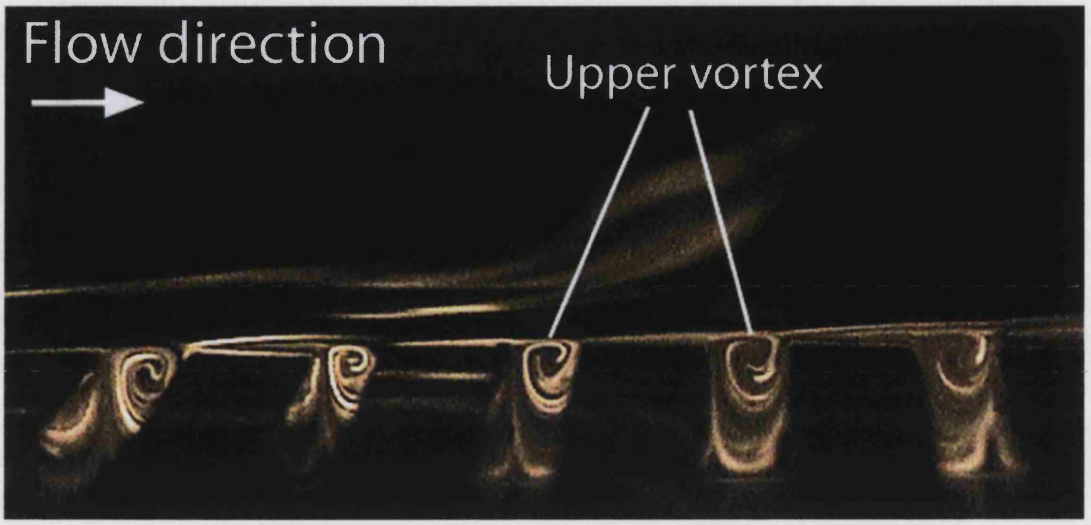

a) Flow visualisation for a gap distance s/k=0.5

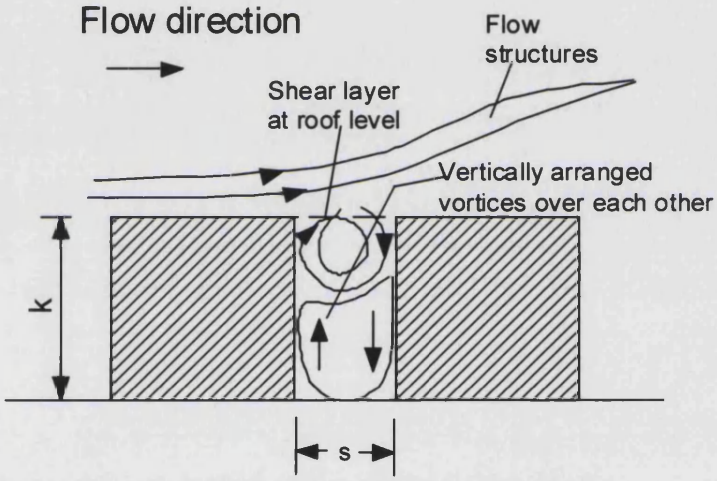

b) Vertically arranged vortices for a gap distance s/k=0.5

Figure 5.33 Vertically arranged vortices in a narrow gap between slats a) dye visualisation for gap distance s/k=0.5 between slats b) schematic

5.9.2 Transition from single vortex to two vortices in gap between slats

Continuing further the discussion in section 5.1, the flow regime has been confirmed from the roughness length scales in figure 5.22a, b to move to transition at $s/k = 2$. The flow pattern inside the cavity for a 10mm roughness spacing was found un-organized i.e. the vortex was unable to fill the whole cavity and started to act as a

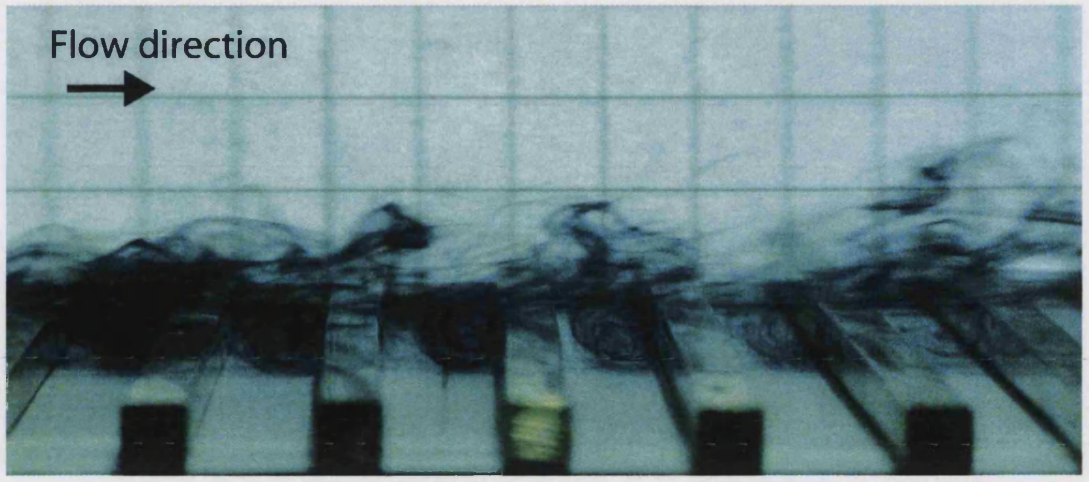

a) Transition between skimming and wake interference flow

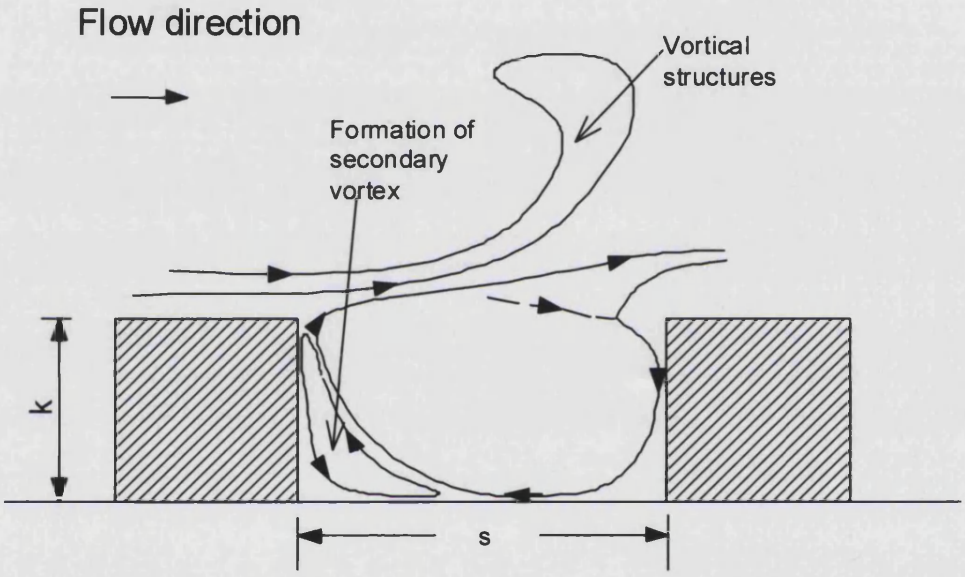

b) Transition vortex formation

Figure 5.34 Critical value of gap spacing s/k=2 between skimming and wake interference flow

three dimensional vortex liable to be ejected into the main flow (figure 5.34a, b). The experimentally calculated length scale and friction velocity for $s/k = 2$ shown in figures 5.22b and 5.27b, confirm that z_o and f are higher than for skimming flow indicating a new flow regime in the cavity. Regarding the ventilation characteristic of the cavity and looking back to figure 5.6, it is illustrated that the plume width inside

the cavity is similar for injector *dl* and *ul*. It is therefore proved that the formation of the secondary vortex has a significant impact on the ventilation of pollutant produced at the upstream corner of the cavity.

5.9.3 Transition from two vortices to multiple horizontal vortices in the gap between roughness elements

Looking at the calculated roughness length scales (figure 5.22a,b) for the various rough bed geometries, it was found that z_o increased very rapidly for gap distances between 12.5mm and 25mm. The flow dynamics inside the cavity for a 30mm gap distance were at a critical value, behaving alternately as wake interference flow and isolated roughness flow. Figures 5.35, 5.36a show the intermittent absence of the downstream vortex, because of which the dye seeps against the flow direction toward the upstream vortex. The upstream vortex was found more stable and was seen to expand and contract at its position and allow the interaction with the downstream flow. Figures 5.35, 5.36b shows the flow with the downstream vortex present acting independently and able to eject pollutant from the cavity. Figure 5.35, 5.36c show the mutual interaction of the upstream and downstream vortices. This evidence supports the concept that $s/k = 6$ was a critical value between wake interference flow and isolated roughness flow.

The behaviour of the cavity plume width plotted in figure 5.6 provides the evidence that the injector in the direction of the flow (*dl*) is more efficient from the pollutant ventilation point of view than the injector facing against the flow direction (*ul*). This is because the flow has the properties of wake interference flow and as well as isolated roughness flow.

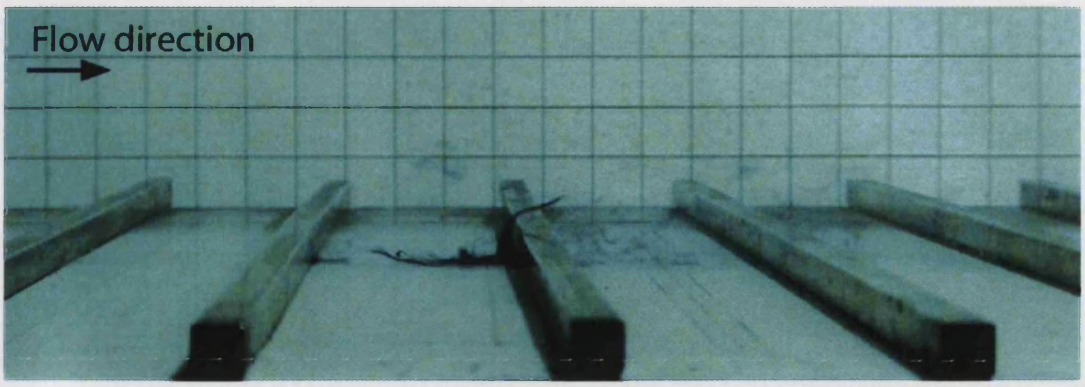

(a) Dye seeping upstream

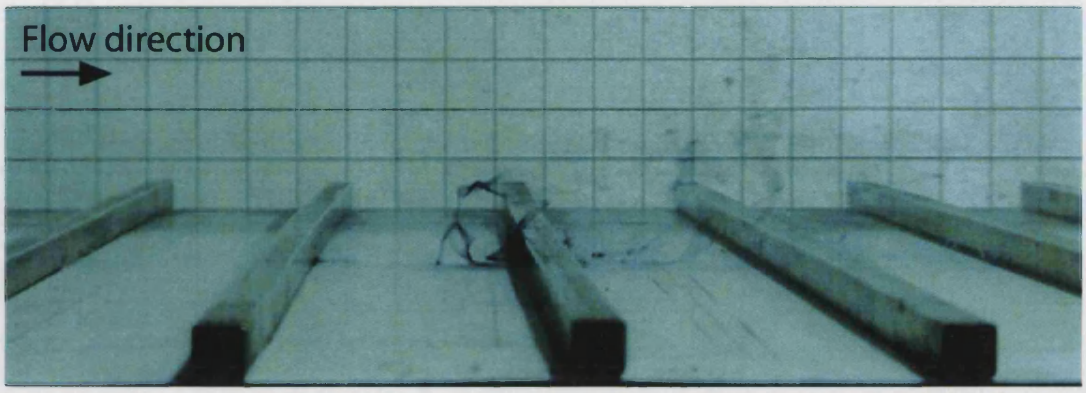

(b) Downstream vortex trapped the dye

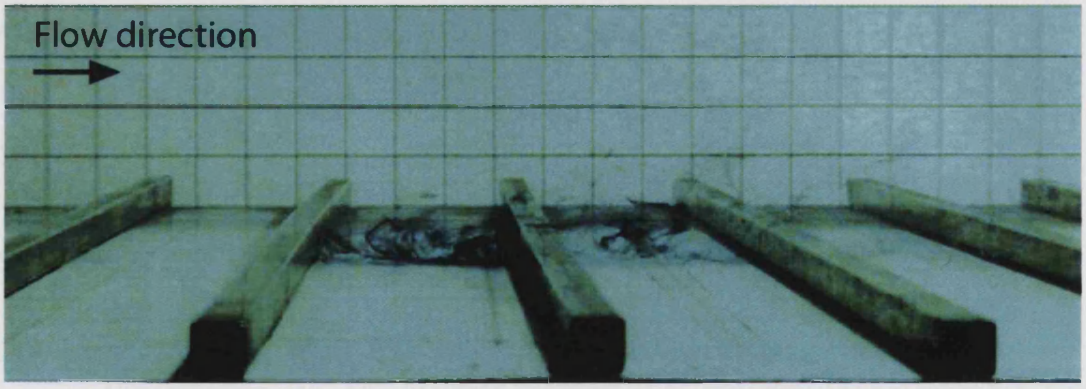

(c) Horizontally arranged vortices diffusing dye

Figure 5.35 Critical region between wake interference and isolated roughness flow at gap distance s/k=6 a) dye seeping upstream b) dye trapped in the downstream vortex c) horizontally arranged vortices inside the gap between the slats

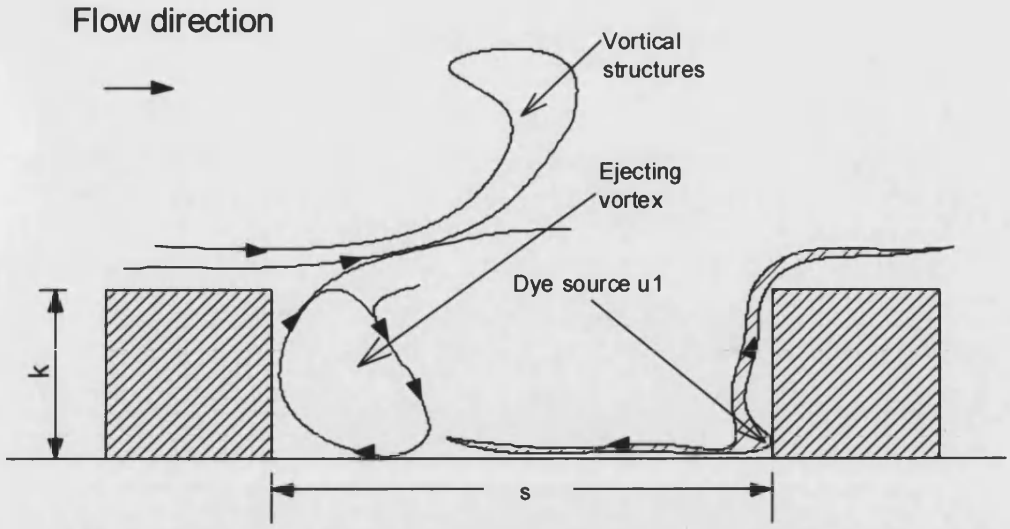

a) Absence of downstream vortex promoting suction from downstream

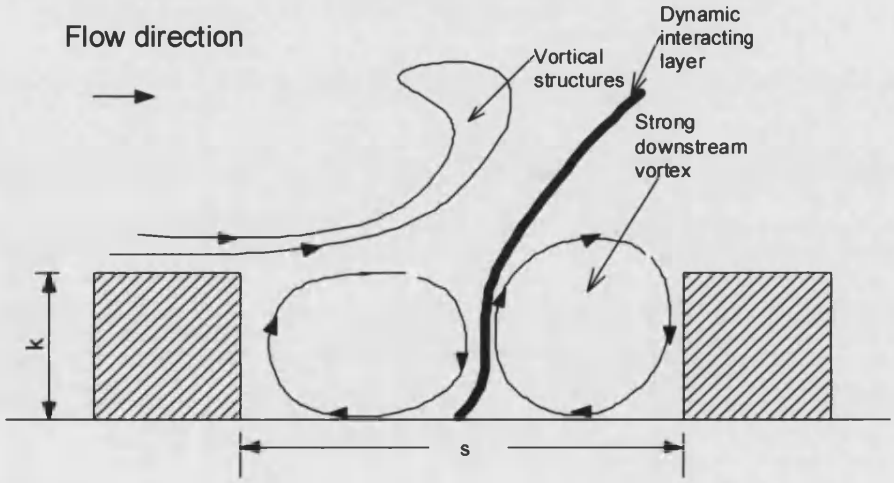

b) Presence of downstream vortex

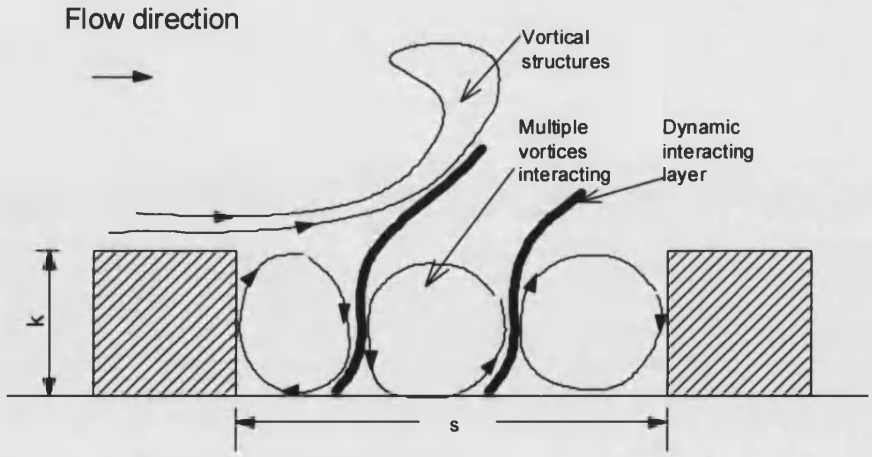

c)Horizontally arranged vortices mixing the flow

Figure 5.36 A schematic of three possible flow patterns for critical gap distance s/k=6; a) absence of downstream vortex b) presence of downstream vortex c) multiple horizontal vortices

5.10 Effect of roughness spacing on dye diffusion

Initial tests were conducted to study dye diffusion on the water surface for a range of different wall roughness spacings. The dye was introduced 3m downstream of the flume inlet, using a specially designed feeder having a nozzle diameter of 2mm and a cylinder 3mm high, in order to ensure test reproducibility. The dye diffusion on the water surface behaved differently for a narrow gap ($s/k = 1.5$) in comparison to a widely spaced ($s/k = 9$) shown in figure 33(a,b).

The vorticity observed on the water surface was found to be more organised for $s/k = 1.5$ in comparison to $s/k = 9$. Another important characteristic was the increased mixing in the case of the larger gap distance. The diffusion structure shows that there is a stronger interaction and mixing between the flow structure for a larger gap distance than for the narrow gap case.

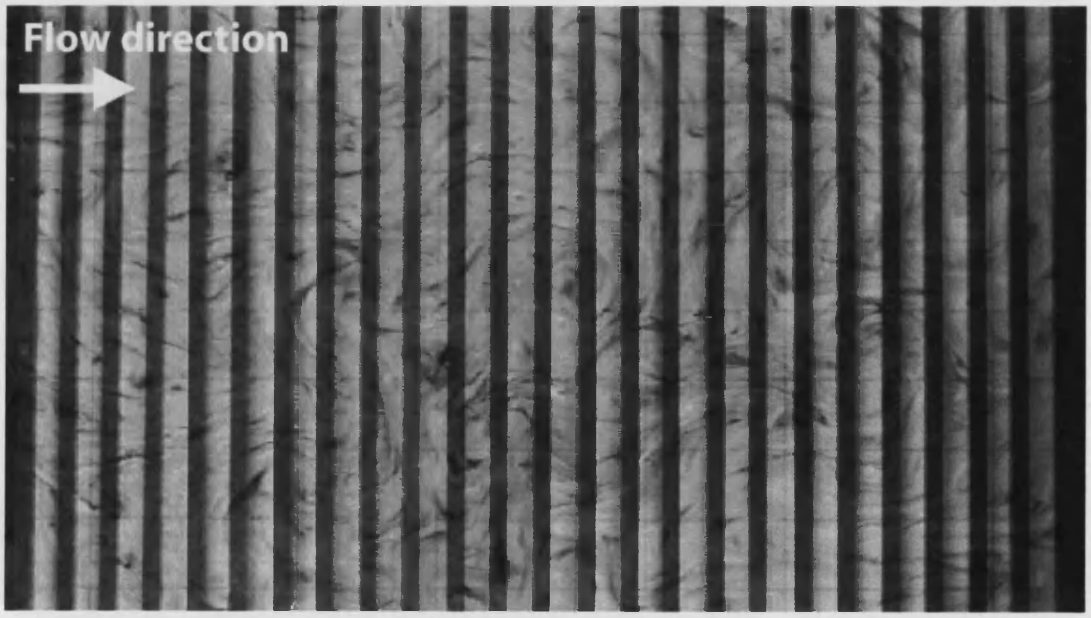

(a) Systematic structure of dye diffusion on water surface for gap distance between slats s/k=1.5

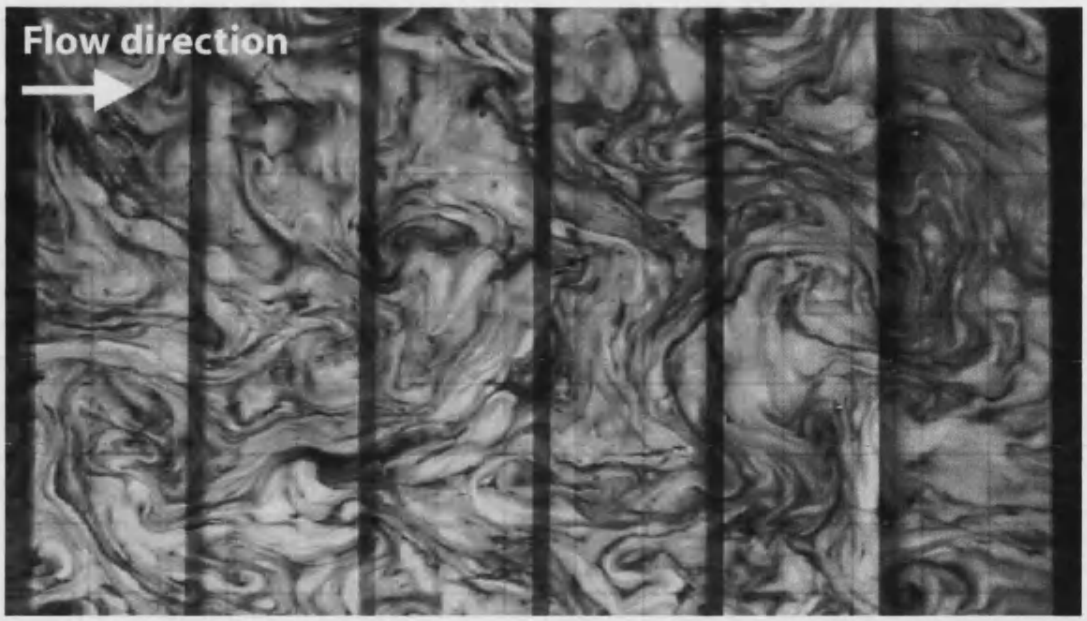

(b) Strong mixing of dye diffusion on water surface for gap distance between slats s/k=9

Figure 5.37 Diffusion of dye on water surface at 3m distance from the introduction of dye at channel inlet for gap distance between the slat a) s/k=1.5 and b) s/k=9

The point injectors were used to introduce dye at the test section for the assessment of horizontal and vertical diffusion. This has been sketched from the average position of the diffusion plume based on visualisation in the x-z and x-y planes. Measurements in the x-z plane were made against a scaled grid, 10mm square, on the back wall of the channel. The second grid, 25mm square, was drawn on white fablon adhesive plastic sheeting and used for measurements in the x-y plane. This was placed on the surface of the glass plate.

5.10.1 Dye plume observations in the x-z (streamwise-vertical) plane

Dye released from the injector *c1* at the top of the surface roughness (equivalent to roof level) was traced against the grid on the back of the channel wall (see for example figure 5.38). The grid was laid over a distance of 1000mm in the streamwise direction. The flow visualization was recorded 3m away from the channel glass in the x-z plane with a wide angle lens. The flow visualization has been quantified in two

different ways. The first involved measuring the shortest distance (*L1*) at which the dye touched the water surface, the second gave the average distance (*L2*) at which the dye touched the water surface. A frame by frame analysis of the diffusion behaviour is shown in figure 5.39 recorded at 25 frames per second. This shows the motion of a specific cloud of dye from the bed up to the water surface. The positions for the shortest and the average distances at which the dye touched the water surface are shown in figure 5.40. This clearly provides evidence that the distance travelled to touch the water surface is shortest for bed roughness spacing providing the greatest effective roughness (roughness length scale) shown in figure 5.22a, b.

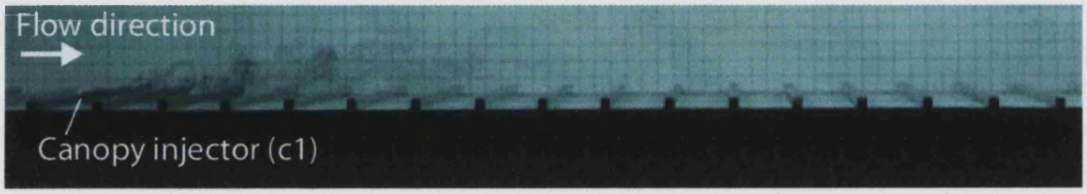

Figure 5.38 Vertical plume growth observation traced against the grid for gap distance s/k=6 between roughness elements in (x-z) plane

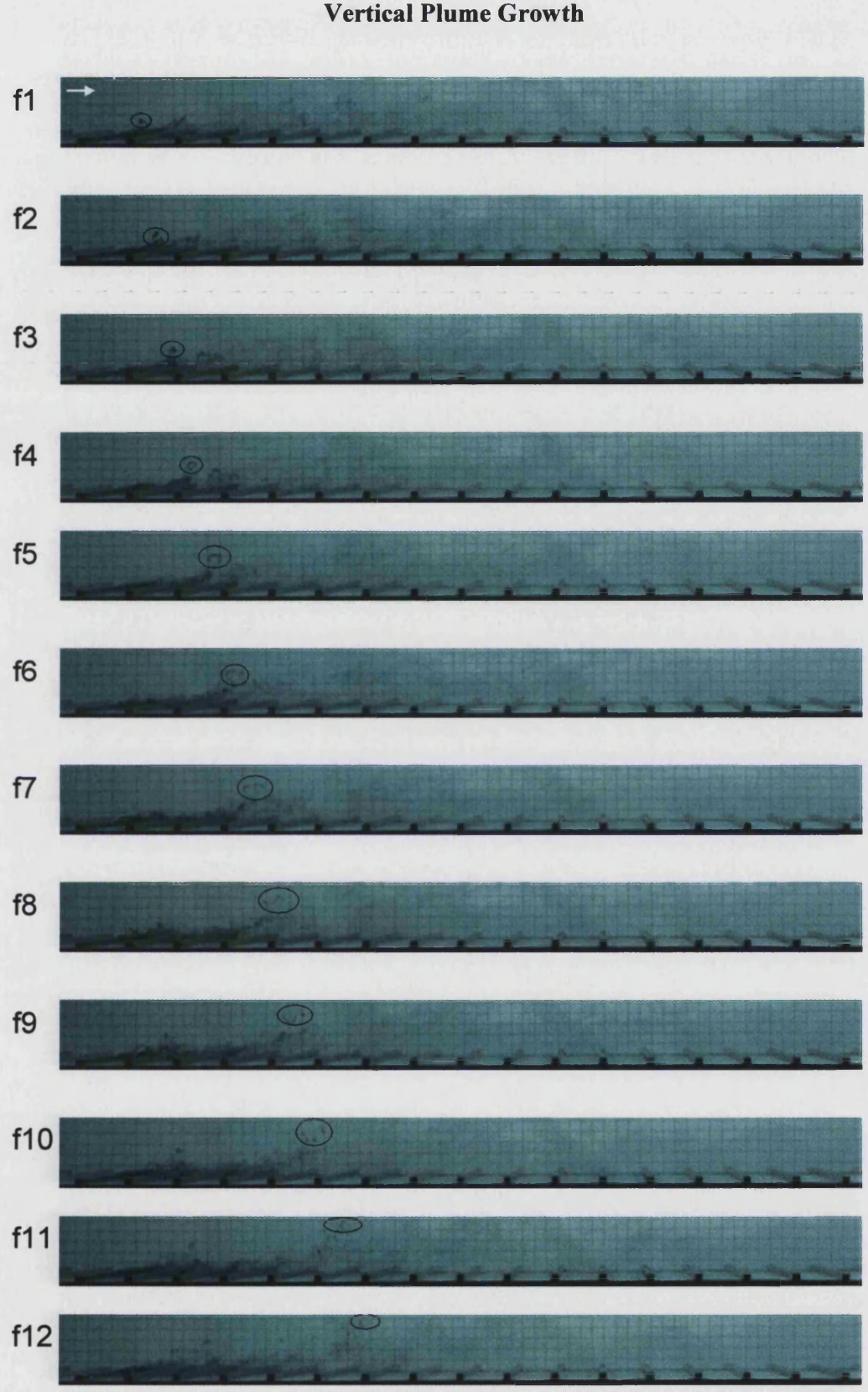

Figure 5.39 Vertical plume growth at 0.16 second time step from canopy injector for gap distance s/k=6

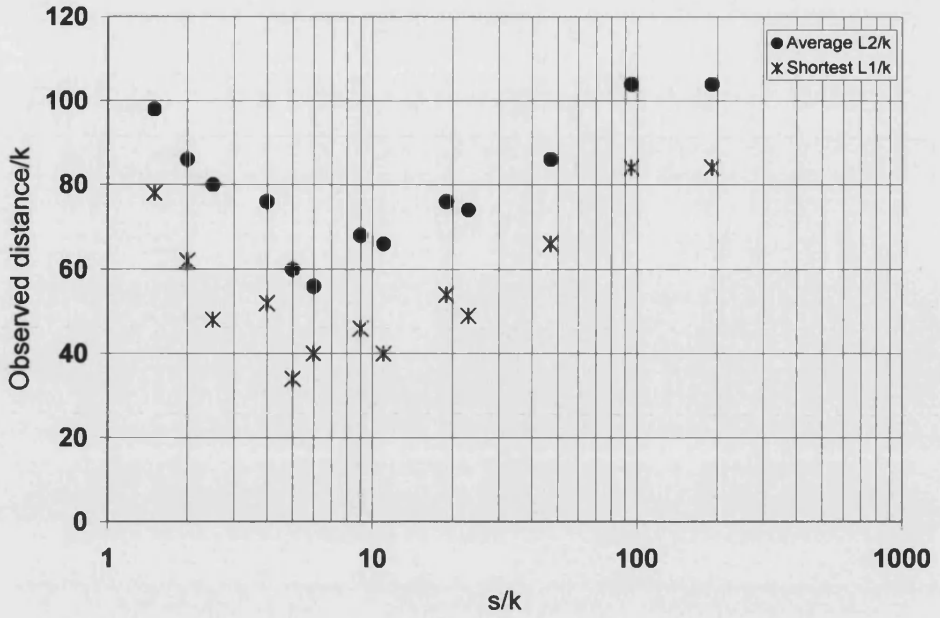

Figure 5.40 Average and shortest observed distance for dye to reach the water surface (injector c1)

5.10.2 Initial plume width (*wo*) observations in the x-y (streamwise-lateral) plane

Tests were carried out using video to investigate the spanwise change in plume width as a result of increasing the gap distance between the roughness slats. The regimes considered for investigation included skimming, wake interference and isolated roughness flows. A video was recorded in the x-y plane covering 500mm in the streamwise and 275mm in the lateral direction. The initial plume width was calculated for each of the tests for the same injection rate of dye at the test section. The purpose was to ensure consistency in the tests. The plume shown in figure 5.41 is the averages from images taken over a period of 4 seconds observations. This has been achieved by digital addition of the images. Frame by frame analysis of the dye plume is shown in figure 5.42.

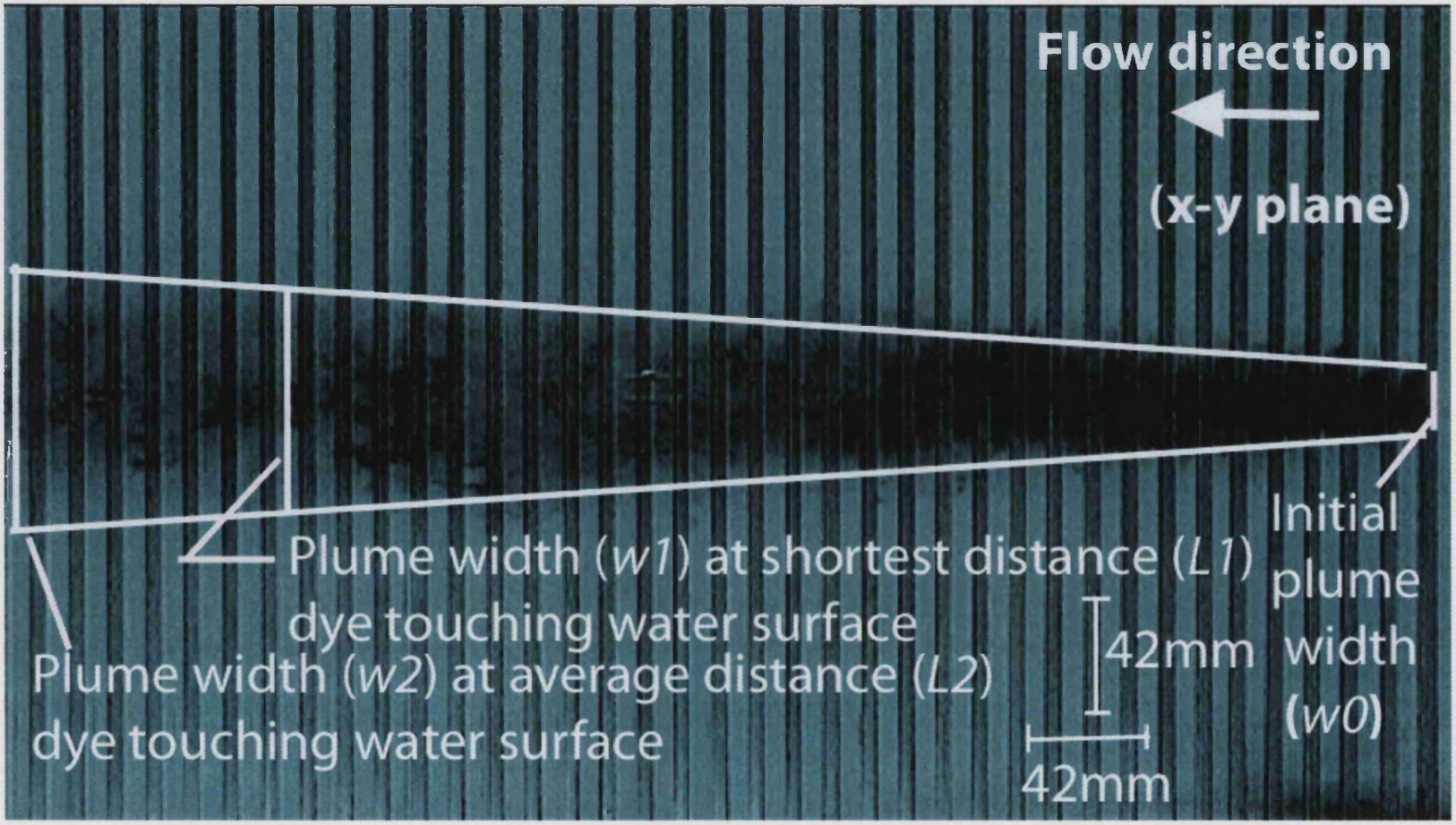

Figure 5.41 Average plume growth from canopy injector for gap distance s/k=1.5

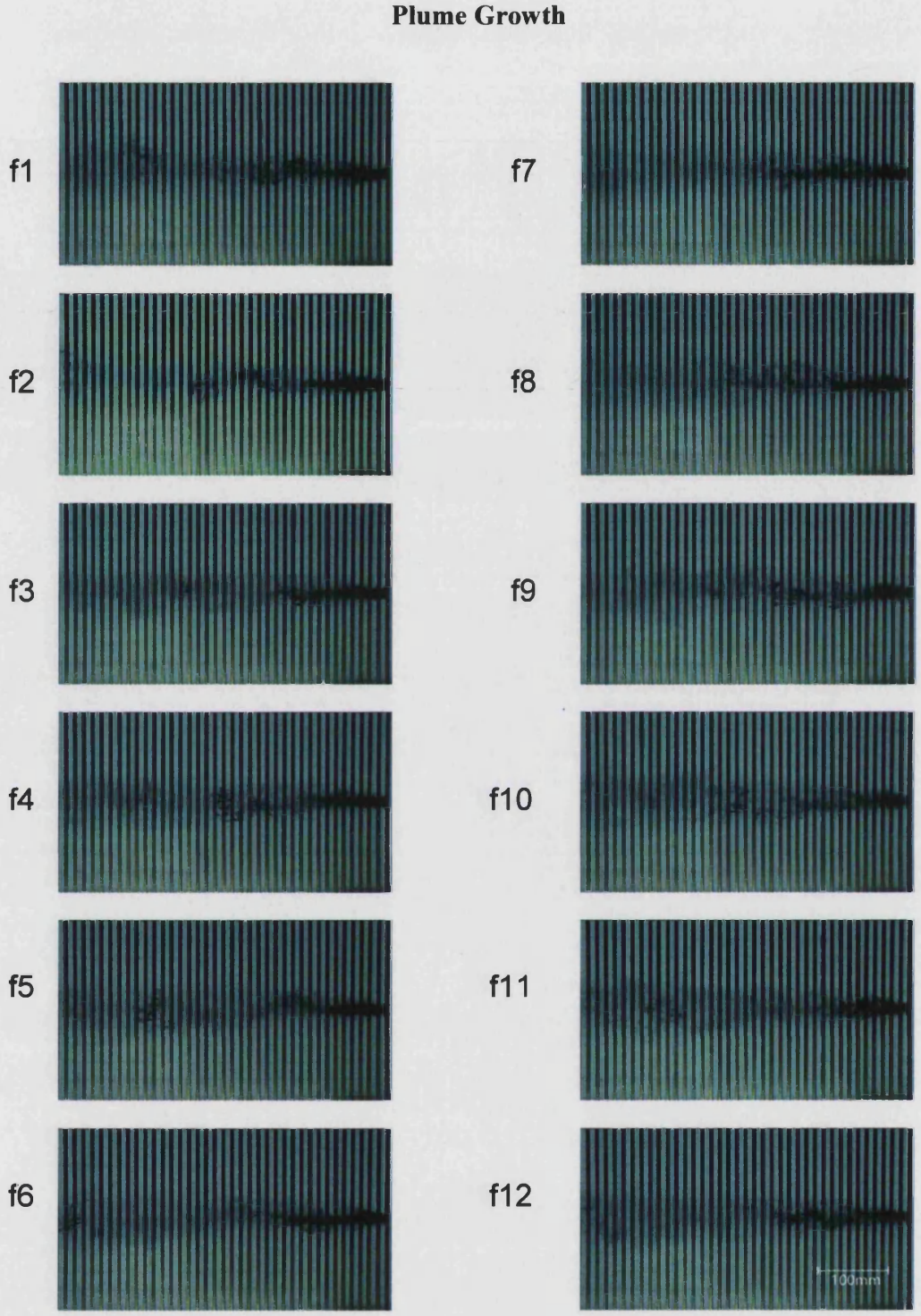

Figure 5.42 Plume growth at 1 second time step from canopy injector c1 for gap distance s/k=1.5

Figure 5.43 shows the increase in the initial plume width, *wo*, with increasing roughness spacing for the injector drilled through the top of a roughness element. This demonstrates that initial plume width is sensitive to the bed roughness for gap widths varying from (s/k) 1.5 to 23. The turbulence structure of the flow is investigated at roof level ($z''= 5mm$ position s2) by considering the local mean velocity gradient and the corresponding Reynolds stresses shown in figure 5.44 and 5.45 respectively. The dispersion behaviour was found significantly influenced by the gradient of velocity and Reynolds stresses. Interpreting these observations in terms of near bed flow regimes, in the case of skimming flow one can see very organized 2-d flow inside the cavity promoting very little lateral spreading. This is the reason why the initial plume width (*wo*) was found least for skimming flow. The distance downstream before the plume touches the water surface is greatest for skimming flow because turbulence is at its lowest. In wake interference flow the vortices start interacting inside the cavity and encourage lateral motion which influences the plume width. The downstream distance taken by the dye to touch the water surface is reduced significantly. Under isolated roughness flow conditions, turbulence in the boundary layer is reduced and consequently the distance for the dye to touch the water surface is increased again. For space to height ratio greater than 23, the initial plume width remains constant. The initial spanwise plume width (*wo*) achieves its maximum value at a gap to height ratio (s/k) of 20.

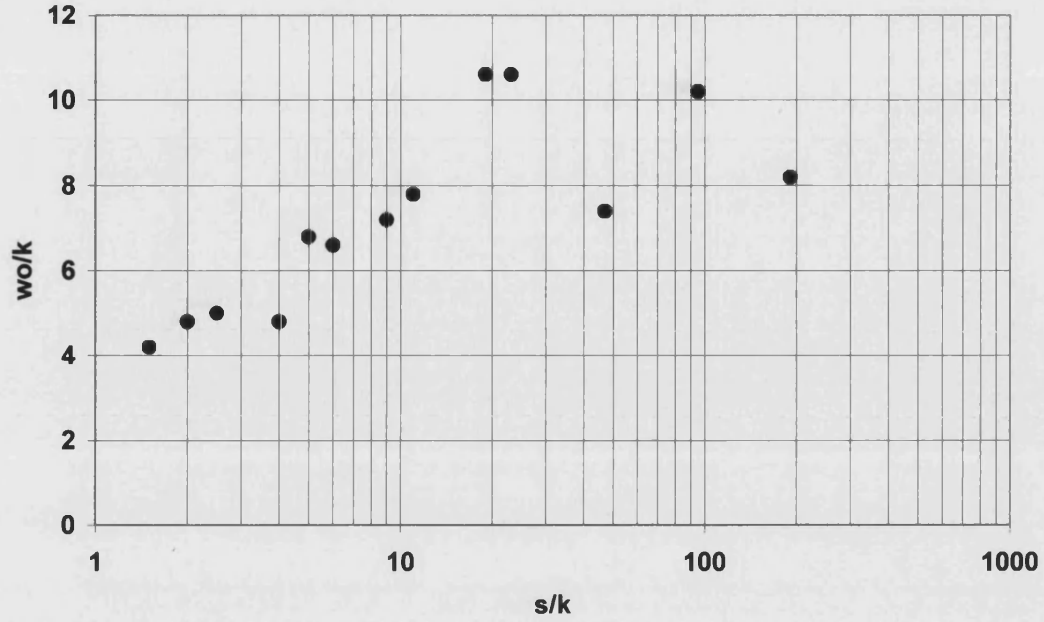

Figure 5.43 Initial plume width growth for injector c1 at the top of roughness element

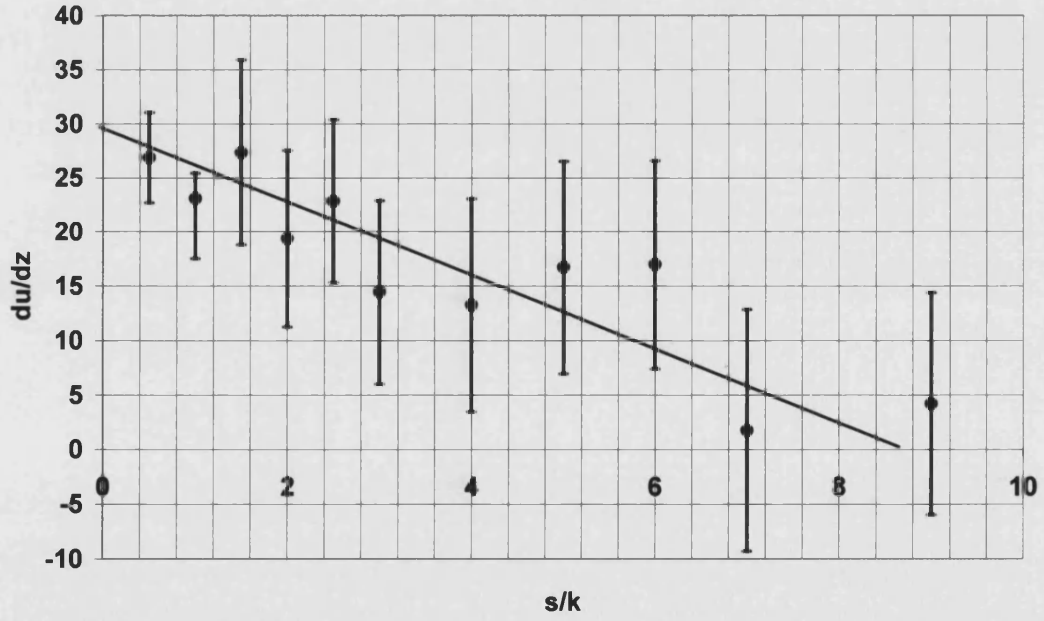

Figure 5.44 Velocity gradient at roof level (z"= 5mm) at position S2

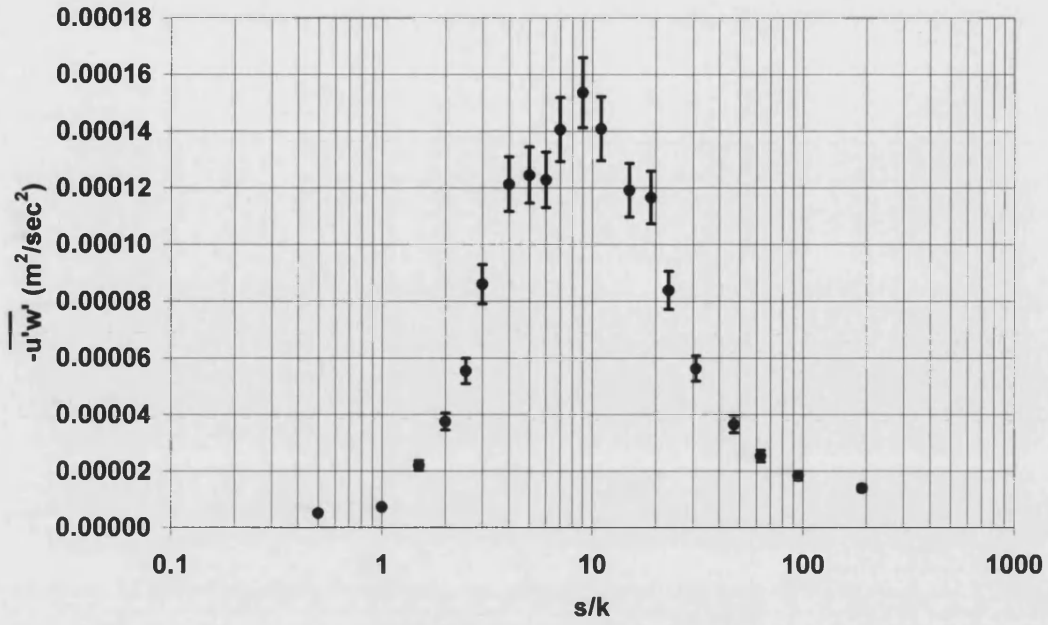

Figure 5.45 Reynolds stresses at roof level (z''= 5mm) at position S2

5.10.3 Lateral plume growth observations in the x-y (streamwise-lateral) plane

The lateral growth of the plume as it propagates downstream from the injector at the top of the roughness element was investigated. The width of the plume was estimated at two positions, corresponding to where the dye touched the water surface, one at the shortest distance (*L1*) at which the dye touched the water surface and the other at the average distance (*L2*). The ratio of the plume widths (*w1,w2*) to the corresponding distances travelled downstream (*L1,L2*) are shown in figure 5.46.

The plume width was found to increase with increasing gap to height (s/k) ratio from 1.5 to 6. The peak plume width was found at a roughness spacing (s/k) of 6. This is because turbulence fluctuations tend to increase and peak roughness length scales is achieved. This evidence confirms that an increase in turbulence fluctuations increases the rate at which the plume grows both in the horizontal and vertical planes.

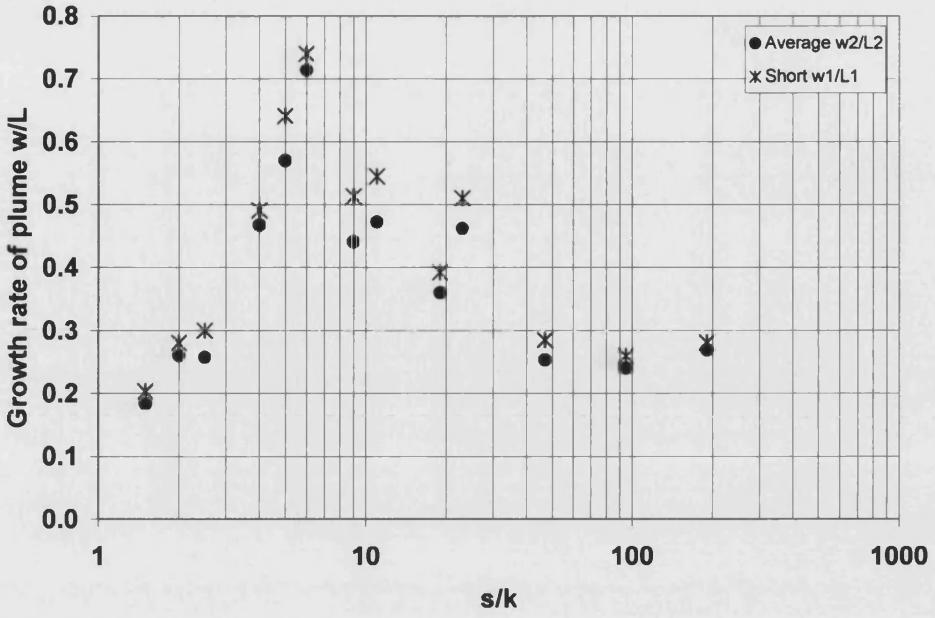

Figure 5.46 Variation in plume growth rate (w1/L1, w2/L2) from injector at canopy c1

In this chapter it was found that different flow regimes were formed inside the cavity and the boundaries between these regimes have been estimated by systematically varying the gap distance between the roughness slats. The effect of varying the gap distance was observed on the diffusion plume released from the line source on the roughness slat. The maximisation of the effective roughness length scale was linked with the maximisation of turbulence production, maximisation of the upward ejection of pollution, and maximisation of lateral plume width. The next chapter focuses on sudden change in local bed geometry and its effect on dispersion behaviour.

CHAPTER 6

FLOW OVER IRREGULAR ROUGHNESS

The purpose of this chapter is to describe experiments to investigate turbulence at and above roof-level in an urban environment, and to predict the behaviour of street pollution from experiments using dye dispersion, for different roughness conditions and bed geometries.

Experiments have been carried out in which flow in the boundary layer above an idealised urban environment has been simulated in a laboratory water flume. Comparisons have been made for the same model street canyon with and without the presence of upstream roughness. In the tests reported here, model street canyons have been aligned perpendicular to the flow direction, and velocity measurements made within and above the model street canyons using a laser Doppler velocimeter (LDV). Flow visualisation techniques have also been used to confirm the gross flow features from streak images. The aim was to identify the differences in mean flow and turbulence in and above model street canyons and to provide an insight into the mechanisms by which roughness geometry and turbulence interact to influence flow and air quality in the urban environment.

The tests reported here were designed to reproduce those reported earlier used by Gerdes and Olivari (1999) in their wind tunnel experiments and subsequently modelled by Xia and Leung (2001) in their study of pollutant dispersion (see chapter 1 and 3).

6.1 Experimental setup

The experimental work was carried out in the re-circulating water flume described in Chapter 3. A water flume has several advantages over the wind tunnel i.e. the lower kinematic viscosity permits lower mean flow velocities, thus slowing down the

turbulent dispersion process. This facilitates high quality flow visualization with a dye tracer and polystyrene beads. Mineral particles present in typical quality laboratory water also provide natural seeding for laser Doppler velocimetry measurements.

The upstream turbulent boundary layer was developed over a 2-d slat type bed roughness (*k-type*). The slat elements had a rectangular cross section 10mm thick and 20mm high and were spaced at a pitch of 100mm (figure 3.7). The roughness slats were placed normal to the flow direction from the channel inlet over a 3.3m length of the flow. The flow depth was kept constant at 0.191m by altering the bed slope in order to maintain a uniform flow.

The variables considered for investigation which define the model street canyon are the gap distance between slats and the slat height. Comparisons were made for the same model street canyon with and without the presence of upstream urban approach roughness. Model street canyons were investigated using four different geometries; each was tested in isolation (Table 3.2, series-1, test 1 to 4), with the upstream bed roughened with '*k*' roughness (figure 3.7) and with large scale roughness immediately upstream of the model street canyon (Table 3.2, series-2, test 5 to 8) to simulate an urban environment. Sketches of typical test geometry with model street canyon and large scale roughness immediately upstream of the model street canyon geometry are shown in figures 3.9 to 3.12. The legend at the test section or elements of the same height and tall elements is shown in figure 3.13a, b.

6.2 Measurement technique

Flow interaction inside the test section and above roof-level for the simulated urban street canyon was studied with different colour dyes. Methyl Orange was introduced through a stainless steel tube of 1.5mm internal diameter under gravity feed. The probe was located at a distance of 190mm from the upstream element of section S9

(figure 3.8 to 3.11). Potassium permanganate crystals (pink) were used inside the centre of the test street canyon, and nigrosine crystals (black) were placed just downstream of the test street canyon. Flow was recorded at 25 frames per second using a standard camcorder for flow visualization. The two-component laser Doppler velocimeter (LDV), described in chapter 3, was employed for quantitative measurements of instantaneous velocities around the test street canyon at sections marked S0 to S4 and S8 to S14 in figures 3.6 and 3.8 to 3.11. The water was uniformly seeded with titanium (IV) dioxide. The signals were processed using TSI IFA655 signal processors with FIND software. The processors were operated in coincident mode to ensure that measurements of both velocities were made for the passage of each seeding particle detected. The LDV system is described in Chapter 3.

6.3 Turbulent boundary layer development

The mean free stream velocity at the model street canyon in the water flume was set to 0.156m/sec corresponding to a wind tunnel velocity of 1.7m/sec used by Gerdes and Olivari (1999). The Reynolds number based on roughness element height (30mm) ($R_k = \frac{uHu}{\upsilon}$) was 4680 for model street canyon. The vertical variation of the wind speed under neutral stability can generally be described by the logarithmic law:

$\frac{u}{u_\tau} = \frac{1}{\kappa}\ln(\frac{z}{z_o})$, where u_τ is the friction velocity, κ the Karman constant, and z_o is the wall roughness length scale; the approach boundary layer in the present tests was characterised by this logarithmic "law of the wall" profile. The vertical origin was determined using the method proposed by Perry and Joubert (1963); expressed as a function of the roughness height, k, this was found to be $0.57k$ below the level of the roughness crests. The bed friction velocity u_τ was estimated using total stress measurements and the slope of the mean velocity profile in the log region. The

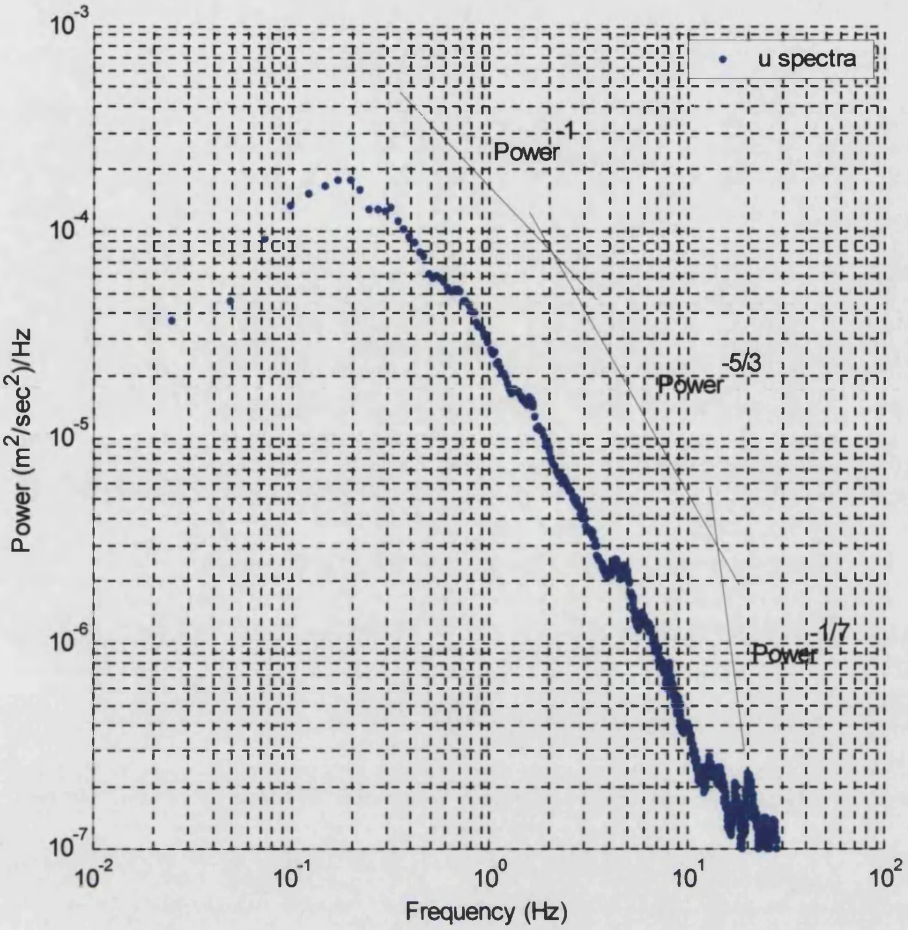

Figure 6.1 Logarithmic scale u-frequency spectra of turbulence at z'= 60mm for "k-type" isolated roughness at S2

Reynolds number based on roughness length scale, $\frac{u_\tau z_o}{\nu}$, was found to be 98, which is larger than the minimum value of 2.5 recommended by Snyder (1972) for model studies of the atmospheric boundary layer. The frequency spectrum of the horizontal turbulent velocity fluctuations was found to obey the Kolmogorov $K^{-5/3}$ law as shown in figure 6.1.

From the foregoing, it is reasonable to assume that the approach boundary layer in the water flume gives an acceptable simulation of an atmospheric boundary layer.

6.4 Effect of additional upstream large scale roughness

Upstream roughness has a significant influence on the structure of the Reynolds shear stresses at and above roof-level in an urban environment. The effect of adding large scale roughness (Table 3.1) was investigated and compared to the same model street canyon with only a uniform approach roughness.

6.4.1 Effect on reverse flow circulation inside cavity

From the discussion in section 5.1.1 for a cavity having gap to height ratio (s/k) of 1 to 1.5 a single vortex is found to be formed inside the cavity. This is illustrated by the flow visualization in figure 6.2a, b, showing a single vortex formed inside the cavities with aspect ratio (s/k) of 1 (Test 1 and 5) and 1.5 (Test 2 and 6).

The model street canyon was studied under two conditions i.e. with and without the presence of additional upstream roughness. It was found from the LDV measurements that circulation velocities inside the model canyon increased by 7% (figure 6.3a) for a square section canyon (test 1 and 5) but reduced by 9% (figure 6.3b) for a wider street canyon (test 2 and 6) in the urban environment in comparison to the isolated canyon case. Circulation velocities within the canyon were increased significantly (by 63% for the isolated street canyon, 37% in a simulated urban environment) when the canyon was made wider (keeping the slat height constant).

From this discussion it was demonstrated that reverse flow circulation close to the cavity wall was independent of the additional upstream roughness. The most important parameter found to effect the reverse flow circulation was the gap distance 's' between the roughness elements forming the cavity.

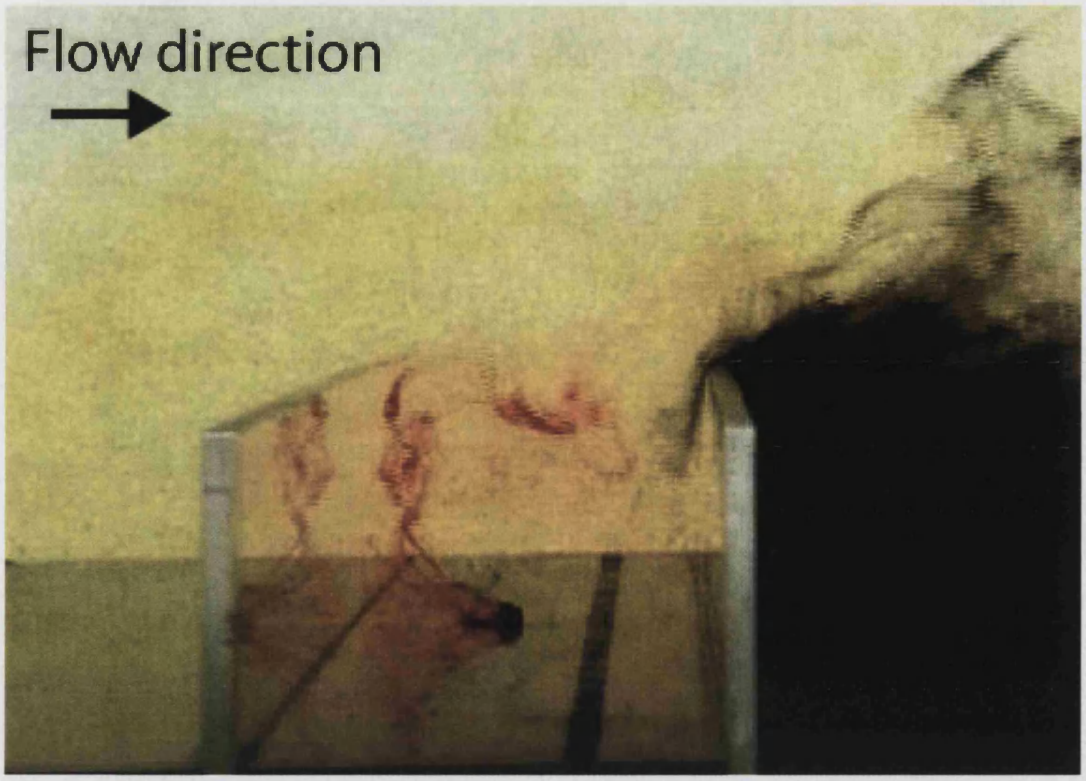

a) Reverse flow at roof-level for isolated street canyon, Test 2

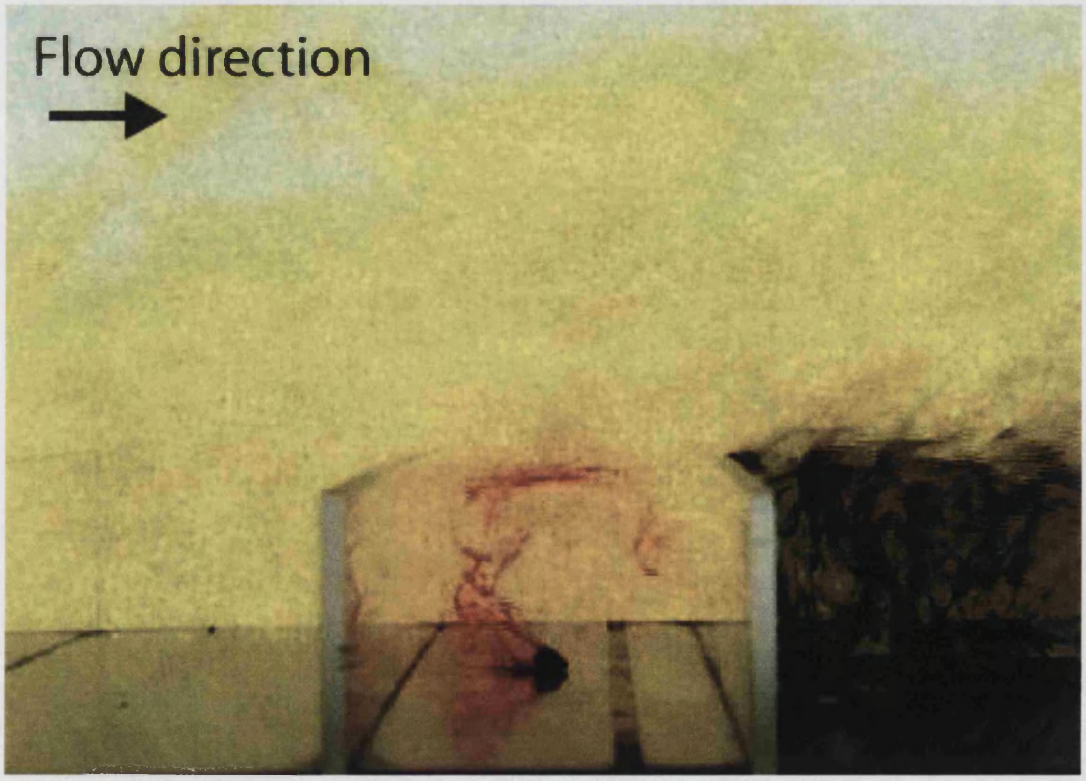

b) Strong shear at roof-level in simulated urban environment, Test 6
Figure 6.2 Flow visualisation a) Interaction at roof level b) Presence of vortex

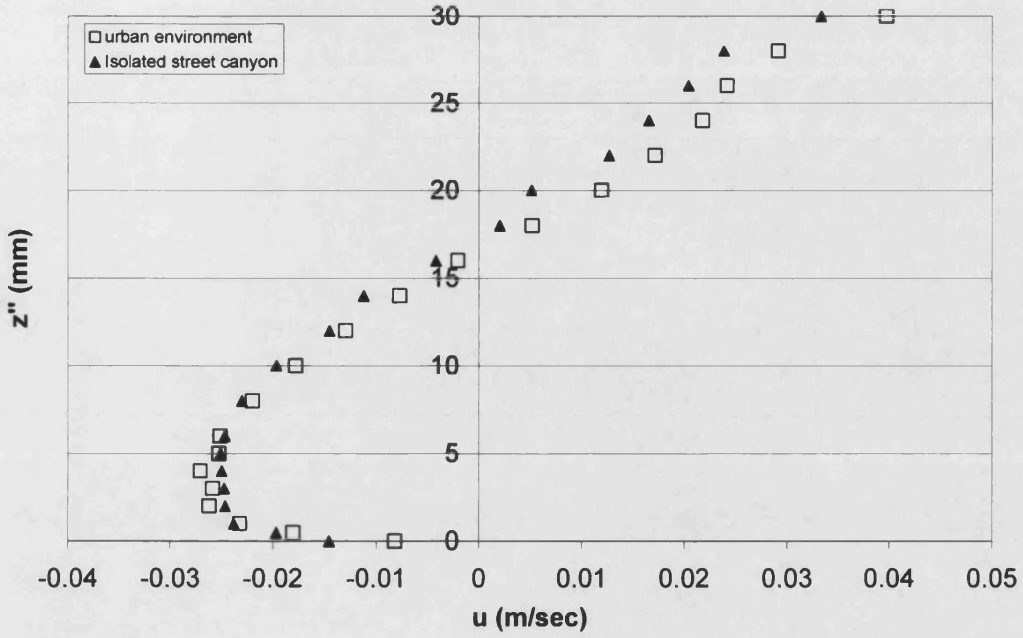

a) Test 1 and Test 5 (measured mid way between roughness elements at position S11)

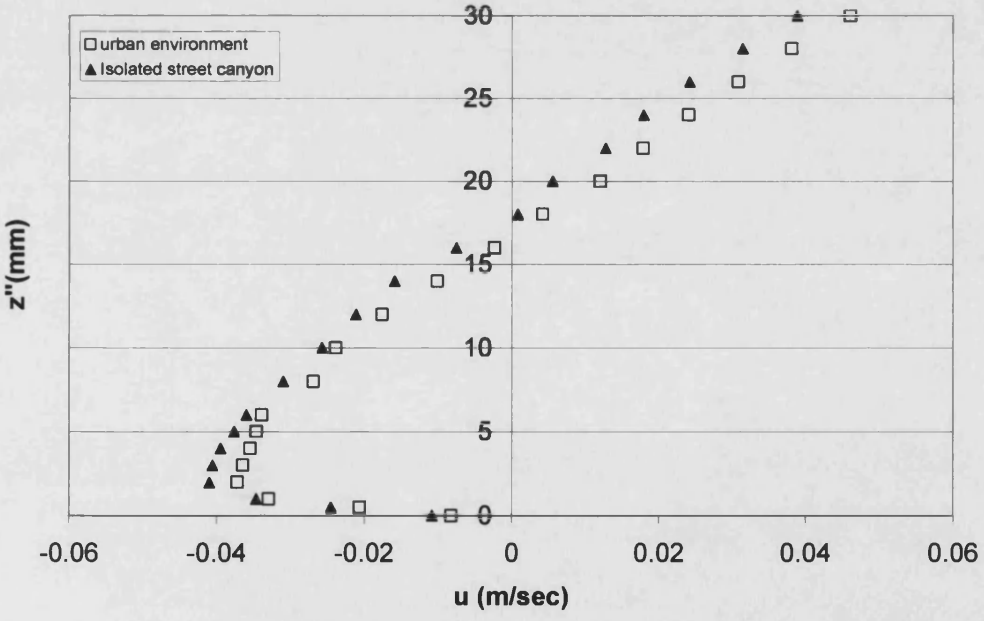

b) Test 2 and Test 6 (measured at S11)

Figure 6.3 Comparison of reverse flow circulation inside cavity a) Square section b) Rectangular section

6.4.2 Observation of shear formation at roof level

When the ambient wind direction is perpendicular to the street canyon, a vortex flow is generated within the street as shown in figure 6.2a, b. Coherent trails of nigrosine dye were seen rising higher into the flow, and they also occasionally moved back upstream into the adjoining street canyon (figures 6.2a and 6.4a). This contrasted with the tests with large scale roughness immediately upstream, simulating an urban environment, where the flow was seen to skim over the tops of the elements, trapping the dye in the street canyon (figure 6.2b and 6.4b). This behaviour is shown clearly in the vector plots (figure 6.5 a, b) generated from LDV measurements of the two cases. A Vortex formation inside the street canyon with uniform approach bed roughness was found very dynamic and changed its position relative to the downstream roughness element. Vortex which initially followed a circular trend quickly transformed to oval-shaped (figure 6.4 a) occasionally and started forced ejections of pollutants at an angle varied from 40 to 50 degree with the bed. The change in vortex shape from circular to oval was found to be associated with significant energy which helped in forcing ejections of pollutants from the street canyon. The effect of forced ejection was observed up to 0.80Hu from the roof-level of the street canyon, dissipating further downstream over the adjoining street canyon. Vortical structures above roof level were influenced by these forced ejections and moved vertically away from the roof level at such occasions. The reverse flow at roof level was found associated with forced ejections and the displacement of vortical structures away from the roof level. Reverse flow at roof-level into the adjoining street canyon was prevented by an observed increase of more than 15% in streamwise mean velocity at roof-level as a result of the additional large scale roughness immediately upstream. The dye streaks were seen to spread more in the isolated street canyon than when it

was placed in the urban environment. The frequency of dye emergence at roof-level was also more in the isolated case than for the urban environment. In the isolated case, dye was ejected from the upstream central part of the street canyon at roof-level. Using the method of quadrant decomposition introduced by Lu and Willmarth (1973) to analyse the instantaneous velocity data above the test street canyon at roof-level, it was found that higher ejection-to-sweep ratios were observed with uniform upstream roughness than for the urban environment at a distance 0.17a downstream from location S9 (figure 6.6). For the tests on a model street canyon with a square section in the simulated urban environment, dye was observed to be ejected from the downstream quarter of the gap

a) Reverse flow over roughness slat of model street canyon from downstream (tracing styrocell particles), Test 2

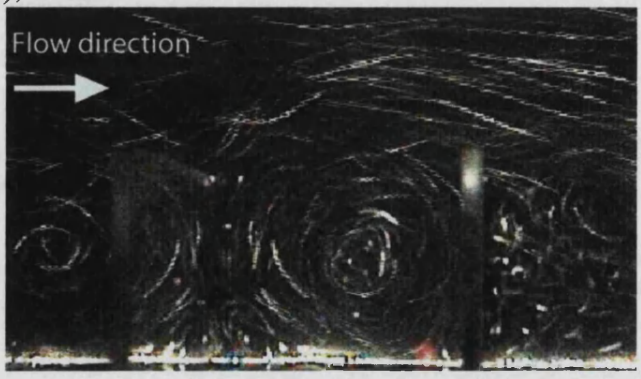

b) Urban environment with no reverse flow over roughness slat from downstream, Test 6

Figure 6.4 Flow visualisation with styrocell particles a) isolated street canyon b) urban environment

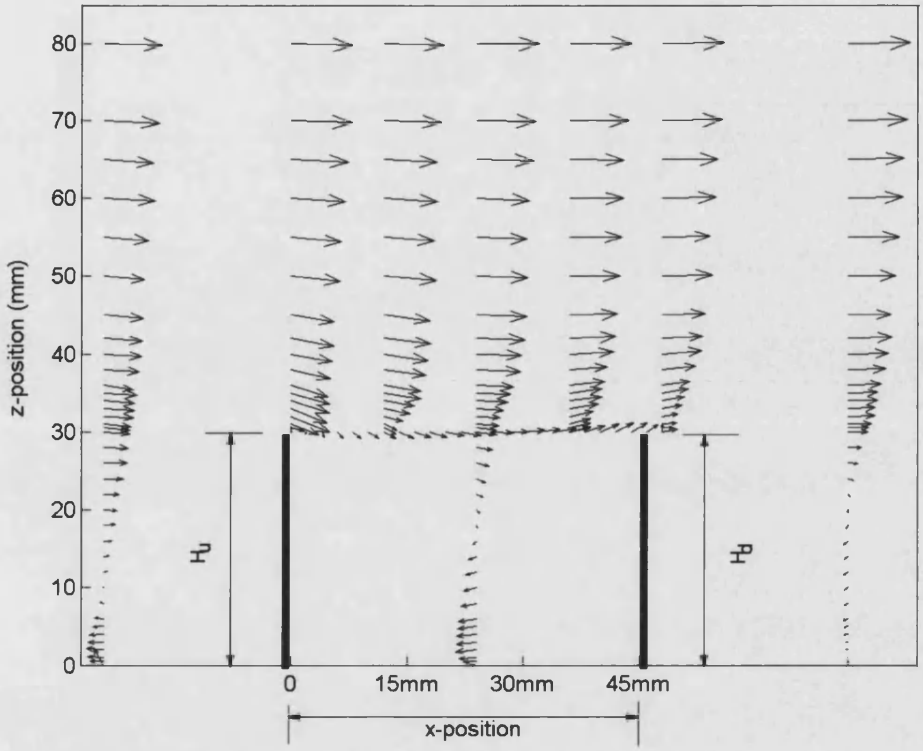

a) Local mean flow velocities from LDV for isolated street canyon, Test 2

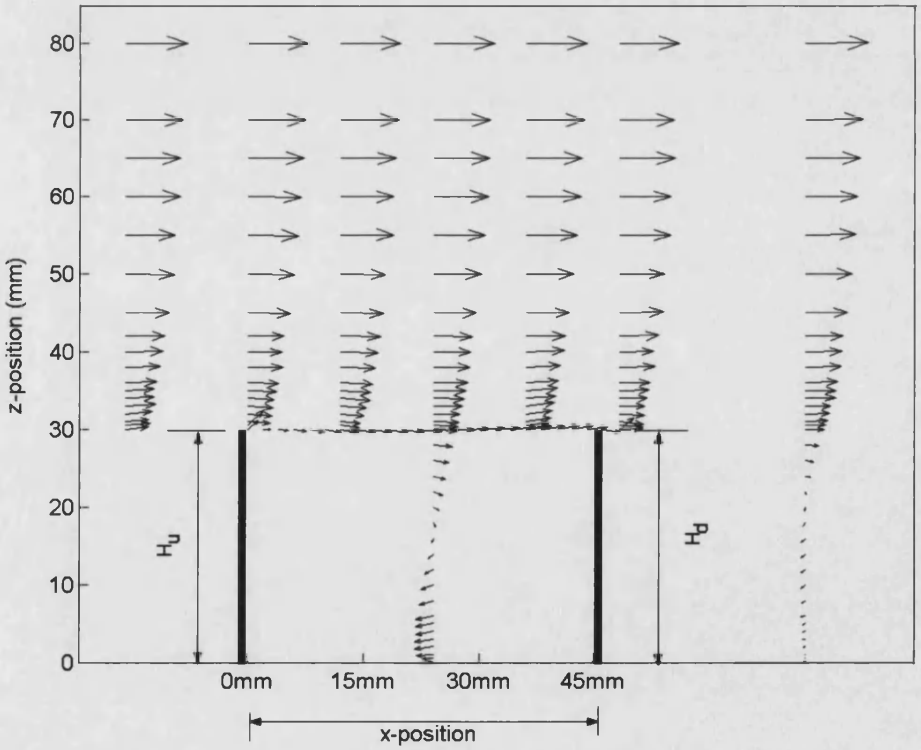

b) Local mean flow velocities from LDV for urban environment, Test 6

Figure 6.5 Evidence of single vortex formation and shear observation at roof level Hu=30mm, s=45mm, Hd=30mm a) isolated street canyon b) urban environment

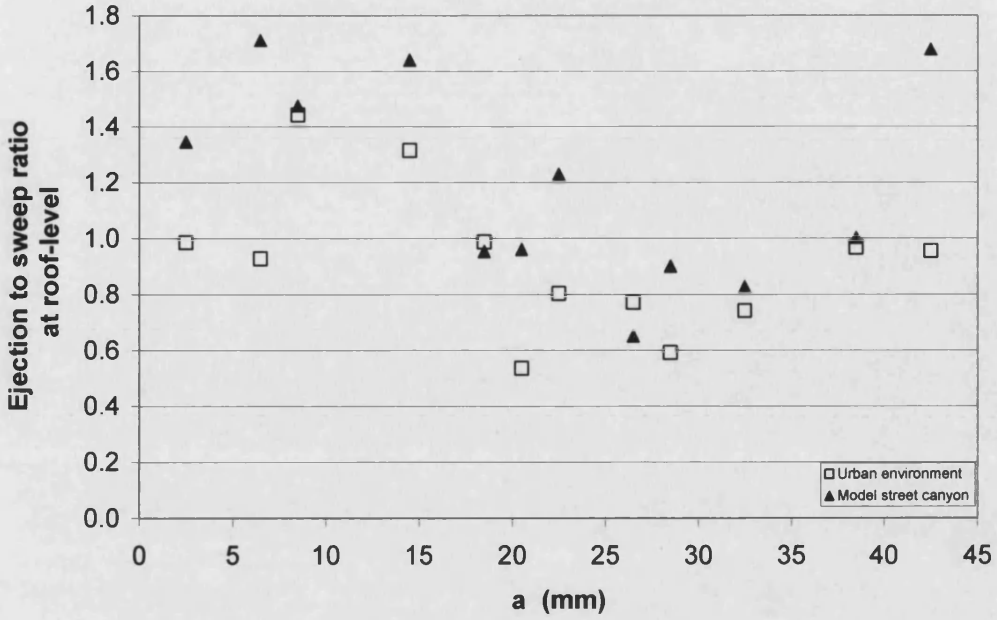

Figure 6.6 Ejection to sweep ratio for model street canyon at H=0 Test 2 and Test 6

at roof-level. This contrasted with tests using a wider street canyon where dye ejected uniformly over the entire width of the street canyon at roof-level.

6.4.3. Effect on local mean flow velocity above roof level

The effect of additional large scale roughness is compared to the isolated street canyon case. It was found from figure 6.7a that upstream roughness offers drag to the flow over the model street canyon (Test 2 and 6). On the other hand, for a cavity having a tall roughness element downstream (Test 4 and 8) the flow was unable to feel the drag from upstream roughness as shown in figure 6.7b. Comparable Reynolds stress profiles over a model street canyon with equal height (Test 2 and Test 6) and tall roughness (Test 4 and Test 8) are shown in figure 6.8a, b. The evidence observed from these graphs shows that friction velocity is increased in the model street canyon in comparison to the case with additional upstream roughness. The increase in friction velocity is evidence of the coupling between the flow in the boundary layer and the surface roughness. It can be deduced that ventilation of pollutants is more in the isolated street canyon in comparison to when we have

additional roughness upstream. Now looking back to the model street canyon with a tall roughness element (Test 4 and 8), it was found that friction velocity is high in the presence of additional large scale roughness in an urban environment. More ventilation can be expected in a city when the roughness elements have uneven height which actually breaks the shear formation at roof level. The evidence for an increase in friction velocity for model street canyon of even height was shown in figure 6.9a from the bed shear stresses. Similarly a street canyon with a tall slat within an urban environment promotes an increase in friction velocity, and this is demonstrated by the bed shear stresses shown in figure 6.9b. The reduction in friction velocity in the simulated urban environment indicates an increase in the zero plane displacement height and consequently an increase in shear at the roof level.

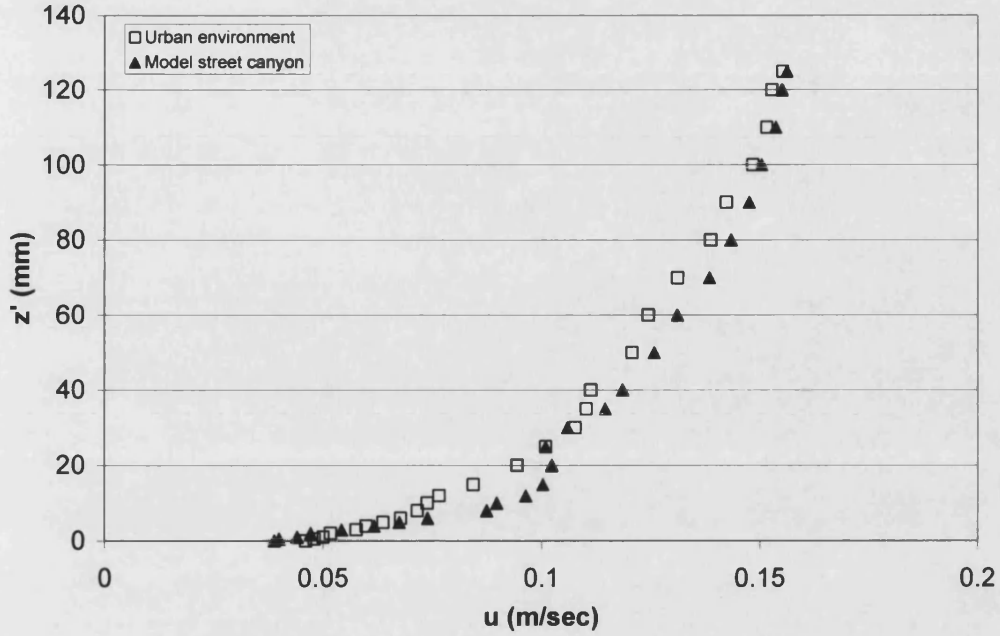

a) Test 2 and Test 6 measured at S11

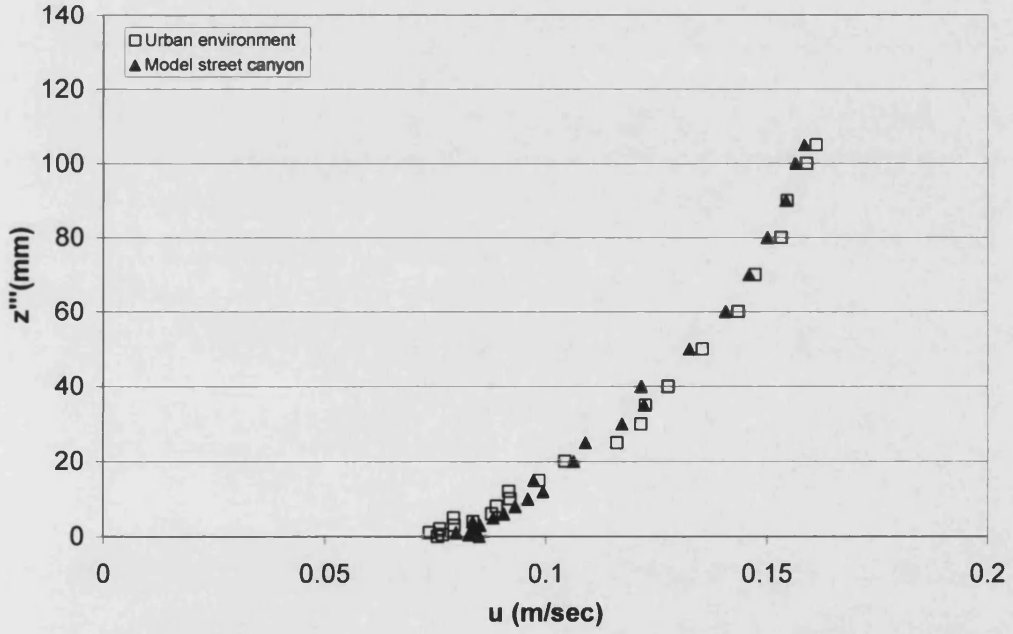

b) Test 4 and Test 8 at S11

Figure 6.7 Local mean velocity profile a) equal height b) tall slat

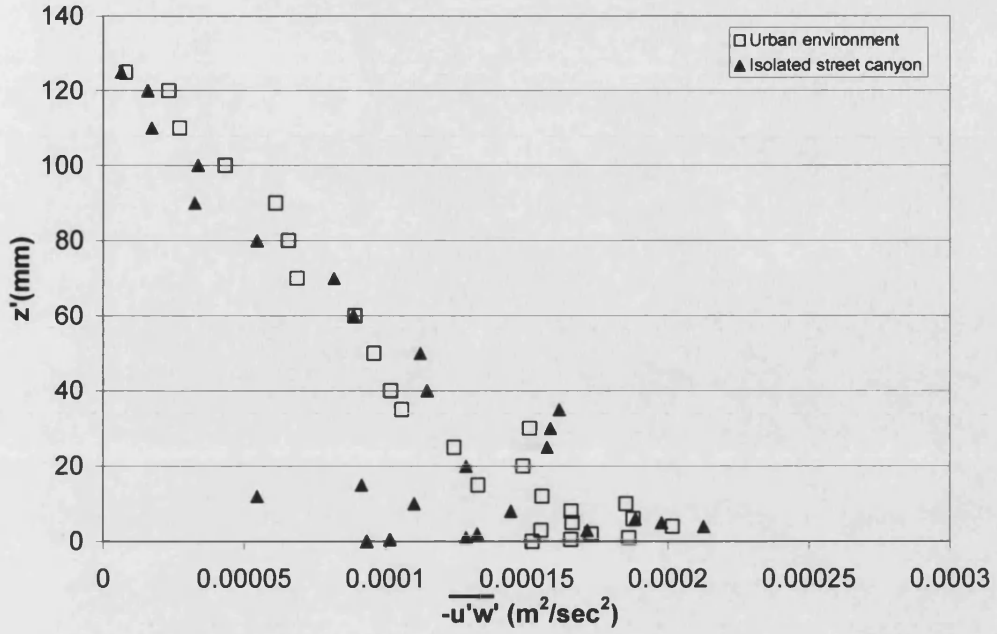

a) Test 2 and Test 6 measured at S11

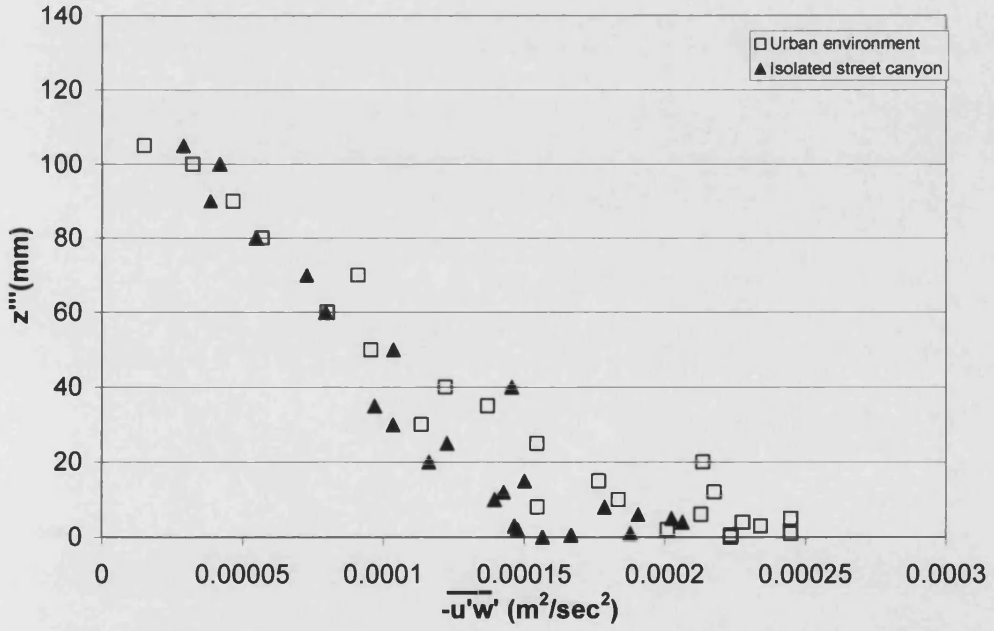

b) Test 4 and Test 8 at S11

Figure 6.8 Reynolds stress profiles a) equal height b) tall slat

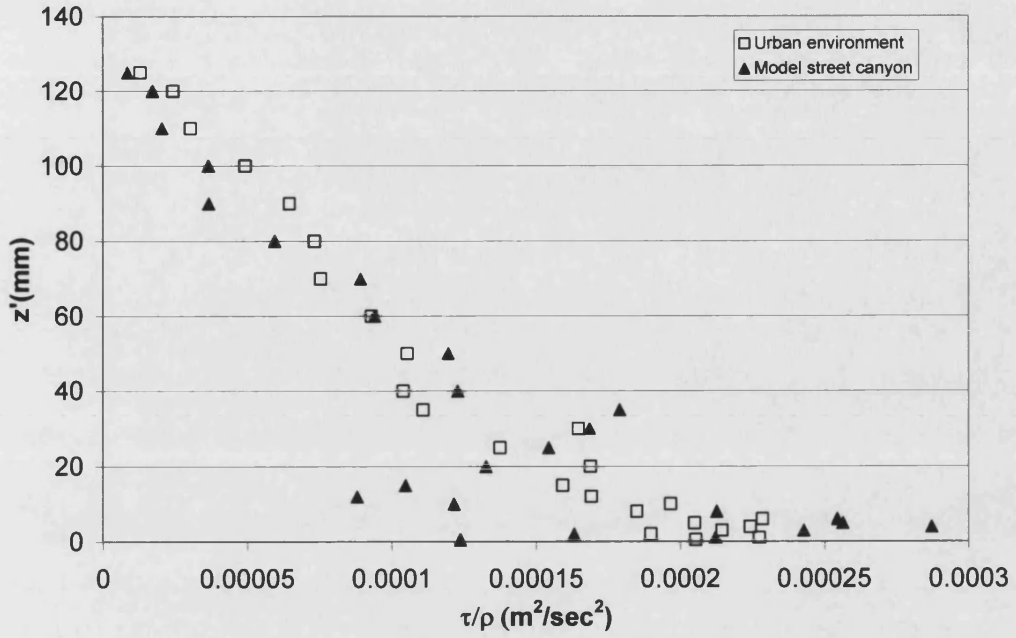

a) Test 2 and Test 6 measured at S11

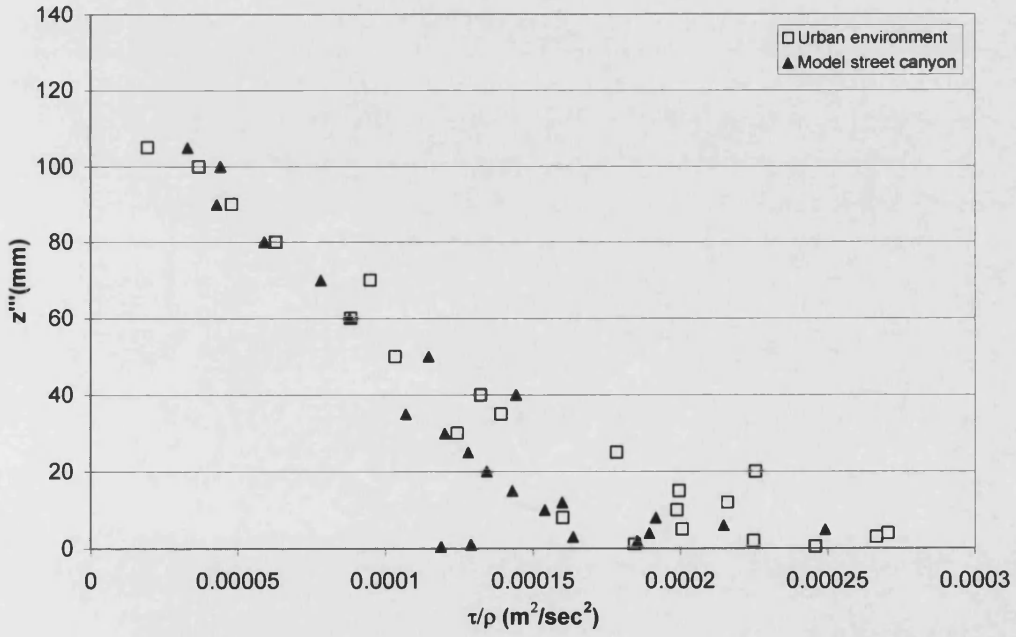

b) Test 4 and Test 8 at S11

Figure 6.9 Bed shear stress a) equal height b) tall slat

6.4.4. Effect on turbulence fluctuations

The comparison of urms and wrms values at S11 for different approach conditions above roof-level is shown in figures 6.10a, b. This reveals that urms and wrms is higher for the model street canyon than when the large roughness elements were inserted upstream. That is the reason why the dye streaks were spread more rapidly and ventilated from the isolated street canyon more efficiently than for the simulated urban environment, as demonstrated in the LDV vector plots (figure 6.5a, b).

With a relatively tall roughness slat inserted on the downstream wall of the model street canyon (figure 6.11a, b), urms and wrms were increased in the roughness sublayer by the presence of additional upstream roughness (test 7 and 8) in comparison to the uniform approach roughness (test 3 and 4). It was found that relatively high buildings upstream or downstream increased ventilation and reduced local pollutant concentration levels in the presence of upstream urban roughness.

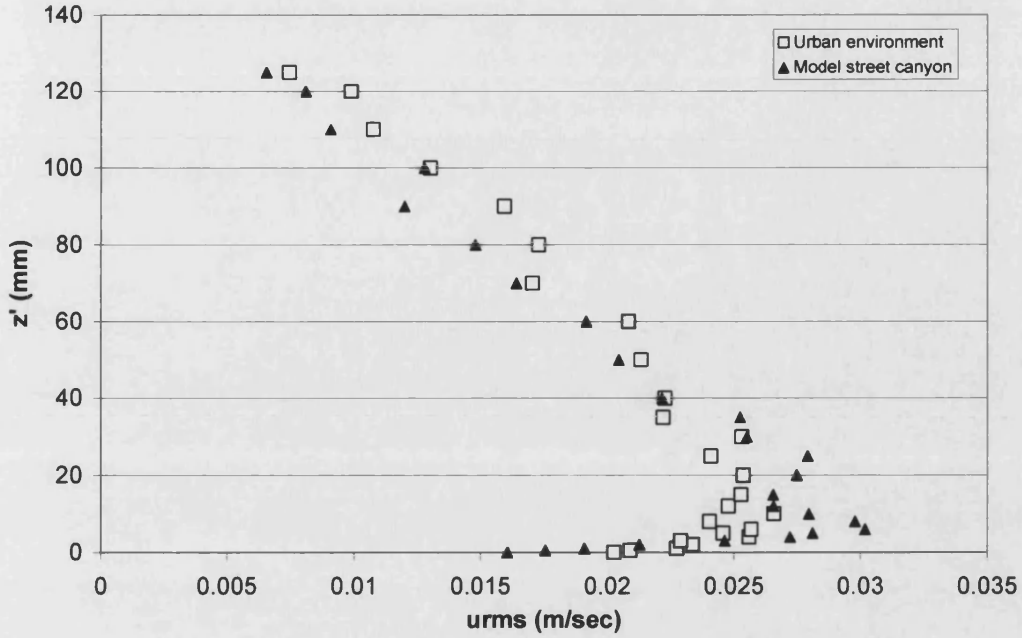

a) Test 2 and Test 6, equal height measured at S11

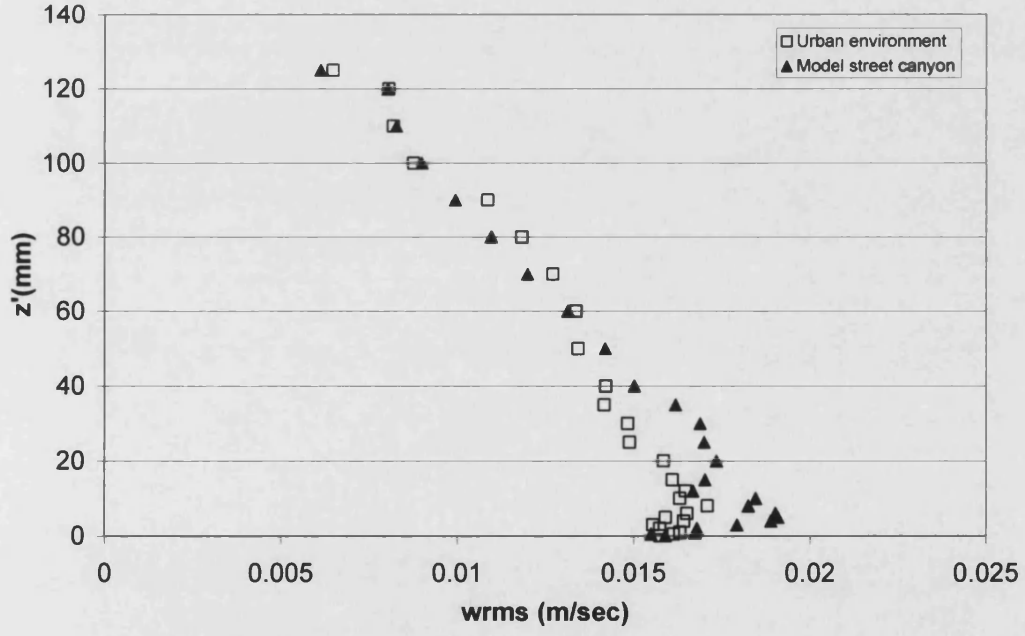

b) Test 2 and Test 6, equal height at S11

Figure 6.10 Turbulence fluctuations above slats of same height a) streamwise turbulence b) vertical turbulence

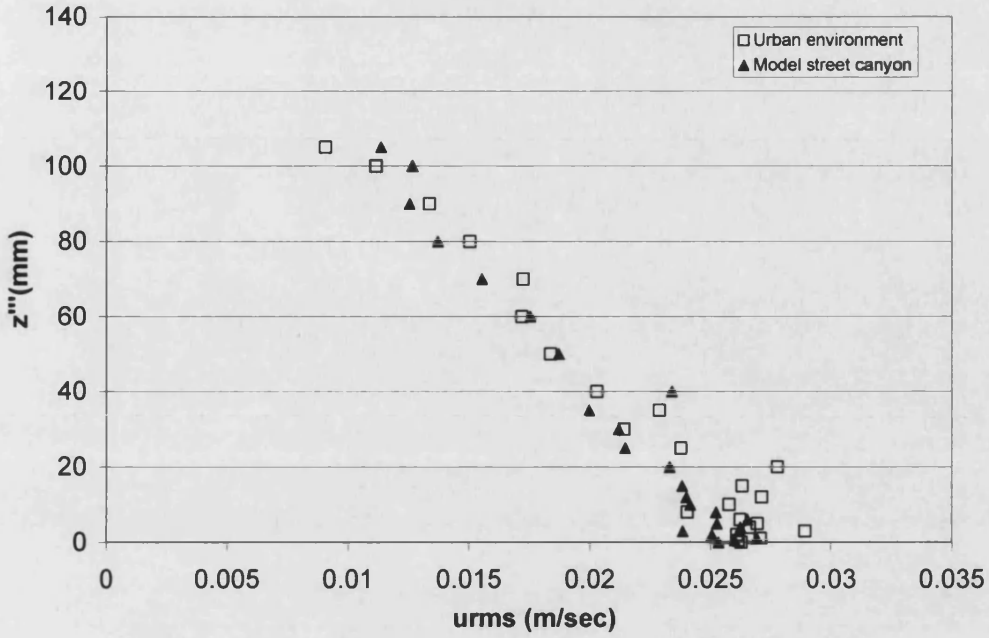

a) Test 4 and 8, tall slat at S11

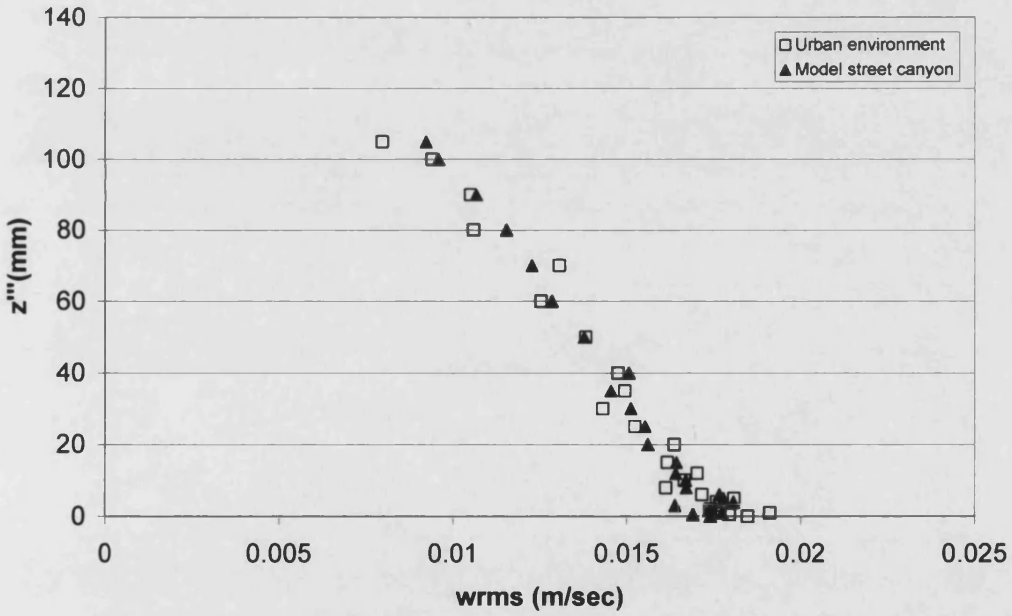

b) Test 4 and 8, tall slat at S11

Figure 6.11 Turbulence fluctuations above tall slat a) streamwise turbulence b) vertical turbulence

CHAPTER 7

CONCLUSIONS AND RECOMMENDATIONS

Tests have been carried out to investigate the effects of systematic variation in bed roughness geometry on the characteristics of a turbulent boundary layer and dye dispersion. The dispersion of dye was investigated from three injectors located at specific positions. Two injectors were placed opposite to each other inside the cavity, while the third injector was positioned at the centre of the top of a slat.

7.1 Square slat roughness

The following are the conclusions derived from tests over square section slat roughness:

- Characterising flow over 2-d slat type roughness in terms of skimming, wake interference and isolated roughness flow, the boundaries between these modes of flow have been identified at different gap distances between the roughness slats. This classification was based on flow visualisation and point measurements from LDV.
- At transition between these regimes, there were special patterns observed. Two vortices were observed, one above the other, inside the cavity for $s/k = 0.5$, just before transition to skimming flow. There was little chance for ventilation of pollutant trapped inside the lower vortex close to the wall, because of lower turbulence intensity. Momentum transport in such a narrow cavity was found governed by the upper vortex which was more dynamic, having direct interaction with the outer flow. The nature of the sweep events generated by the upper vortex at roof level was similar to the one generated over a smooth wall at the same position.

- At larger gap distances, between $s/k = 1$ *to* 1.5, it was confirmed by flow visualisation that a single vortex is formed inside the cavity. Turbulence inside the cavity was governed by the presence this single vortex which was very dynamic at the opposite end of the cavity. This was confirmed by the dispersion behaviour at the upstream end than the downstream end. Two injectors were facing in opposite directions were run, one after the other. Dye from the injector facing downstream spread more in the lateral direction than dye from the injector facing upstream.
- At $s/k = 2$, the transition from skimming to wake interference flow was observed. The ventilation behaviour of the cavity was significantly improved at upstream of the cavity and lateral spreading of dye inside the cavity is significantly reduced in comparison to skimming flow regime.
- A second vortex was noticed in the gap interacting with the primary vortex in the cavity. This regime is termed wake interference flow and was found at $s/k = 2.5$ *to* 5. The two vortices were actively interacting with each other and their communication with the flow in the boundary layer was quite effective in terms of getting into the body of the flow.
- Vortices above each other in a narrow cavity adversely affect the ventilation; on the other hand, horizontally-arranged vortices in a relatively wide gap promote ventilation.
- The transition from wake to isolated roughness flow (critical roughness density) was found at a gap distance $s/k = 6$, where the flow behaviour inside the cavity was found to switch between isolated and wake interference flow. The upstream vortex in the cavity was found quite stable whereas the downstream vortex was dynamic and changed its position inside the cavity.

- The next flow regime identified was the isolated roughness flow. This is comprised of more than two vortices within the gap between adjacent roughness elements. They interact in a random fashion. Two vortices, one at the upstream end and the other at the downstream end of the cavity, were formed. Between them, the streamlines were observed to touch the floor of the glass plate. Flow visualisation revealed that the two vortices were acting independently from each other at $s/k = 9$.
- The vortex patterns between the roughness elements are related to the macroscopic boundary layer characteristics, in particular the roughness length scales of the logarithmic profile.
- Von Karman constant was found to vary between 0.31 to 0.41for flow over a systematically varying wall roughness conditions.
- The variation in gap distance between the roughness slats has an important impact on the turbulence production in the boundary layer. Turbulence production depends on the correlation of the Reynolds stresses and the local mean velocity gradient. The Reynolds stresses achieve their highest value at critical roughness density of $s/k = 9$. The maximum velocity gradient was found for skimming flow because of the viscous effects and gradually reduced at $s/k = 9$ because of the higher turbulence observed in the flow.
- The increase in turbulence production in the boundary layer was found associated with the increase in mixing length scale of the turbulence. The turbulence diffusion coefficient was found to have increased.
- The rate of increase in turbulence production in the boundary layer has significant influence on the growth rate of a plume of pollutant in the both vertical and horizontal planes.

- The increase in turbulence induced by the increased effective roughness helps pollutant to disperse upwards towards the water surface.
- The initial plume width from a line source injector increases in plan when the flow transforms from skimming to wake and isolated roughness flow. This is caused by the turbulence generated from upstream roughness.
- Skimming flow was found to be organised and 2-dimenstional, and promotes little lateral spread of the dye plume. This feature indicates cavity ventilation was not strong.
- Wake interference flow on the other hand was found to be fully 3-dimensional. This was because of increasing turbulence production in the boundary layer. Two vortices interact with each other, increasing the chance for ejection of pollutants from any point along the cavity.
- Rough surfaces enhance the ejection and sweep events in comparison to a smooth wall case.
- The measurement of ejection and sweeps at roof level reflect vortex activity inside the cavity. An interesting feature of isolated roughness flow was the high ratio of ejections and sweeps induced by the vortex at the opposite ends of the cavity. In skimming flow, ejections are dominant at the upstream and downstream walls of the cavity and sweeps dominant midway across the cavity.
- The longitudinal turbulence fluctuations increases with increasing gap spacing between roughness elements until the transition from wake interference flow to isolated roughness flow at $s/k = 6$.
- The drag coefficient (f) is greatest at the transition from wake interference flow to isolated roughness flow at $s/k = 6$ *to* 10.

- The maximum value of z_o / k is obtained at the transition from wake interference flow to isolated roughness flow (critical density) at $s / k = 6$.
- The maximisation of the effective roughness length scale was linked with the maximisation of turbulence production, maximisation of the upward ejection of pollution, and maximisation of lateral plume width.

7.2 Irregular roughness

Experiments have been carried out over an idealised urban environment to investigate turbulence at and above roof level under different bed geometry conditions. The parameters considered for investigation were roughness element height and gap distances between the slats. Comparison has been made between flows with the roughness arranged to simulate an urban environment in the presence of additional large scale roughness and with no upstream roughness.

The conclusions derived from these tests over irregular roughness are as follows:

- Street canyon configuration and upstream approach roughness have a significant influence on the dispersion of pollutants in an urban environment.
- Uniformity in height of buildings along parallel streets in an urban environment promotes shear at roof-level, thereby trapping fluid and pollution within the canyon. This observation confirms earlier work by Meroney et al. (1996). On the other hand, non-uniformity in building height and the presence of substantial upstream buildings promotes turbulence which helps in ventilation of street canyons. In order to reduce pollutant concentration the objective should be to reduce shear at roof-level and promote turbulence.
- Analyzing this further using quadrant analysis, turbulent ejection-to-sweep ratios are reduced and ventilation is suppressed due to uniformity in building heights.

- In an urban environment, wider street canyons promote pollution ejection at the roof-level over the entire width of the street canyon. This helps in the reduction of pollution on the downwind face of the street canyon. This confirms the field observation by Chan and Kwok (2001).
- Flow in the roughness sublayer was found to be highly influenced by the upstream urban approach roughness. An understanding of the turbulent nature of the roughness sublayer can help in characterizing the ventilation behaviour of different urban roughness geometries.

7.3 Recommendations

In this research an attempt has been made to show the effect of turbulence generated because of 2-d surface roughness on the dispersion of pollutants. The characteristics of the flow inside a cavity (modelling an urban street canyon) were investigated and the effects of different cavity widths were identified. This can play an important role in urban planning. The research study has demonstrated an appropriate minimum width (s/k=2) to avoid the trapping of pollutant inside the street canyon.

However, there are other important factors that also influence the flow field and pollutant dispersion in the urban environment. For instance, temperature gradients have significant effects on dispersion. Also, cities are comprised of roughness arrangements, having 3-d characteristics. One can commonly observe openings between buildings, and it would be interesting to simulate such roughness arrangements for comparison to the present work. The following are the recommendations for further experiments:

- To study density stratification between two fluids of different density mixing in an urban environment. This will illustrate how the dispersion behaviour is effected by temperature in an urban environment.

- To study the flow structure and dispersion behaviour of flow over slat-type roughness with systematic variation in lateral openings between the slats. This will allow the flow to move easily in the cavities. It would be interesting to compare the length scales estimated from the tests with the present tests on 2-d slat type bed roughness with a 3-d roughness arrangement.

REFERENCES

1. Balachandar, R., Blakely D., Tachie, M. and Putz, G.,2001, A study on turbulent boundary layer on a smooth flat plate in open channel, Transactions of the ASME, 123, 394-400

2. Bandyopadhyay, P.R., 1987, Rough wall turbulent boundary layers in the transitional regime, Journal of Fluid Mechanics, Vol. 180, 231-266

3. Belcher, S.E., Jerram, N. and Hunt, J.C.R., 2003, Adjustment of a turbulent boundary layer to a canopy of roughness elements, Journal of Fluid Mechanics, Vol. 488, 369-398

4. Blackwelder, R.F., 1979(a), Boundary layer transition, Physics of Fluids, 22(3),583-584

5. Blackwelder, R.F. & Eckelmann, H., 1979(b), Streamwise vortices associated with the bursting phenomenon, Journal of Fluid Mechanics, vol.94, part 3, 577-594

6. Briggs, G.A., Britter R.E., Hanna. S.R., Havens, J.A., Robins, A.G. and Snyder,W.H., 2001, Dense gas vertical diffusion over rough surfaces: results of wind-tunnel studies, Atmospheric Environment 35, 2265-2284

7. Britter, R.E., Hanna, S.R., Briggs, G.A. and Robins, A., 2003, Short-range vertical dispersion from a ground level source in a turbulent boundary layer, Atmospheric Environment 37, 3885-3894

8. Brundrett, E. and Baines, W.D., 1964, The production and diffusion of vorticity in duct flow", Journal of Fluid Mechanics, 19, 375

9. Cardoso, A.H., Graf, W.H., and Gust, G., 1989, Uniform flow in a smooth open channel, Journal of Hydraulic Research, Vol. 27(5), 603-615

10. Chan, L.Y. and Kwok, W.S., 2000, Vertical dispersion of suspended particulates in urban area of Hong Kong, Atmospheric Environment, 34, 4403-4412.

11. Chang. C.H. and Meroney. N.R., 2001, Numerical and physical modelling of bluff body flow and dispersion in urban street canyons, Journal of Wind Engineering and Industrial Aerodynamics 89, 1325-1334

12. Clauser, F.H., 1954, Turbulent boundary layers in adverse pressure gradients, Journal of the Aeronautical Sciences, vol.21, 91

13. Clauser, F.H., 1956, Turbulent boundary layer, Adv. Applied Mechanics, Vol. IV,1

14. Colebrook, C.F. and White, C.M.,1937, Experiments with fluid motion in roughened pipes, Proc. Roy. Soc. London, Vol. A161, 367-381

15. Coles,D., 1956, The law of the wake in the turbulent boundary layer, Journal of Fluid Mechanics, 1,191-226

16. Cook, N. J., 1985, The designer's guide to wind loading of building structures Pt.1, Background, damage survey, wind data and structural classification, London : Butterworths [for] Building Research Establishment, Department of the Environment, 371

17. Counihan, J., 1971, Wind tunnel determination of a roughness length as a function of the fetch and the roughness density of three-dimensional roughness elements. Atmospheric Environment 5, 637-642

18. Dong, Zengnan, and Ding Y.,1990, Turbulence characteristics in smooth bed open channel flows, Sciences in China (Series A), Vol. 33(2), 244-256

19. Eames, I., and Gilbertson, M.A., 2004, The settling and dispersion of small dense particles by spherical vortices., Journal of Fluid Mechanics, Vol. 498, 183-203

20. Elder, J.W., 1958, The dispersion of marked fluid in turbulent shear flow, Journal of Fluid Mechanics, 2, 544-560

21. Fang, F., and Sill, B.L., 1991, Aerodynamic roughness length: correlation with roughness elements. 8th International Conference Wind Engineering London, Canada

22. Finnigan, J.J., and Brunet, Y., 1995, Turbulent airflow in forests on flat and hilly terrain, In: Wind and Trees, edited by Coutts, M.P. and Grace, J., Cambridge University Press, 3-40

23. Garde, R.J., 1994, Turbulent flow, John Wiley & Sons India

24. Gerdes, F., and Olivari, D., 1999, Analysis of pollutant dispersion in an urban street canyon, Journal of Wind Engineering and Industrial Aerodynamics 82, 105-124

25. Goldstein, S., 1936, A note on roughness, Aero. Res. Council, R&M, 1763

26. Grass, A.J., 1967, Boundary layer turbulence in open channel flow, Ph.D. Research Thesis, Department of Civil and Environmental Engineering, University College London.

27. Grass, A.J.,1971, Structural features of turbulent flow over smooth and rough boundaries, Journal of Fluid Mechanics, vol. 50, 233-255

28. Grass, A. J., Stuart R. J. and Mansour, T., 1991, Vortical structures and coherent motion in turbulent flow over smooth and rough boundaries, *Phil. Trans. R. Soc. London*, 336, 35-65

29. Head, M.R. and Bandyopadhyay P. 1981, New aspects of turbulent boundary layer structure, Journal of Fluid Mechanics, vol. 107, 297-338

30. Hinze, J.O.,1959, Turbulence, McGraw-Hill Series, USA

31. Holmes, P.J., Berkooz, G. and Lumley, J.L., 1996, Turbulence, coherent structures, dynamical systems and symmetry. Cambridge University Press, Cambridge

32. Hunt, J. C. R., and Eames, I., 2002, The disappearance of laminar and turbulent wakes in complex flows, Journal of Fluid Mechanics, Vol. 457,111-132

33. Jimenez, J. and Pinelli, A., 1997, Wall turbulence: How it works and how to damp it. AIAA paper 97-2122

34. Jones, M.E., 1968, Wind turbulence and buildings: a literature review, Building Research Establishment, England

35. Karman, T.V. and Lin, C.C., 1961, On the concept of similarity in the Theory of isotropic turbulence, Turbulence classic papers on statistical theory, edited by Friedlander.S.K., and Leonard Topper, Interscience Publishers, New York, 179-185

36. Kim, J. and Moin, P., 1986, The structure of the vorticity field in turbulent channel flow. Part 2, Study of ensemble-averaged fields. Journal of Fluid Mechanics, vol. 162, 339-363

37. Kline, S.J., Reynolds, W.C., Schraub, F.A. & Rundstadler, P.W., 1967,The structure of turbulent boundary layers, Journal of Fluid Mechanics, Vol.30, Part 4, 741-773

38. Knight, D.W., Patel, H.S., Demetriou, J.D., and Hamed, M.E., 1982, Boundary shear stress distribution in open channel and closed conduit flows, The Mechanics of sediment transport. Editor Sumer, B.M., BalkemaPublications, Netherlands

39. Laufer, J., 1951, Some recent measurements in a two dimensional turbulent channel, N.A.C.A. Report No. 1033

40. Lettau, H., 1969, Note on aerodynamic roughness parameter estimation on the basis of roughness element description. Journal of Applied Meteorology, 8, 828-832

41. Ligrani, P.M. and Moffat, R.J.,1986, Structure of transitionally rough and fully rough turbulent boundary layers, Journal of Fluid Mechanics, Vol. 162, 69-98

42. Louka, P., Belcher, S.E., and Harrison.R.G., 1998, Modified street canyon flow, Journal of Wind Engineering and Industrial Aerodynamics 74-76, 485-493

43. Lu S.S. and Willmarth W.W., 1973, Measurements of the structure of the Reynolds stresses in a turbulent boundary. Journal of Fluid Mechanics, 60, 481-571

44. Macdonald, R.W., Griffiths, R.F. and Hall, D.J., 1998, An improved method for the estimation of surface roughness of obstacles arrays, Atmospheric Environment, 32, 1857-1864

45. Macdonald, R.W. and Ejim, C.E., 2002, Hydraulic flume measurements of mean flow and turbulence in a scale model array of 4:1 aspect ratio obstacles, 5th UK Conference on Wind Engineering, University of Nottingham, 49-52

46. Mansour, T. M., 1992, Spatial distribution and scaling of bursting events in boundary layer turbulence over smooth and rough surfaces, Ph.D. Research Thesis, Department of Civil and Environmental Engineering, University College London

47. Melling, A. and Whitelaw, J.H., 1976, Turbulent flow in a rectangular duct, Journal of Fluid Mechanics, 78, 289

48. Meroney, N.R., Pavagaeu, M., Rafailddis, S. and Schatzmann, M., 1996, Study of line source characteristics for 2D physical modelling of pollutant dispersion in street canyons, Journal of Wind Engineering and Industrial Aerodynamics 62, 37-56

49. Millikan, C., 1938, A critical discussion of turbulent flows in channels and circular tubes, Proc. 5th International Congress Applied Mech., Cambridge,386-392

50. Moin, P. & Kim, J., 1982, Numerical investigation of turbulent channel flow, Journal of Fluid Mechanics, Vol 118, 341

51. Moin, P. & Kim, J., 1985, The structure of the vorticity field in turbulent channel flow. Part 1, Analysis of instantaneous fields and statistical correlations, journal of Fluid Mechanics, Vol.155,441

52. Moore,W.F.,1951, An experimental investigation of the boundary layer development along a rough surface, Ph.D. dissertation, State University of Iowa

53. Morris, H.M., 1959, Design methods for flow in rough conduits, Journal of the hydraulic division, ASCE, 85, No. HY7, 43-62

54. Nezu, I., and Rodi,W.,1986, Open channel flow measurements with a Laser Doppler Anemometer, Journal of Hydraulic Engineering, ASCE, Vol. 112(5), 335-355

55. Nikuradse,1933, Stromungsgesetze in rohnen, Forsh. Arb. Ing. Wes No. 361

56. Oke,T.R.,1987, Boundary layer Climates, 2nd Edition, London : Rout ledge, 435
57. Owen, P.R. 1961, A classification of the problems involving the effects of wind shear on buildings, Second meeting Industrial Aerodynamics Research N.P.L.

58. Panofsky, H.A., and Dutton, J.A., 1984, Atmospheric Turbulence, John Wiley & Sons, USA, 1-397

59. Pearson, B.R., Elavarasan, R. and Antonia R.A., 1997, The response of a turbulent boundary layer to a square groove, Transactions of the ASME, 119, 466-469

60. Perry, A.E. and Joubert, P.N.,1963, Rough-wall boundary layers in adverse pressure gradients, Journal of Fluid Mechanics 17,193-211

61. Perry, A.E., Schofield, W.H., and Joubert, P.N., 1969,Rough-wall boundary layers in adverse pressure gradients, Journal of Fluid Mechanics 37,Part 2, 383-413

62. Perry, A.E., Lim, T.T., and The, E.W.,1981, A visual study of turbulent spot, Journal of Fluid Mechanics, Vol. 104, 387-405

63. Peterson, R.L.,1997, A wind tunnel evaluation of methods for estimating surface roughness length at industrial facilities, Atmospheric Environment, 31, 45-57

64. Prandtl, L., 1925, Bericht Uber Untersuchungen Zur Aubgebildeten Turbulenz, Z. Angew. Math. Mech.,Vol. 5, No. 2, 136

65. Rajaratnam. N., and Muralidhar D.,1969, Boundary shear stress distribution in rectangular open channels, La Houille Blanche, Vol. 6, 603-609

66. Ratti, C., Di Sabatino, S., Britter, R., Brown, M., Caton, F. and Burian, S., 2004, Analysis of 3-d urban databases with respect to pollution dispersion for a number of European and American cities, http://www2.dmu.dk/AtmosphericEnvironment/trapos/abstracts/CERC_2.pdf

67. Raupach, M.R., Coppin, P.A. and Legg, B.J., 1986, Experiments on scalar dispersion within a model plant canopy. Part 1: the turbulence structure, Boundary layer Meterology, Vol. 35, 21-52

68. Raupach, M.R., Antonia,R.A. and Rajagopalan,S.,1991, Rough wall boundary layers, Appl. Mech. Rev., 44,1-25

69. Raven, P.W.J., 1977, Turbulent boundary layer characteristics in open channel flow over fixed and mobile sand beds, Ph.D. Research Thesis, Department of Civil and Environmental Engineering, University College London

70. Reynolds, A.J.,1974, Turbulent flows in engineering, John Wiley and sons

71. Reynolds, O., 1883, An experimental investigation of the circumstances which determine whether the motion of water shall be direct or sinuous and the laws of resistance in parallel channels, Phil. Trans. Royal. Soc. London, 174,51

72. Robinson,S.K.,1991, Coherent motions in the turbulent boundary layer, Ann. Rev. F.Mech., Vol.23

73. Roy, A.G., Buffin, Belanger, T., Lamarre, H. and Kirkbride, A.D., 2004, Size, shape and dynamics of large-scale turbulent flow structures in a gravel-bed river, Journal of Fluid Mechanics, Vol 500, 1-27

74. Sandham,N.D., and Kleiser,L., 1992, The late stages of transition to turbulence in channel flow., Journal of Fluid Mechanics, Vol. 245, 319-348

75. Schlichting, H., 1979, Boundary layer theory, Mc Graw Hill, 2nd Edition, New York

76. Schoppa, W., and Hussain, F., 2000, Coherent structure dynamics in near-wall turbulence, Fluid Dynamics Research, Vol. 26, 119-139

77. Schultz, F. and Drunow., 1940, Neues Reibungswiderstandsgesetz fur glatte platen, Luftfahrt Forschung (NACA TM986),Vol. 17, 239

78. Sladek, I., Kozel, K., Janour, Z., and Gulikova, E.,2004, In Procs Int. Conf. On Urban Wind Engineering and Building Aerodynamics, von Karman Institute, Belgium, 5-7 May. 2004; von Karman Institute for Fluid Dynamics; C.9.1-C.9.10

79. Steffler, P.M., Rajaratnam, N., and Peterson, A.W.,1983, LDV measurements of mean velocity and turbulence distribution in a smooth rectangular open channel, Water Resources Engineering Report, WRE 84-4, Department of Civil Engineering, University of Alberta

80. Stuart, R.J., 1984, Three-dimensional characteristics of coherent flow structure in a turbulent boundary layer over a rough surface, Ph.D. Research Thesis, Department of Civil and Environmental Engineering, University College London

81. Snyder, W.H.,1972, Similarity criteria for the application of fluid models to the study of air pollution meteorology, Boundary Layer Meteorology, 3, 113

82. Tennekes, H. and Lumley, J.L.,1972, A first course in Turbulence, MIT-press,Cambridge, 300

83. Theodorsen, T.,1952, Mechanism of turbulence, 2nd Midwestern conference on Fluid Mechanics, Ohio State University, 1-18

84. Theurer, W.,1993, Dispersion of ground-level emissions in complex built-up areas. Ph.D. Thesis, University of Karlsuhe

85. Townsend, 1976, The structure of turbulent shear flow, 2nd edition, Cambridge University Press, Cambridge

86. Wallace, J.M., Eckelmann, H. and Brodkey, R.S.,1972, The wall region in turbulent flow, Journal of Fluid Mechanics, Vol 54, Part 1, 39-48

87. Xia, J. and Leung, Y.C., 2001(a), Pollutant dispersion in urban street canopies, Atmospheric Environment 35, 2033-2043

88. Xia, J. and Leung, Y.C., 2001(b), A concentration correction scheme for Lagrangian particle model and its application in street canyon air dispersion modeling, Atmospheric Environment 35, 5779-5788